Universidade de Évora - Escola de Ciências e Tecnologia

Mestrado em Engenharia Geológica

Dissertação

CONTRIBUTION FOR HEAT FLOW DENSITY ESTIMATION IN THE MESO-CENOZOIC BASINS OF PORTUGAL

Anuri Nwadimma Chiamaka Nwagbara

Orientador(es) | António Correia

Évora 2021

Universidade de Évora - Escola de Ciências e Tecnologia

Mestrado em Engenharia Geológica

Dissertação

CONTRIBUTION FOR HEAT FLOW DENSITY ESTIMATION IN THE MESO-CENOZOIC BASINS OF PORTUGAL

Anuri Nwadimma Chiamaka Nwagbara

Orientador(es) | António Correia

Évora 2021

A dissertação foi objeto de apreciação e discussão pública pelo seguinte júri nomeado pelo Diretor da Escola de Ciências e Tecnologia:

Presidente	|	Isabel Maria Ratola Duarte (Universidade de Évora)
Vogais	|	António Correia (Universidade de Évora) (Orientador) Júlio Ferreira Carneiro (Universidade de Évora) (Arguente)

Évora 2021

ABSTRACT

CONTRIBUTION FOR HEAT FLOW DENSITY ESTIMATION IN THE MESO CENOZOIC BASINS OF PORTUGAL

The evolution of temperature in sedimentary basins is a fundamental tool for the evaluation and exploration of hydrocarbons, for the evaluation of geothermal potential, for paleogeographic reconstruction, for carbon sequestration and for the hydrogeological evaluation of a given region. Estimates of heat flow density (HFD) on the surface in the Portuguese Meso Cenozoic basins are difficult to obtain. The small number of HFD estimates in the Meso Cenozoic basins is a consequence of the high drilling costs for determining HFD and strict drilling regulation measures. Most of the temperature data available for estimating HFD is obtained in oil exploration holes; however, the temperature data obtained from them are subject to high uncertainty. Twelve oil exploration holes carried out in Portugal, with temperature records, were considered in this work; only one hole was rejected because they did not present the minimum quality requirements for HFD estimation. The values of thermal conductivity of the rock formations traversed by the various holes were assumed since there are no laboratory determinations for those geological formations. Bottom temperatures (BHT) have been corrected with Zetaware software that uses the Horner method and produces results with acceptable uncertainties. Only three sedimentary basins (Lusitanian, Porto, Alentejo) were identified and possessing a regional HFD estimates ranging from 61 to 174 mWm^{-2}. The average geothermal gradient and average HFD estimates of the Lusitanian basin were found to be 33 °C km^{-1} and 113 mWm^{-2}, Porto (24 °C km^{-1}, 78 mWm^{-2}) and Alentejo (21 °C km^{-1}, 61 mWm^{-2}) respectively. Compared to previous geothermal and HFD values, the new estimates obtained had a fair correspondence with a high regional sedimentary HFD estimates. Nevertheless, a heat flow density map was generated and an attempt to geothermally characterize the Portuguese Meso Cenozoic basins is made.

KEYWORDS: Heat flow density, geothermal gradient, thermal conductivity, Portuguese Meso Cenozoic basins

RESUMO:

CONTRIBUIÇÃO PARA A ESTIMATIVA DA DENSIDADE DO FLUXO DE CALOR NAS BACIAS MESO CENOZÓICAS DE PORTUGAL

A evolução da temperatura nas bacias sedimentares é uma ferramenta fundamental para a avaliação e exploração de hidrocarbonetos, para a avaliação do potencial geotérmico, para a reconstrução paleogeográfica, para o sequestro de carbono e para a avaliação hidrogeológica de uma determinada região. Estimativas da densidade do fluxo de calor (DFC) na superfície das bacias Meso Cenozóicas Portuguesas são difíceis de obter. O pequeno número de estimativas de DFC nas bacias Meso Cenozóicas é uma consequência dos elevados custos de perfuração para a determinação do DFC e de medidas rigorosas de regulação da perfuração. A maioria dos dados de temperatura disponíveis para estimar o DFC é obtida em furos de prospeção de petróleo; no entanto, os dados de temperatura neles obtidos estão sujeitos a uma elevada incerteza. Neste trabalho foram considerados doze furos de prospeção de petróleo realizados em Portugal com registos de temperatura; apenas um furo foi rejeitado por não apresentar os requisitos mínimos de qualidade para a estimativa do DFC. Assumiram-se os valores de condutividade térmica das formações rochosas atravessadas pelos diversos furos uma vez que não existem determinações laboratoriais para essas formações geológicas. As temperaturas de fundo de furo (BHT) foram corrigidas com o software Zetaware que utiliza o método de Horner e produz resultados com incertezas aceitáveis. Apenas foram identificadas três bacias sedimentares (Lusitanianas, do Porto, do Alentejo) e com uma estimativa regional de DFC que varia entre 61 e 174 mWm^{-2}. Verificou-se que o gradiente geotérmico médio e a DFC média na bacia Lusitaniana são, respectivamente, 33 $°Ckm^{-1}$ e 113 mWm^{-2} Porto (24 $°C\ km^{-1}$, 78 mWm^{-2}) e Alentejo (21 $°C\ km^{-1}$, 61 mWm^{-2}) respectivamente. Em comparação com valores geotérmicos e de DFC anteriores, as novas estimativas obtidas correspondem a uma DFC sedimentar regional elevada. Foi desenhado um mapa da densidade de fluxo de calor e é feita uma tentativa de caracterizar geotermicamente as bacias Meso Cenozóicas Portuguesas.

PALAVRAS-CHAVE: Densidade de fluxo de calor, gradiente geotérmico, condutividade térmica, bacias Meso-Cenozóicas Portuguesas.

APPRECIATION

Firstly, all gratitude to God Almighty for his divine guidance and protection in my life.Without him, I will not be here and made it this far and to several people whose contributions were indelible.

Many thanks to my advisor, Prof. Doctor António Correia from the Physics Department from the University of Évora, for the scientific rigour, data provision, patience, and guidance he administered to me in the course of this work which broke boundaries in my transition from my Chemical Engineering discipline to Geological Engineering and contribution in the discipline of Applied Geophysics.

I thank Prof. Isabel Maria Ratola Duarte, the program coordinator for Masters in Geological Engineering, for granting me the opportunity in this program and her ever-ready availability and rapid response to problems associated with being a foreign student. I thank Prof. Rita Maria Ferreira da Fonseca, director of the Environmental Biogeochemistry Laboratory at the University of Évora, for her sisterly support and contribution in the discipline of Applied Geochemistry. I cannot forget to mention Prof.António Chambel, President of the International Association of Hydrogeologists, for well drilling exercises and contribution in Hydrogeology elective of Geotechnical discipline, and, to Prof. António Pinho, for his support and contribution in Geotechnical discipline. Also, I thank Prof. Jorge Manuel Costa Pedro, director of the Department of Geoscience, for his support, brainstorming sections, and contribution to the discipline of Energy Resources.

A special thanks to Helena Lucas, a sister from another mother, for her non-seizing prayers, encouragement, and support in my career goals. Immense love to my bosom buddies - Josephine Azoba, Regina Onye, and Victoria Bassey, for your friendship andsupport in my life goals.

To those I fail to mention, I love you all.

INDEX

LIST OF FIGURES

LIST OF TABLES

NOMENCLATURE

Q	*Heat flow*
K	*Thermal rock conductivity.*
$\left(\frac{\partial T}{\partial z}\right)$	*Geothermal gradient.*
Δz	*Depth at a segment.*
R	*Radiant energy per second.*
σ	*Stefan-Boltzmann constant.*
T	*Absolute Temperature (Kelvin).*
H	*Rate of supply of heat to well.*
Δt	*Elapsed time between cessation of fluid circulation and T measurement.*
Tc	*Elapsed time between cessation of drilling and cessation of fluid circulation.*
λ_B	*Mean conductivity.*
λ_i	*Thermal conductivity of the ith bed.*
ϕ_i	*Thickness of the zth bed.*
Z_i	*Thickness of the zth bed.*
Z	*Total thickness of the sequence ($Z=\sum Z_i$).*
ϕ_0	*Porosity of sediments at time of deposition.*
Az,Bz	*Constant compaction coefficient of A, B.*
Z_{max}	*Depth at which all fluid is expelled.*
a	*Mean interatomic distance.*
V_m	*Mean phonon velocity.*
V_p	*P-wave velocity.*
Q_r	*Radioactive heat generation.*
A	*Heat generation.*

CHAPTER ONE: GLOBAL HEAT FLOW DENSITY

1.1 INTRODUCTION

Crustal movements, seismicity, hydrocarbon maturation are phenomena induced by the internal energy of the Earth. A measure of Earth's thermal energy is the heat originating from the Earth's surface and Sun. The Earth's thermal budget is the primary controlling parameter for the lithosphere and asthenosphere's activities and the formation of the innermost structure of the Earth. Common knowledge has those regions of high heat flow characterized by high temperatures, mostly at shallow depths, more than regions with low heat flow (Morgan, 2014). It is evident with the heat flow density map of North America illustrating the differences between continental and oceanic heat flow density, except in the active regions of the North American continent where heat flow density is low, and lowest in the Canadian Shield. Comparatively, higher heat fluxes are prevalent in the oceans than in the continent and higher on the western than on the eastern margin (Blackwell & Richards, 2004, Jaupart & Mareschal, 2007). From a global perspective, the oceanic lithosphere trends a transient thermal state in its short residence time on the Earth's surface as a function of age, which parallels elevation or bathymetry. The continental lithosphere being almost in a thermal steady state, has endured a long evolution, and is distinguished by a complicated structure and composition. It is noteworthy that the continental crust has radioactive elements that contribute a significant component to Earth's surface heat flow density (Jaupart & Mareschal, 2007).

The era of heat flow density measurements started in Great Britain in the late 1930s, with the first heat flow data measured in boreholes. A significant breakthrough was witnessed in the 1950s for the first heat flow density measurement in the Atlantic Ocean by Sir Edward Bullard when pioneering marine investigations (Benfield, 1939; Cermak, 1979). These triggered and motivated similar studies in the USA and Canada a decade later. The

1960s ushered a series of rapid development on measurement techniques for heat flow density, collation, and publishment of heat flow data at irregular intervals throughout the years (e.g., Cermak, 1979; Jessop et al., 1976; Lee & Uyeda, 1965; Pollack et al., 1993; Simmons & Horai, 1968). The latest compilation of heat flow density dataset is collected and compiled by the Global Heat Flow Database of the International Heat Flow Commission, and presently, more than 30,000 heat flux measurements on Earth's solid surface is distributed about equally between continents and oceans (Davis & Davis, 2010; Lee & MacDonald, 1963; Lee & Uyeda, 1965; Simmons & Horai, 1968). Notwithstanding, heat flow data measurement and interpretation are reported in journals such as the Journal of Geophysical Research, Pure and Applied Geophysics (Pageoph), American Association of Petroleum Geologists Bulletin, Geophysics, Geothermics, and so on or unpublished thesis or dissertations (Beardsmore & Cull, 2001).

The knowledge of global heat flow density is instrumental in the deduction of the mechanism of the Earth's processes. Direct information about geological processes underlain in the Earth's interior is revealed, more specifically in the study of the interactions of the solid interior with the hydrosphere, cryosphere, and atmosphere (Fahnestock et al., 2001; Mashayek et al., 2013; Scott et al., 2001). Heat flow density distribution provides valuable information for reconstructing the tectonic history of the Earth's crust. The patterns of heat flow density inside a given tectonic unit reverberate differences in fault distribution regions, hydrogeology, crustal radioactivity, hydrothermal activity, and subsequent heat flow density maps generated (Cermak, 1983; Condie, 1997; Sclater et al., 1980a). Understanding of the subsurface temperature field is vital to the study of the generation of oil and gas, ore bodies deposition, sedimentary basin evolution, earthquakes, and volcanism occurrence (Cathles & Smith, 1983; Muffler & Cataldi, 1978; Nielsen, 1986; Tissot et al., 1987). The impact of the Earth's thermal structure on the crust

is evident in the nonvolcanic eruption of volatiles gases (CO_2 and CH_4) (Etiope & Klusman, 2002; Mörner & Etiope, 2002).

However, the recent massive advancement of computer packages of Comsol, PetraSim, Leapfrog, Ground Loop Design software, SVHeat, and SVFlux, Etc., simplified the path of evaluations of the thermal regimes of geological processes, the assessment of the deep lithosphere temperature, and geothermal modeling, both on local, regional, and global scales. Nevertheless, a significant amount of knowledge of the underlying physical concepts and a wealth of reliable data is needed for the most efficient use of these sophisticated software applications. Constraints are met with accurate integral information on terminologies regarding thermal conductivity, vitrinite reflectance, xenolith geochemistry, diffusivity, Etc., especially by industry professionals as they are poorly understood. Existing is a shortage of scholars and experts with the necessary experience in new data generation and quality critiques of significant constraints associated (Beardsmore & Cull, 2001).

This section aims to summarize the general knowledge of heat flow density on Earth and pursue two different goals; (i) explain the underlying mechanism of heat transport on Earth, which involves an analysis of heat transmission at molecular levels (ii) illustrate different fundamental thermal properties responsible for heat flow density generation and numerical analysis in the estimation of these thermal properties. These goals are met by analyzing available measurement techniques employed at different terrains and their uncertainties.

1.2 EARTH´S HEAT FLOW DENSITY

Heat emerges from the Earth's surface from its interior and Sun. The Sun radiation incident on the Earth is mainly reflected into space; part enters the atmosphere and is reflected by the clouds or is absorbed and reradiated into space. Earth's surface heat flux is an elemental output of our dynamic solid Earth's heat engine**.** The detailed estimate of the global surface heat flux undertaken by Pollack et al. (1993) (abbreviated to PHJ93) yielded a value of 44.2TW±10 TW, from a dataset of 24,774 observations at 20201 sites. Jaupart et al. (2007) (abbreviated to JLM07) made alternative interpretations of the same heat flow dataset, resulting in a reasonable estimate of Earth's total surface heat flux of 46TW±3TW. A recent estimate of 47±2TW equivalent to an average heat flux of 91.6 mWm^{-2} has been regarded as the best estimate for the Earth's surface heat flux irrespective of the inhomogeneous nature of heat flow density measurements globally, i.e., poor sampling in Antarctica, Greenland, Africa, Canada, Australia, South America, and parts of Asia (Davies & Davies (2010), abbreviated as DD10). This estimate was derived from an improved heat flow dataset measurement with 38,374 heat flow density values, and the methodologies of Geographical Information Systems to produce a global heat flow density map. Figure 1 shows the global heat flow dataset distribution illustrating the inhomogeneous layout of measurements, while Figure 2 displays the heat flow density map, including data sets from PHJ93 (in blue).

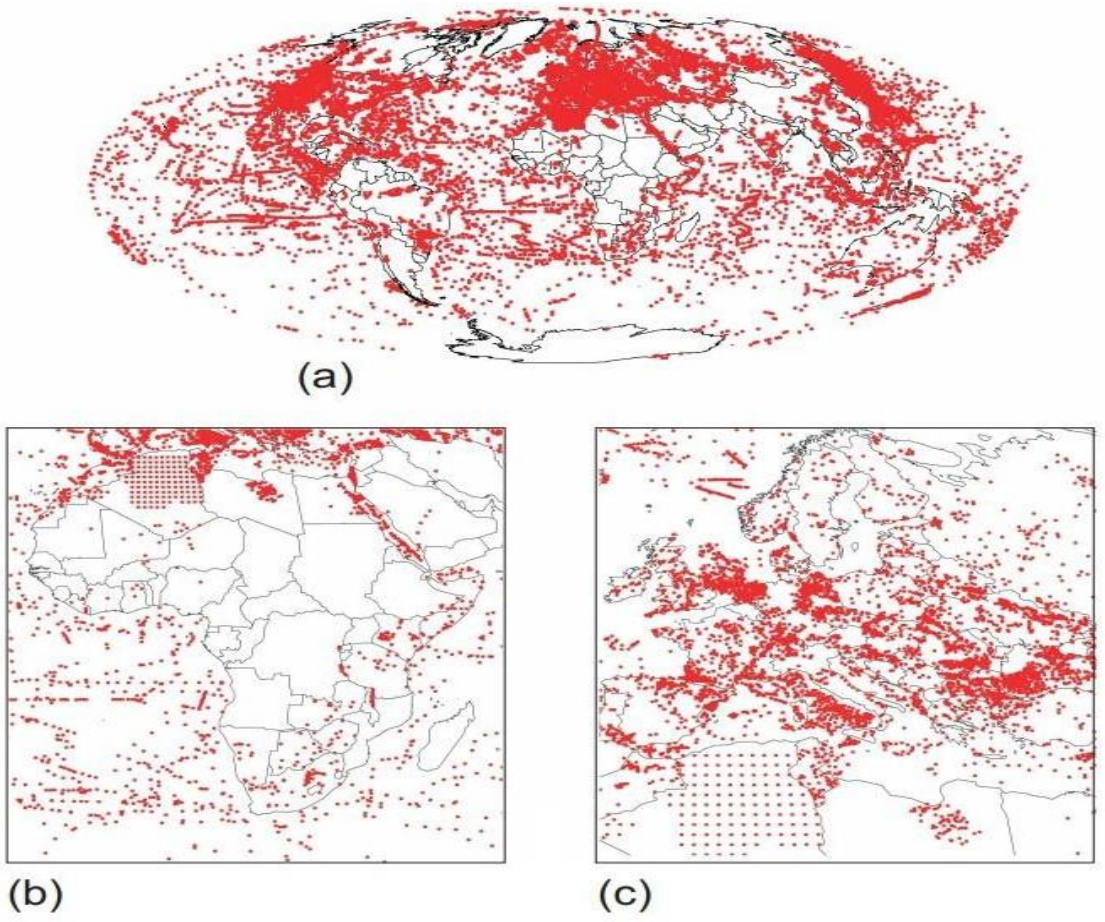

Figure 1: (a) Global distribution of heat flow density measurements. (b) African continent. (c)Europe continent (Davies & Davies, 2010).

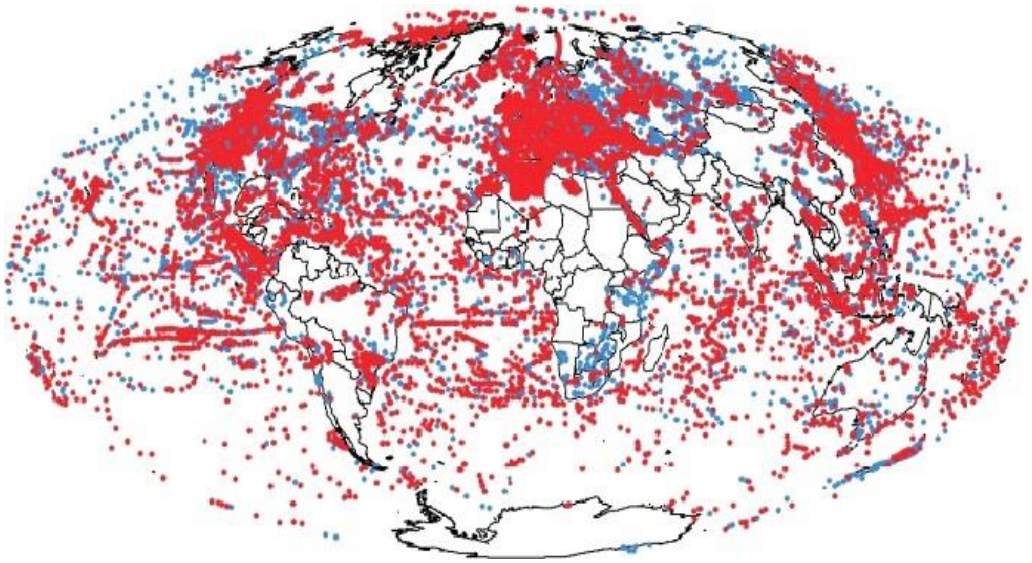

Figure 2: As in Fig. 1a with PHJ93 (blue) (Davies & Davies, 2010).

Heat flux data are distributed sparely and non-uniformly across the globe. Table 1 summarizes major modes of heat loss from Earth and Table 2 compares various estimates used in the past. Nearly 75% of the global heat loss is through the oceans, 85% of which is associated with the new oceanic lithosphere creation. On comparison,over 60% of the 25–30% of the global heat loss from the continents is derived by radioactive decay in the crust (Morgan, 2000).

Table 1: Major Modes of Heat Loss from the Earth (Sclater et al., 1980b).

Mode Of Heat Loss	**Estimated Power; Estimated HFD**
Heat loss through continents	3.1×10^{13} W
Heat loss through the oceans	1.2×10^{13} W
Total	4.2×10^{13} W
Heat loss by hydrothermal circulation	1.0×10^{13} W
Heat lost in plate creation,	2.6×10^{13} W
Mean heat flow density	
Continents	50 mW m^{-2}
Oceans	100 mW m^{-2}
Global	84 mW m^{-2}
Convective heat transport by surfaceplates[a]	~65% heat loss
Radioactive decay in crust	~17% heat loss

[a] Includes lithospheric creation in oceansand magmatic activity in continents.

Table 2: Estimates of the continental and oceanic heat flux and global heat loss (Jaupart et al., 2007).

	Continental (mWm^{-2})	**Oceanic** (mWm^{-2})	**Total** (TW)
Williams & Von Herzen (1974)	61.0	93.0	43.0
Davies (1980)	55.0	95.0	41.0
Sclater et al. (1980)	57.0	99.0	42.0
Pollack et al. (1993)	65.0	101.0	44.0
Jaupart et al. (2007) [a]	65.0	94.0	46.0
Davis & Davis (2009)	70.9	105.4	91.6

[a] The average oceanic heat flux does not include the contribution of hot spots. The total heat loss estimate does include 3TW from oceanic hot spots.

1.3 HEAT SOURCES OF EARTH

The Earth's internal heat originates from several sources. Heat is generated from the creation of new lithosphere at oceanic ridges. The widening of the sea-floor releases heat in the marginal basins behind island arcs. Hotspots from rising plumes of magma emerging deep in the mantle liberate heat to Earth's surface. However, almost for some decades, the Earth's heat has been chiefly derived from two distinctive sources: the heat associated with its formation and the heat derived from the decay of long-lived radioactive isotopes in the Earth.

Primordial heat is heat lost by the Earth as it cools from its original formation. Earth's accretion from a hot cloud of gas and dust began more than 4550 million years ago. The release of kinetic energy from the accreting masses, solar heating, short-lived radioactive isotopes, compressional heating, and potential energy released during core formation contributed to the thermal structure of Earth. A vast amount of heat from the events associated with the formation and initial differentiation of the Earth was liberated early in Earth history, and the Earth has since been slowly dissipating heat through its surface. The Earth's mantle primordial heat loss is estimated to be within the range of 7 - 15 TW, which is calculated as the heat remnant after core heat flow and bulk-Earth radiogenic heat production removal from the observed surface heat flow (Dye, 2012).

The radioactive element's decay in the Earth's mantle and crust leads to the production of daughter isotopes and the release of geoneutrinos and heat energy, or radiogenic heat. The heat contribution from a radioactive element is proportional to its absolute abundance, its half-life, and the heat generated from a single decay event of each isotope of the element (Beardsmore & Cull, 2001). Four long-lived radioactive isotopes (^{232}Th, ^{238}U, ^{40}K, and ^{235}U) are responsible for most radiogenic heat because of their enrichment relative to other radioactive isotopes. Figure 3 illustrates the decrease of Earth's radiogenic heat flow over time and Table 3 shows heat production rates of major radioactive isotopes.

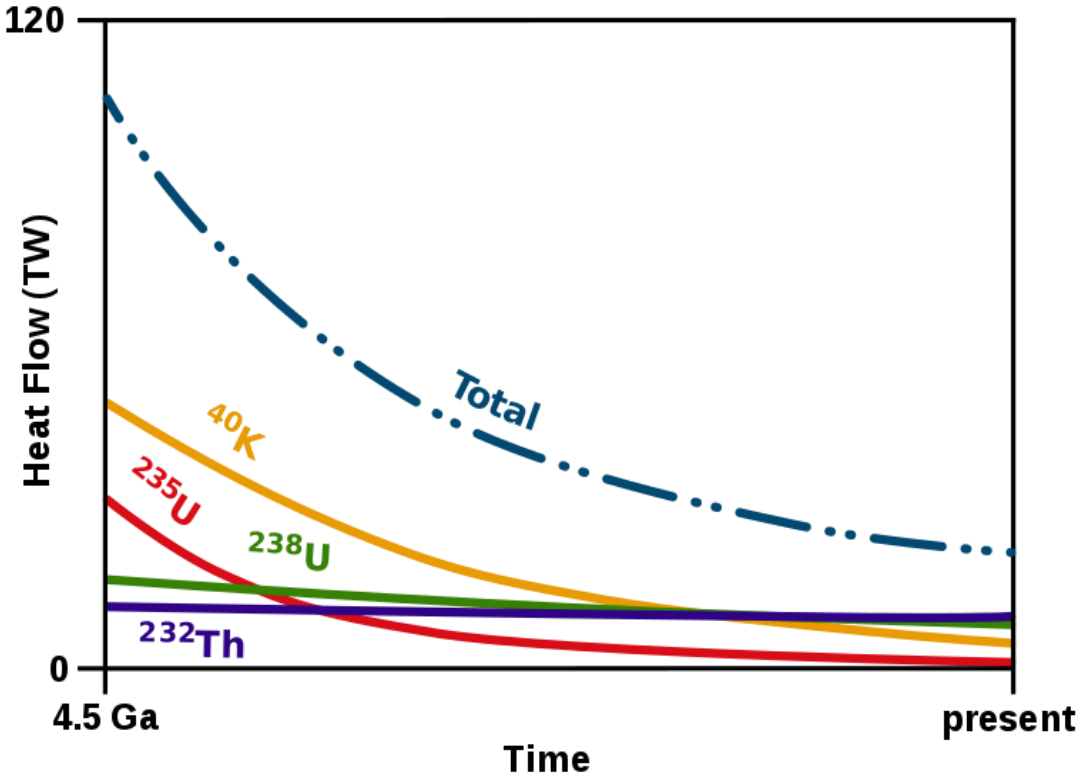

Figure 3: Earth's radiogenic heat fluxes over time (Arevalo Jr et al., 2009).

Table 3: Rate of heat release (H) and half-lives ($\tau^{1/2}$) of the most important radioactive isotopes in the Earth's interior (Turcotte & Schubert, 2014).

Isotopes	**H** (W kg^{-1})	**$\tau^{1/2}$** (yr)	**C** (kg kg^{-1})
^{238}U	9.46×10^{-5}	4.47×10^{9}	30.8×10^{-9}
^{235}U	5.69×10^{-4}	7.04×10^{8}	0.22×10^{-9}
U	9.81×10^{-5}	31.0×10^{-9}	
^{232}Th	2.64×10^{-5}	1.40×10^{10}	124×10^{-9}
^{40}K	2.92×10^{-5}	1.25×10^{9}	36.9×10^{-9}
K	3.48×10^{-9}	31.0×10^{-5}	

H = Heat releases, $\tau^{1/2}$ = Half-lives, C = Concentration.

Note: Heat release is based on the present mean mantle concentrations of the heat-producing elements. Today's heat generation is by ^{238}U and ^{232}Th but in the past was by ^{235}U and ^{40}K because of their short lives.

As the total internal Earth heat flow to the surface is well limited, the high uncertainty of the Earth's radiogenic and primordial heat sources contributions are as a result of their direct measurement difficulties. However, a modern balance of Earth formation and differentiation has been estimated to be 80% radiogenic heat and 20% primordial heat (Morgan, 2000).

1.4 MECHANISM OF EARTH'S HEAT TRANSFER

Heat can be conveyed by conduction, convection, radiation, and advection. Heat Conduction involves the interaction of atoms or molecules within a material. Conduction is the most effective heat transport process in the crust and lithosphere and less effective when the molecules are mobile. In convection, heat transport takes place due to a molecule's mobility within a material, and it is more rapid than conduction. Heat convection occurs in the Earth's mantle as the mantle appears to behave as a viscous fluid over time with the passage of seismic waves through it. Convection is also significant in the transfer of heat in the outer core, where fast changes in the geomagnetic field result from it. Radiation heat transfer is only significant in the hottest areas of the core and lower mantle. Within the Earth, three heat transfer mechanisms are effective, namely: (1) lattice (or phonon) conduction, (2) convection or advection, and (3) radiation (or photon conduction).

1.4.1 TRANSFER BY CONDUCTION

Heat conduction occurs in liquids, gases, or solids by direct microscopic transfer of kinetic energy of particles (molecules or atoms) through the boundary between two systems. The majority of the Earth's surface heat loss is by conduction, and Fourier's law of conduction governs heat transport. Heat flow from Earth is assumed to be vertical and can be expressed by the relationship given below:

$$Q = -k(\partial T/\partial z) \quad (1.1)$$

Where heat flow density (Q) is the product of thermal rock conductivity (k) and, the rate of temperature increase (T) with depth (z) (by convention, z is defined as positive downward) (Morgan, 2014).

At a molecular level, conduction is perceived as vibrations spreading along inter-atomic bonds as atoms in a solid occupy definite positions that form a lattice with a certain symmetry. The distribution, number of neighbouring atoms, and the types of external forces determine the atoms' countless numbers of vibrational states. These vibrational states are considered quantized particles or phonons that form a gas; thus, phonon conduction. As the vibrational states increase, coupling between atoms and vibrational energy is transferred to the lattice. In a perfect, infinite lattice, free atomic movement is limited only by collisions between two or more phonons. These phonons behave in a wave-like manner in their relationship to the lattice**.** Hence, thermal conduction in Earth is more evident in crust and mantle, where there are few conduction electrons and low lattice vibrational energy**.**

1.4.2 TRANSFER BY CONVECTION

Heat convection is the method of transfer of heat by the movement of fluid (liquid or gas) between areas of different temperatures. In solid Earth, convective heat involves the movement of Earth materials physically across a temperature difference (i.e., rock or ascending and descending fluids, such as magma or water). Convection currents can be produced by thermally induced buoyancy forces known as natural or free convection or by external forces (as in lithosphere tectonic deformation and regions of gravity-driven groundwater flow) as forced convection. Convection is the dominant heat transfer process below the lithosphere base with depths greater than 100–200 km. Hydrothermal

convection occurs in fractures and pores, which get closed by the confining pressure deeper than 10 km. Hydrothermal circulation currents are crucial in shallow environments where heat flux measurements are made (Jaupart et al., 2007). Advection is a unique form of convection where heat transfer is by non-thermally produced buoyancy but can be driven by hydraulic forces (in thermal springs) or pressure differences (as in magma intrusion) with no return flow.

1.4.3 TRANSFER BY RADIATION

Radiation takes place through any transparent medium (solid or fluid or gas) or a vacuum. Thermal radiation is the process of the transfer of energy as atoms and molecules move randomly in matter. These atoms and molecules consist of charged particles, and their movement results in energy emission away from the surface in the form of electromagnetic waves. Radiative heat transfer becomes effective at high temperatures, and the rate of transfer of radiant energy can be defined by the Stefan-Boltzmann equation below:

$$R = \sigma T^4 \tag{1.2}$$

Where R represents the radiant energy per second emitted per unit area of the body's surface at temperature, σ is the Stefan-Boltzmann constant (5.6704 x 10-8 $Wm^{-2}K^{-4}$), and T is the absolute temperature in Kelvin (Lowrie, 2007). Inside the Earth, radiation is only essential for phenomena that occur at high temperatures. As radiation is considered the least significant heat transport on Earth, solar radiation is harvested for heat and power, unlike conduction and convection (Mojiri, 2013).

1.5 HEAT GENERATION BY THE DECAY OF RADIOACTIVE ELEMENTS

Heat is obtained in rocks chiefly through the radioactive decay of unstable isotopes that emits energy occurring as alpha (α), beta (β), and gamma (γ) particles, geoneutrinos. The α-particles are positively charged and equal to helium nuclei, while β-particles are electrons. Geoneutrinos are electron antineutrinos generated within the Earth by beta-minus decay when a neutron decays to a proton through a weak interaction. Rocks are virtually transparent to neutrinos and antineutrinos, and most of the particle's energy is lost into space (Hamza & Beck, 1972; and Dye, 2012). The criteria of a radioactive isotope as a significant source of heat includes:

- half-life comparable to the Earth's age,
- complete conversion of the energy of its decay into heat, and
- the abundance of the isotope.

Nevertheless, the energy release and decay rate depend only on the radioactive isotope species (see Table 4), so the absolute abundance of individual isotopes in a rock wholly determines the heat production rate.

Table 4: Decay constants and half-lives of some naturally occurring, radioactive isotopes (Lowrie, 2007).

Parent Isotope	Daughter Isotope	Decay Constant ($10^{-10}10yr^{-1}$)	Half-Life (Ga)
^{40}K	89.5% ^{40}Ca, 10.5% ^{40}Ar	5.543	1.25
^{87}Rb	^{87}Sr		
^{147}Sm	^{143}Nd	0.1420	48.8
$2^{32}Th$	^{208}Pb	0.0654	106.0
^{235}U	^{207}Pb	0.4948	14.01
^{238}U	^{206}Pb	9.8485	0.704
		1.5513	4.46

Radioactive heating of the mantle and crust is ascribed to the decay of the uranium isotopes ^{235}U and ^{238}U, the thorium isotope ^{232}Th, and the potassium isotope ^{40}K (Table 4). The natural isotopic abundance of a unit mass of Rb is higher than K, but its contribution to the total radiogenic heat power is expected to be less than 1% (Fiorentini et al., 2007), given the relative decay rates and a K/Rb ratio of ~400 in the bulk silicate Earth (BSE) (McDonough & Sun, 1995). Gamma-ray spectrometers are considered the most direct method for measuring uranium, potassium, and thorium abundance in rock.

The quantity of heat generated per second by these elements (in Wkg^{-1}) is natural uranium, 95.2; thorium, 25.6; and natural potassium, 0.00348 (Rybach, 1976, 1988). The radioactive heat generation (Q_r) in rock with concentrations C_U, C_{Th}, and C_K of these elements is:

$$Q_r = 95.2C_U + 25.6C_{Th} + 0.00348C_K \quad (1.3)$$

In a petroleum exploration setting, heat generation (A) is computed directly from Well logs of uranium, thorium, and potassium concentration, using below expression,

$$A = -0.96(FQ) + 1.29 \quad (1.4)$$

where A is in Wm^{-3} and (FQ) is the fractional proportion of quartz (Issler & Beaumont, 1989) or using the empirical relationship with total gamma-ray count (GR) following the revised expression of Bucker and Rybach (1996),

$$A = 0.0158(GR - 0.8) \quad (1.5)$$

For deeper formations of the Earth's middle and upper crust, the expression for empirical correlations with seismic velocity may be used and is given below:

$$In(A) = B - 2.17Vp \quad (1.6)$$

where V_p is the p-wave velocity.

1.6 HEAT FLOW DENSITY PARAMETERS

Various nomenclature was developed for understanding heat flow density in the Earth. A set of elements employed in the systematization and quantification of heat distribution over a region is known as heat flux parameters. Heat flux parameters are thermal properties providing essential information useful in geothermal investigations of the Earth's crust. Heat flux parameters play an essential role in the prediction of heat flow provinces. These parameters are heat generation, thermal gradient, and thermal conductivity (see table 5). Despite these terminologies' simplicity, the process of deducing heat flux from thermal properties has surprising complexity on measurement methodology, instrumentation, and correction procedures on varying terrains.

Table 5: Basic Parameters in Heat flow density (Stein, 1995).

Property	Symbol	Approximate ranges
Heat flow	Q	0 - 125 mWm^{-2}
Vertical temperature gradient	dT/dz	10 - 80 $°Ckm^{-1}$
Thermal conductivity	K	0.6 - 1.2 $Wm^{-1}K^{-1}$
marine sediments		1 - 5 $Wm^{-1}K^{-1}$
continental sediments	A	0 - 8 10^{-6} Wm^{-3}
Heat generation		

1.6.1 HEAT GENERATION

Current heat flow density is ascertained by the amount and distribution of radioactive isotopes, their secular decrease with time, the retardation between heat production and its surface appearance, earthly cooling of the interior, and various minor heating sources, which are usually neglected due to several controversies and paradoxes associated with it. To appreciate how impressive heat is generated on Earth, the initial conditions of the Earth

cannot be overlooked. In concession with the cold accretion model of the formation of the planets, the Earth's internal heat sources originate from converting potential gravitational energy and the colliding bodies of a primordial cloud of dust, gas into heat. Another model suggests the interaction of the cosmic neutrino with the Earth as a potential heat source on Earth. Other models proposed internal heat sources as the frictional heat of intraplate strain and plate motions, exothermic metamorphic and diagenetic producing heat processes, tidal dissipation emerging extensive melting and differentiation of the Moon, and some meteorite parent bodies, the energy of short-lived radioactive nuclides. The energy released by short-lived radioactive isotopes is consumed quite quickly during most of Earth's thermal evolution (Safronov, 1972; Hamza & Beck, 1972; Anderson, 1989).

1.6.2 GEOTHERMAL GRADIENT

The geothermal gradient is the rate of variation of temperature with depth in the Earth. It varies significantly from place to place, depending on the region's thermal history, underlying rock's radioactivity, and the conductivity of the upper rocks. Geothermal gradients range from very low to near zero in zones of groundwater recharge and fore-arc regions. However, gradients above 20,000 °C km^{-1} have been recorded like in the sediments beneath Yellowstone Lake inside the caldera of Yellowstone National Park, Wyoming, USA. However, such high gradients are lost as soon as temperatures reach the boiling temperature at depth. Thus, a wide range of geothermal gradients exists in the upper continental crust (Morgan, 2014).

A geothermal gradient is a vector quantity dependent on temperature distribution in three dimensions. As a rule, it is assumed that the maximum gradient direction within the upper crust is vertical, so the gradient is the temperature derivative with respect to depth (dT/dz). By convention, this quantity is positive when increasing downward and expressed as:

$$(\partial T/\partial z) \approx (T_1 - T_0)/\,\Delta_z \quad (1.7)$$

where$(\partial T/\partial z)$ is the geothermal gradient, T_0 is the surface temperature, T_1 is the hole temperature at depth Δz, and Δz is the depth difference between point $T_1 - T_0$ measurements at a segment.

1.6.2.1 MEASUREMENTS TECHNIQUES OF GEOTHERMAL GRADIENT

Temperature measurements can be conducted in marine or land environments. The measurement is dependent on instrument technique, geological formation, and type of measurement. The instrument technique could require inserting a temperature sensor into the crust or without utilizing techniques such as drilling, which perturbs the natural regime to measure the thermal gradient. The geological formation could consist of a rock or sediment, or water, and the type of measurement required may be surface or underground measurement. Temperature-sensitive components of the measuring device in use are thermistors or platinum resistance sensors. Platinum resistance thermometers are more stable than thermistors, with a nearly linear resistance-temperature response over an extensive temperature range. The vertical temperature gradient is estimated from measured temperatures at known depths below the surface. The process of surface penetration to measure the temperatures disturbs the thermal structure, i.e., a steady-state must be achieved for a measurement to be made.

(A) MARINE MEASUREMENT

Due to deep ocean topography, temperature measurement accessibility is difficult. Specialized instruments with thermistor-lined probes are utilized in the perforation of the soft sediment on the seafloor. This method requires thrusting a probe into the sediments to depths of about 5 m resulting in frictional heating along the probe shaft, which takes from 5 - 30 minutes to dissipate depending primarily on the probe diameter, attaining thermal equilibrium, and the temperature is measured.

Specific designs of instruments have evolved following improvements in technology to three categories: (i) Bullard probe: solid shafts with regularly spaced thermistors. Long heat dissipation time with slow results. Prone to bending on penetration. (ii) Ewing probe: similar in operation with Bullard probe but different in construction. Incorporates a hollow shaft to collect a core sample for thermal conductivity analysis, and the thermistors arrangement greatly reduces the heat dissipation time. (iii) Lister probe: a violin bow appearance. Consisting of a thin sensor tube supported away from a thick strength member. Advances in digital technology and engineering have paved the way for probes modification with fast multiple logging rate, digital data gathering system, and no withdrawal to the surface, which, unlike earlier probes that are fully returned to the ship between measurements with a maximum rate of four locations per day (Davis, 1988).

Surface temperature measurement in water is conducted both onshore and offshore. In offshore surface temperature, the thermal profiles recognize surface temperatures at the top of the sediment column or the bottom of the water, i.e., at the sediment-water interface. The bottom-water temperature (BWT) is used as the top boundary of the conductive heat flow models. In shallow water and enclosed seas, bottom water temperatures are taken to be equal to surface temperature regardless of water depth. Oil exploration companies use the bottom water temperature or assumed value for offshore surface temperature. The onshore surface temperatures are regarded as the temperature in the top layer of a soil or rock (not air). Typically, the rock temperature usually exceeds average air temperature by a few degrees on land due to surface albedo. Local meteorological records are the best resource for evaluating onshore surface temperature.

(B) LAND MEASUREMENT

(i) Direct measurement techniques

Direct measurement of underground temperature requires lowering down a temperature measuring device in a borehole or cave, mineshaft, or other accessible cavities from the surface. The device is usually encased in a pressure-proof, water-tight container to avoid the necessity of applying an uncertain correction for pressure (Weiss, 1938). The device measures the temperature of the boring fluid and not the surrounding rock to obtain significant ambient temperatures of the rock. Temperature logging is not attempted until 10-20 times of the drilling time has elapsed to allow the bore fluid circulation to attain thermal equilibrium with its surroundings and any event in thermal disruption causes a thermal disturbance. The amount of time needed for re-equilibration depends on the magnitude of the thermal disturbance.

Various high-precision instruments with the capacity to yield the most accurate and precise temperature data possible have been available for many years. Mostly are electronic, using thermistors or platinum resistance sensors as the temperature-sensitive component, and these devices fall into one of three classes; (i) Wire-line temperature tools: moderate budget logging outfit in constant electrical contact with the surface. Consisting of a thermistor mounted close to the tip to reduce disturbance during measurement, cables for circuiting, and a motorized or hand winch. (ii) Self-contained computer temperature tools: commercially available with on-board memory for recording a time-temperature log. Expensive, versatile, and more suited for logging in deep, hot, pressurized, producing, or other bad-environment wells. (iii) Distributed optical fiber temperature-sensing systems: cheap and logs more than one temperature readings. It models the Raman effect of temperature-sensitive backscattering of laser light in an optic fiber. It is ideal for studies and regular monitoring of wells. Two methods exist for using thermistor sensors for

temperature logging. One technique is in monitoring thermistor resistance directly from the surface using a Wheatstone bridge or other type of ohmmeter (see Figure 4), and another is using the thermistor in an oscillatory circuit so that the signal frequency from the probe is proportional to the thermistor resistance (Beardsmore & Cull, 2001; Beck & Balling, 1988).

At surface temperature measurement, normal geothermal gradients are enough to cause convection in boreholes with a diameter of more than about 5 cm. Without significantly disrupting broader temperature trends, the convection effect within boreholes assists in decreasing the signal-to-noise ratio on a temperature log. Subsequently, high geothermal regions produce nosier logs compared to other areas with a formation that has been washed out.

(ii) INDIRECT MEASUREMENT TECHNIQUES

Diverse indirect measurement techniques have been developed to supplement direct measurement techniques. These methods estimate the temperature in the deep crust without requiring direct access to boreholes. The indirect temperature indicators used are groundwater geothermometers for dissolved solids in groundwater, Curie depth for magnetic minerals, xenoliths for temperature pressure equilibrium, and upper mantle resistivity method.

1. **Groundwater Geothermometers:** It utilizes the concept of solubility of dissolved solids in groundwater. The solubility of many compounds increases with temperature in water. The ambient temperature of a formation could be evaluated from the amount of dissolved material in the pore water. The geothermometers work best at a high temperature (> 200 °C) which other temperature devices may not operate. They are useful in geothermal reservoir studies where the estimation of the energy content of a high-enthalpy reservoir is achieved by extracting a fluid

sample to the surface and analyzing its chemistry. In the Petroleum setting, the method only applies when the pore water is in chemical equilibrium with the surrounding rocks at in situ temperature conditions.

2. **Curie depth:** This is the depth at which crustal rocks attain Curie temperature, and a Curie temperature is the temperature where rock minerals lose their ferromagnetic properties. Various rock types have different Curie temperatures such as pure magnetite (580°C), titaniferous (<300°C), ferromagnetic minerals within andesites and alkali-basalts (100-300°C), intermediate to mafic compositions (300-450°C), Fe-Co-Ni alloys (620-1100°C) (Gasparini et al., 1979). Curie depth is estimated through spectral analysis of regional aeromagnetic data. Curie depth may be interpreted as temperature isotherm (580°C in most continental regions).
3. **Xenoliths**: This is a piece of country-rock picked up by magma as it rises through the crust. The stability of pressure-temperature conditions is identified with xenolith's mineral. Xenoliths provide an independent estimate of temperature at depths down to hundreds of kilometers (O'Reilly & Griffm, 1985). The measurement technique uses data derived from the xenolith's mineral assemblage, which relates to the thermal conditions existing when the xenolith was emplaced in the host magma.
4. **Upper mantle resistivity**: Magnetotelluric methods yield a value for the upper mantle's electrical resistivity, which strongly depends on temperature (Majorowicz et al., 1993). However, the depth resolution of such temperature estimates is poor.

In Figure 4, the outline of steps for the collection and collation of crustal temperature data for the most accurate possible temperature profile for a specific region is shown. The more

constrained the temperature field, the more accurate gradient values and subsequent heat flow density values in yielding an accurate temperature data.

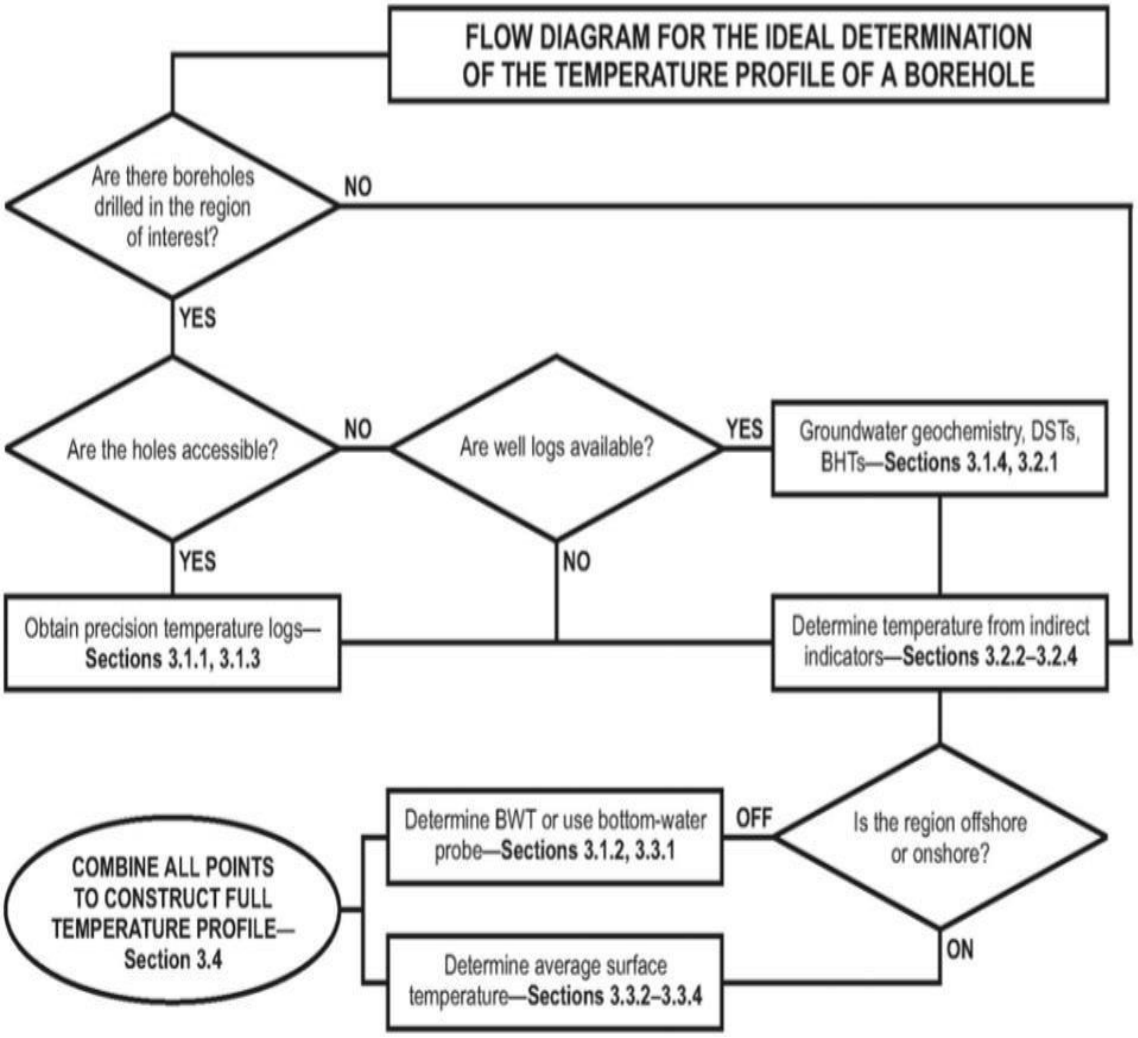

Figure 4: Flow chart for collating all available temperature data (From Beardsmore & Cull, 2001).

1.6.2.2 BOTTOM HOLE TEMPERATURE IN DEEP WELLS

In the oil and gas industry, many temperature data come from bottom hole temperatures (BHTs). Bottom hole temperatures are the highest temperature measurement made at the bottom of the well and sometimes at intervals up the well. BHTs are usually recorded at the end of each logging run with other parameters as resistivity, spontaneous potential

logging (SP), Etc. More than three or four logging runs before a well is completed so that a minimum of four bottom hole temperatures may be available from a single hole. These temperatures can be used for purposes such as corrections application to temperature-dependent physical properties, zone location for cement setting, Etc., where inaccuracies of a few degrees can be ignored or tolerated (Stein, 1995).

Bottom hole temperatures are affected by the thermal effects of mud circulation. It can take several months for a deep well to attain thermal equilibrium after drilling. After drilling in offshore wells, wells are mostly plugged and abandoned, making them inaccessible for future temperature logging. While in onshore wells, there is a possibility of access to the deep borehole for precision temperature logging after a sufficient equilibration time. In a typical excavation process of an oil well, drilling is interrupted at depths to change the drill bit, run wireline geophysical logs, and case the well. During logging, a suite of tools, including a thermometer, is lowered into the well, and the instruments down-hole record maximum temperatures. These temperature data are corrected to get an estimate of equilibrium formation temperature.

Most times after drilling, the most accurate measurement of downhole formation temperature is provided by drill stem tests (DST). The measurement technique requires inserting a tool in a well and left it stationary for some time to collect formation fluid flowing from the Well wall. The fluid is assumed to be from a thermally undisturbed zone around the borehole and thus is assumed to attain equilibrium of the ambient temperature of the surrounding rock rapidly. Drill stem tests are not always available for many wells, and in such cases, alternative data are utilized in the estimation of temperature at depth.

(A) METHODS OF CORRECTION OF BHTS

In the Well logging exercise, more than one temperature readings are recorded at the same depth. The drilling fluid temperature is the actual temperature measured, not the formation. The drilling mud flows during drilling and before inserting the wireline tool, and the drilling mud runs cold compared to the formation. The cold drilling fluid permeates the formation and lowers it down very efficiently via heat convection.

While the drilling fluid circulates, the borehole temperature reaches an equilibrium defined by the drilling fluid's cooling effect and the formation's heating effect. But as drilling mud circulation stops (for instance, in preparation for the insertion of a wireline tool or changing of the drill bit), the borehole gradually recovers the true formation temperature because the large mass of formation surrounding the borehole heats the drilling fluid to its ambient temperature. This process is slow because it materializes via heat conduction which is less efficient than heat convection. Equilibrium may take several months to be attained after cessation of the drilling fluid circulation. Temperature measurements made during drilling continually underestimate the formation temperature because drilling mud is being circulated, and sometimes, after the drilling fluid circulation has stopped also, but less than during drilling as the formation is now in the process of reheating the borehole mud. Temperature measurements made at increasing times after fluid circulation have ceased are much closer to the real formation temperature. Hence, it is necessary to correct the bottom hole temperature (Glover, 2014; Beardmore & Cull, 2001).

Various correction methods have been employed in the past to correct the logged BHT to real formation temperature. The relationship between BHT and the virgin rock temperature (VRT), which is the real formation temperature is complex. The BHT

correction methods depend on the type of information available, and three methods are recognized, namely:

(i) **Horner method:** Most precise common method was originally for correction of pressure build-up data from drill stem tests. Exhibits a temperature versus a dimensionless time parameter on semi-log axes and expressed as:

$$BHT = VRT + \left({}^{H}/_{4\pi\lambda}\right) \times In\ (1 + \left[\frac{t_c}{\Delta t}\right]) \quad (1.8)$$

where BHT is the bottom-hole temperature, H is the heat supply rate to well, Δt is the time elapsed between cessation of fluid circulation, and t_c is the time elapsed between cessation of drilling and cessation of fluid circulation. A plot of BHT against [1 + (t_c/Δt)] gives a line which is a function of ($Wm^{-1}K^{-1}$) and H (Wm^{-1}) (Figure 5). The Horner plot may underestimate the true temperature for temperature data collected less than three times the mud circulation time after drilling ceases.

(ii) **Cooper and Jones method**: Models the physical conditions within the drill hole. The temperature of the fluid approaches that of the strata as heat flows radially inwards from the borehole walls. It is useful for more than three temperature data logs and is calculated as:

$$BHT = \left(VRT - T_f\right)[1 - F(\alpha, \tau)] + T_f \quad (1.9)$$

where T_f is drilling fluid temperature, and F (α, r) is a tabulated function from Jaeger (1956) and Davis (1988)**.** The plot of BHT versus [1 — F (α, τ)] is linear with slope (VRT — T_f) and intercept T_f.

(iii) **Roux, Sanyal, and Brown method:** Method invented to counter the theoretical bias in the Horner method on those occasions when (t_c/Δt) > 1/3. It is expressed as:

$$VRT = Horner\ VRT - (2.303 \times m \times T_D) \quad (1.10)$$

where m is the Horner plot's slope, and T_D is a dimensionless temperature parameter.

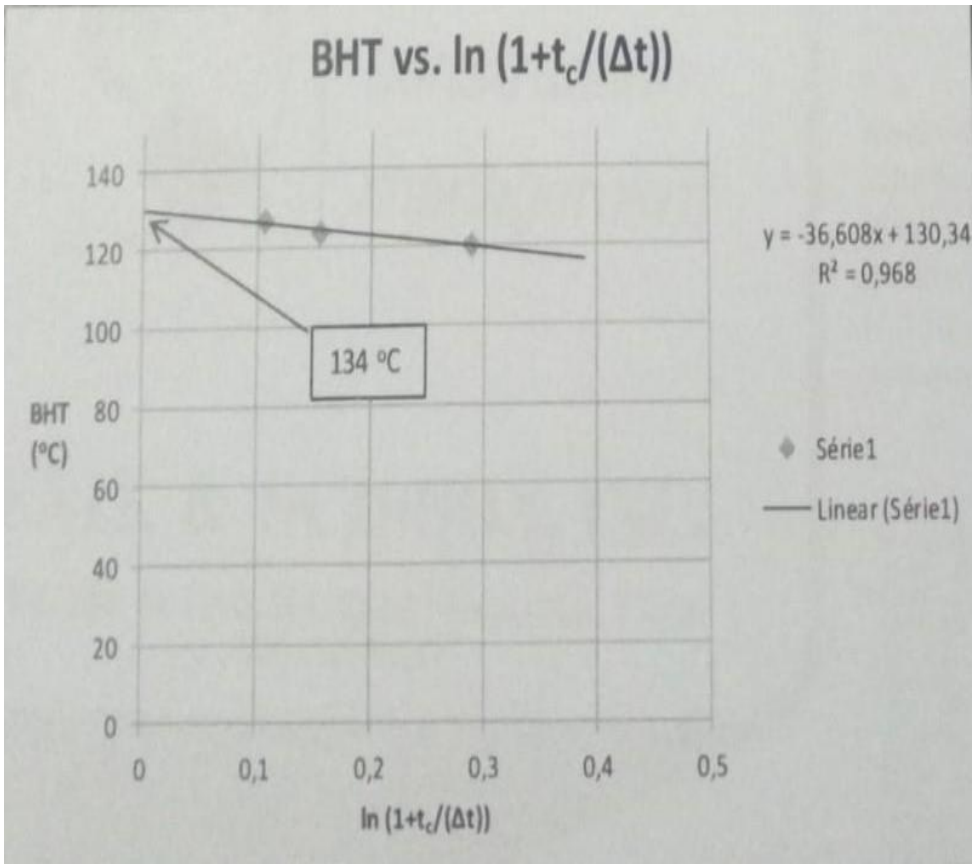

Figure 5: Example of the Horner plot.

(iv) **Zetaware software:** The BHT can be corrected only using a software tool from Zetaware software Inc. Zetaware software is a petroleum system tool developed by Dr. Jeff Corrigan in 2002. His basis stems from an analysis of 983 bottom hole temperature (BHT) and associated equilibrium temperature estimate (Teq) pairs. Based on these investigations, recommended methods for BHT data corrections utilizing information typically available with BHT data (the BHT measurement, time since circulation, and or depth) were established (Figure 6). Depending on the type of information available, three BHT correction methods are recommended below: (a) Horner correction: This is used when three or more BHTs from the same depth are available (see Figure 6). (b) Time since circulation: It is applied

when data available are not suitable for Horner correction but contains only time-since-circulation information. (c) Last resort correction: Mainly for conditions with BHTS that has no time-since-circulation information. This is corrected by adding 18 °C to the BHTs, which is the overall average temperature gradient of depth observed around the world.

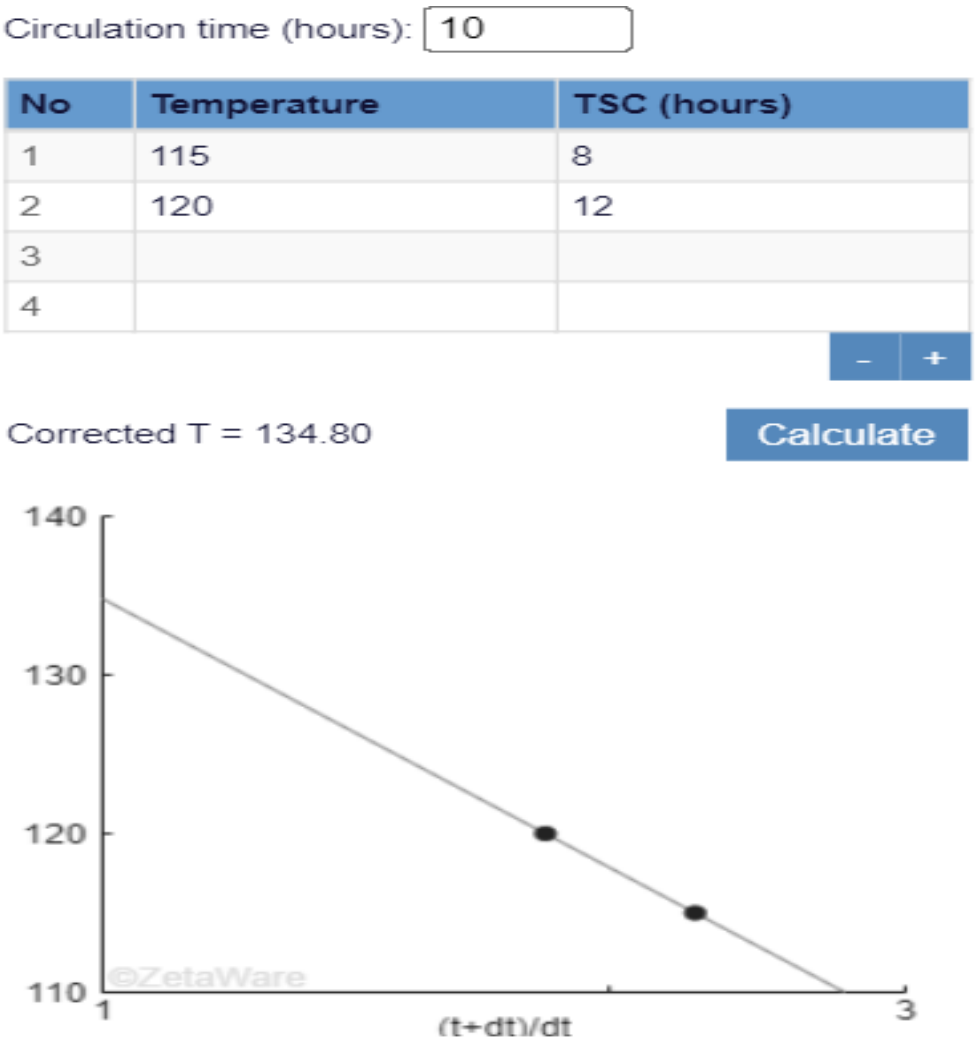

Figure 6: Zetaware software Horner plot correction (Zetaware software, 2003).

(B) FACTORS AFFECTING TEMPERATURE MEASUREMENTS

Some factors influence temperature measurements, such as climate changes, daily and seasonal cycles, etc.

(i) **Climate changes:** Changes in surface temperature result from variation in insolation, long-term climate changes, and glaciation periods. Profile of near-surface temperature records changes in surface temperature as anomalies from equilibrium gradients. These anomalies can be used in the reconstruction of the present climatic history of the region. Offshore surface temperatures are affected by ocean temperatures. The onshore surface temperatures are varied with latitude, altitude, topography, time.

(ii) **Daily and seasonal cycles:** These diurnal and seasonal perturbations affect the temperature in the top layer of Earth. Diurnal changes are the daily temperature rise within the day and night and the sun passage across the sky. Seasonal perturbations are temperature change between the summer and winter periods which is regular and periodic.

1.6.3 THERMAL CONDUCTIVITY

Thermal conductivity is the thermal property that measures the ability of a material to transmit heat. It is an intrinsic physical property essential in heat flow determination as heat flow density is evaluated by the product of the geothermal gradient with thermal conductivity and obeys Fourier's Law of heat conduction. Rocks are poor conductors, and their conductivity varies in a range of less than 1 to 10 $Wm^{-1}K^{-1}$. Thermal conductivity is a crucial factor in thermal modeling as it regulates the temperature within the sedimentary basins.

1.6.3.1 MEASUREMENT TECHNIQUES OF THERMAL CONDUCTIVITY OF THE ROCKS

Unlike the geothermal gradient measurement, measurement techniques are classified based on the specification of regions, but in rock thermal conductivity measurements, the methods are categorized by data availability. Measurement techniques for rock thermal

conductivity are grouped into direct methods and indirect methods. The direct measurement method is conducted in the laboratory on rock samples, i.e., cores or cuttings, or in-situ in boreholes or with marine heat flow probes. Indirect measurement methods are employed when no data are available or no direct measurements can be performed, and such indirect data could be from lithology logs, porosity, and compaction models.

(A) DIRECT MEASUREMENT OF ROCK THERMAL CONDUCTIVITY

Techniques for measuring the rock thermal conductivity of rocks are broadly divided into two classes: steady-state and transient types. Steady-state methods give only the thermal conductivity in the desired direction, while the transient methods give either or both thermal conductivity and thermal diffusivity.

(i) **Steady-state methods:** Steady-state methods compares an unknown thermal conductivity to a known one and are more accurate. Standard steady-state thermal conductivity measurements are conducted only on consolidated rocks with the appropriate rock samples having cylindrical shapes of a diameter similar to the available measuring device, removed along their vertical axes, and polished ends for good thermal contact. The most common apparatus used in steady-state thermal conductivity measurement is the divided-bar apparatus designed to measure the thermal conductivity of discs or cylindrical plugs of material. The apparatus utilizes minimum retaining pressure along with a cylindrical assembly 2-4 cm in diameter. Constant temperature controls are maintained with a thermostatically controlled electrical heating circuit or the use of hollow brass cylinders in the top and bottom sections of the bar. Other comparator apparatus types are stacked disks or divided short bar apparatus with constant temperature

difference across the stack and stacked disks with heat supplied electrically (Beck, 1988).

(ii) **Transient methods:** Transient methods are best suited for poorly consolidated sediment or in situ measurements, especially sea-floor measurements requiring thermal conductivity data usage in temperature conversion for a heat flow estimate. This method is much simpler and rapid than the divided bar method as fewer demands are made on the sample preparation, and the equipment is more standardized than used in the divided bar method. The measurement techniques of the transient method entail that the thermal conductivity of a body is deduced from the rate at which its temperature changes in response to an applied heat source.

Due to local variations in rock composition, large fracture systems, or aggregates composition in parent strata, thermal conductivity measurement on small samples from a single rock differs significantly. In such cases, direct in-situ measurement of bulk conductivity is preferable with line-source probes. The in-situ measurement of thermal conductivity of oceanic sediments is much easier than for boreholes as the sediments have not been disturbed (mainly due to water loss) by the coring and transportation (Stein, 1995; Beardsmore & Cull, 2001).

(B) INDIRECT MEASUREMENT OF ROCK THERMAL CONDUCTIVITY

Thermal conductivity can be estimated from some indirect data such as well-log correlations, saturating fluids, mineralogical composition, and correlations with other physical parameters. Some of these techniques are based on well-defined physical models, while others are purely empirical.

(i) **Lithology logs:** Data sets of lithology columns can be used solely to estimate the thermal conductivity of rocks. It is usually available from commercially drilled wells with the Well completion reports displaying a diagram of the penetrated

formations, lithology, and contact depths. More detailed records of lithology can be realized from mud logs and lithological information of electrical well logs. Sampling for thermal conductivity and porosity analyses are made for all lithologies under investigation. Different regions with similar lithologies can have different thermal conductivities, resulting from minor variations in mineralogy and porosity. In such conditions, the thermal conductivity of the actual formations penetrated should be measured.

(ii) **Rock's mineralogy:** An inter-stratified lithology occurs with various individual conductivities of rock formations. The thermal conductivity of rock is dependent on the different mineral components of the rock. The thermal conductivity of rocks is estimated from their mineral content. Minerals owning to their well-defined composition exhibit a much smaller difference in thermal conductivity than rocks. Mixing-law models are used to estimate the mean conductivities of the rock or formation. The choice of mixing models depends on the lithological distributions, and there are three well-known models, namely,

a) **Harmonic mean:** Useful for wells drilled vertically to sub-horizontal strata and each bed having different thermal conductivity. This model can be used on interbedded units (e.g., sandstone-shale, limestone-shale) when the individual component's proportion is known. The lithology has a layered bed perpendicular to the direction of heat flow (Figure 7). The mean conductivity (λ_B) is given by:

$$\frac{1}{\lambda_B} = \sum_{i=1}^{n} \frac{\phi_i}{\lambda_i} \tag{1.11}$$

where λi is the thermal conductivity of the *i*th bed, ϕi is the thickness of the *i*th bed divided by the total thickness of the sequence ($0 \leq \phi i \leq 1$; $\sum \phi i = 1$). Equation 1.11 can also be written as:

$$\frac{1}{\lambda_B} = \frac{1}{Z} \sum_{i=1}^{n} \frac{Z_i}{\lambda_i} \tag{1.12}$$

where *zi* is the thickness of the *z*th bed and Z is the total thickness of the sequence ($Z=\sum zi$).

b) A**rithmetic mean:** Used for geological formations with faults, igneous intrusion, tight folding, salt pluming, Etc. The strata beds should be parallel to the heat flow direction. The mean thermal conductivity for this model is given as:

$$\lambda_B = \sum_{i-1}^{n} \phi_i \lambda_i \tag{1.13}$$

where all the symbols are the same as earlier stated.

c) **Geometric or Square root mean:** It is the most used model which applies to rock with different minerals and their known conductivities that are randomly distributed in a mixture. The geometric mean is given by:

$$\lambda_B = \prod_{i-1}^{n} \lambda_i^{\phi_i} \tag{1.14}$$

or as a square root mean,

$$\lambda_B = \sum_{i-1}^{n} \phi_i \sqrt{\lambda_i} \tag{1.15}$$

where all the symbols' significances are the same as earlier stated.

Any of these equations can be used to estimate the bulk thermal conductivity of rock from its mineral content and pure mineral thermal conductivities. Pure mineral thermal conductivities can be directly measured or obtained from tables (e.g., Horai & Simmons, 1969; Touloukian et al., 1970). Pore fluid is included as a component of the bulk rock. Figure 7 illustrates the three mixing modes for various lithologies.

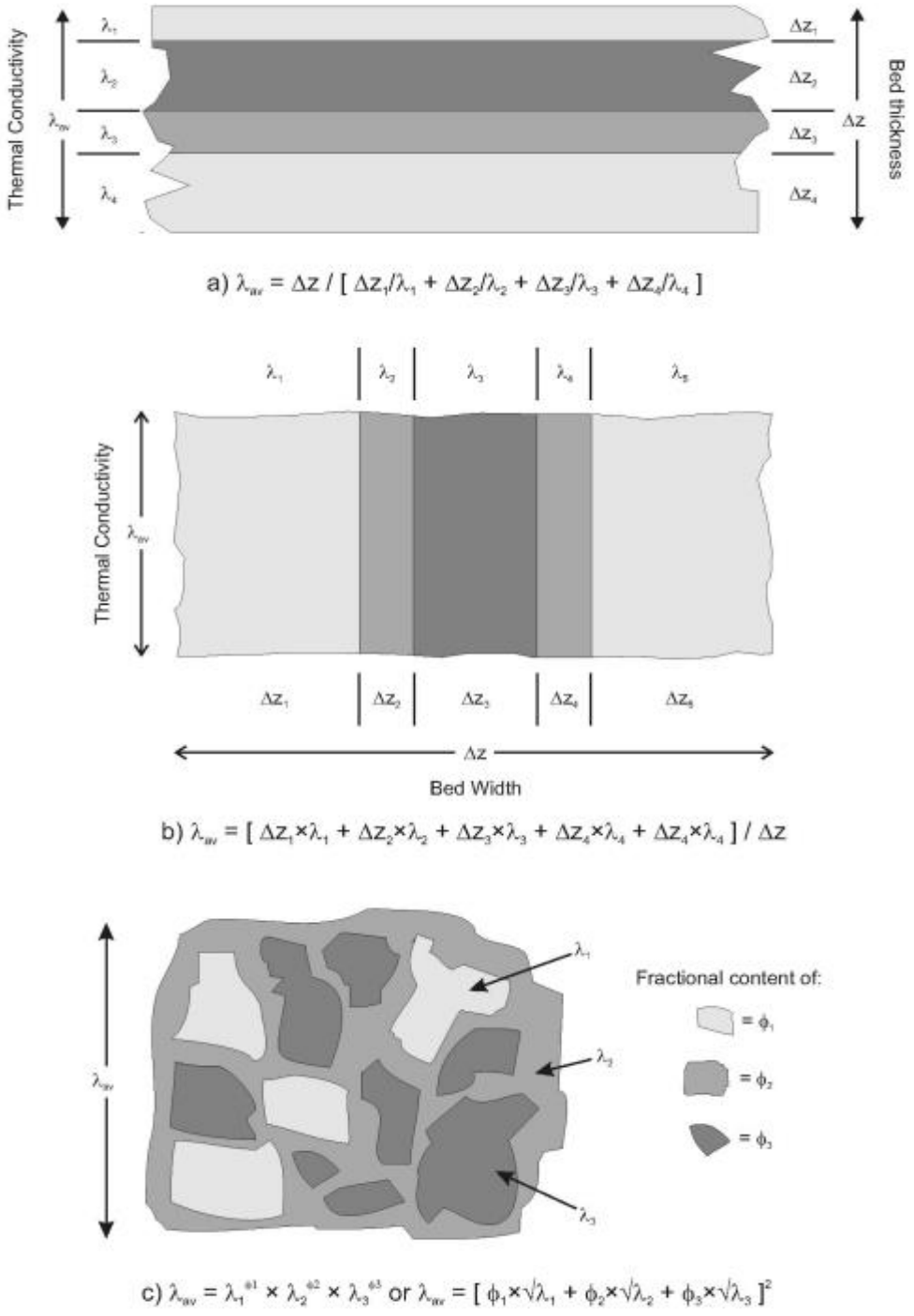

Figure 7: Mixing models for lithologies. (a) Harmonic mean, (b) Arithmetic mean, (c)Geometric/ Square root mean, (From Beardsmore & Cull, 2001).

(iii) **Porosity logs:** Porosity is the primary controlling variable for the thermal conductivity of sedimentary rocks and is very relevant to thermal conductivity

studies. The porosity of core samples is measured before the thermal conductivity testing. Existing porosity data can be extracted from Well completion reports. Porosity data from the same formation and lithology are compiled and collated on a regional scale. The bulk thermal conductivity of a porous rock varies with different saturants, i.e., the thermal conductivity of a rock when it is saturated with other fluids than those used in the laboratory measurement. Laboratory measurement tends to measure first the conductivity of the rock matrix or fluid, which is presumed relatively constant within a formation. Afterward, this matrix conductivity is merged with compaction models to construct in situ conductivity profiles. Therefore, porosity data are utilized in constraining compaction models for different lithologies.

Compaction minimizes the amount of pore fluid in rock and increases the bulk conductivity. When porosity data is unavailable, compaction models are constructed for each lithology to relate their porosity to the burial depth. As porosity is known, it can be merged with matrix conductivity to determine the bulk conductivity of each formation. This matrix conductivity must then be corrected for in situ temperature. Numerous models available for compaction logs are well detailed in Beardsmore and Cull (2001).

Different lithologies compact at different rates. Generally, the thermal conductivity of sedimentary rocks increases with depth through the effect of compaction. Shale constitutes highly anisotropic sheet silicates (Table 6). The vertical thermal conductivity of Shale does not conform to the same trends as other lithologies, i.e., it remains constant or decreases with depth and compaction. However, because of clay platelet rotation, the vertical conductivity of shale may change little or decrease with increasing depth of burial and compaction (Blackwell et. al., 1997).

Table 6: Average thermal conductivity for several sheet Silicates, parallel and perpendicular to the main cleavage plane, and for a mixed aggregate (Diment & Pratt, 1988; Williams & Anderson, 1990).

Minerals	**Average conductivity** ($Wm^{-1}K^{-1}$)		
	Parallel	Perpendicular	Aggregates
Muscovite	3.89	0.52	2.35
Phlogopite	4.01	0.48	
Biotite	3.14	0.52	2.02
Lepidolite		0.48	2.30
Phyrophyllite	6.17	1.15	4.50
Talc	11.5		2.97
Chlorite			2.52
Clinochlore	10.3	1.97	

(iv) **Electric well-log:** Electric well logs are logs about the penetrated well formations and are available for many wells with no rock samples. Even though there is no logging tool for direct measurement, thermal conductivity is estimated by the application of various methods in different logs. The most accurate method can be those that estimate mineral content and porosity, which are then merged to estimate thermal conductivity. Three different approaches exist for which well-logs can be used to deduce estimates for in-situ thermal conductivity:

(i) One technique is establishing empirical relationships between thermal conductivity and well logs parameters, such as porosity and sonic (p-wave) velocity, and bulk density. Theoretically, this approach is unlimited to well logs when there are known petrophysical parameters from laboratory measurement. Blackwell & Steele (1989) presented a good summary of different approaches to illustrate their application to a specific case.

(ii) The second method is on a theoretical basis in which there is an extension of the mixing-model approach to the borehole scale. Various mineral (or fluid) phases have their volume fractions extracted directly from induced gamma-ray spectroscopy logs (Williams & Anderson, 1990) or estimated from a joint analysis of other logs such as gamma-ray (GR), sonic velocity (DT), density (RHOB) and neutron porosity (NPHI), (Demongodin et al., 1991). Subsequently, an appropriate mixing model is applied. A limitation of both methods is that mineralogy-based conductivity models cannot account for the effect of anisotropy observed in many sedimentary and metamorphic rocks.

(iii) The third method applies a phonon conduction model for thermal conductivity, which uses well-logs derived measurements of acoustic velocity, temperature, and bulk density (Williams & Anderson, 1990). Its application is only for unfractured rocks since fracturing effects on compressional and shear velocities generate inaccurate results. The approach has an accuracy of ±15 %, both in isotropic and anisotropic formations, even as shear-wave birefringence indication can pose a limitation in this method application on foliated rocks as well (Pribnow et al., 1993; Clauser & Huenges, 1995).

In quantifying the thermal conductivity of rock formations, significant knowledge of the mixing laws and theoretical models are essential. Rock's thermal conductivity measurements aim at estimating the average thermal conductivity between temperature data points. This is achieved by the construction of an appropriate conductivity profile of the entire section under investigation and subsequent examination of sections between temperature data. The specific steps taken through the investigation are summarised in Figure 8.

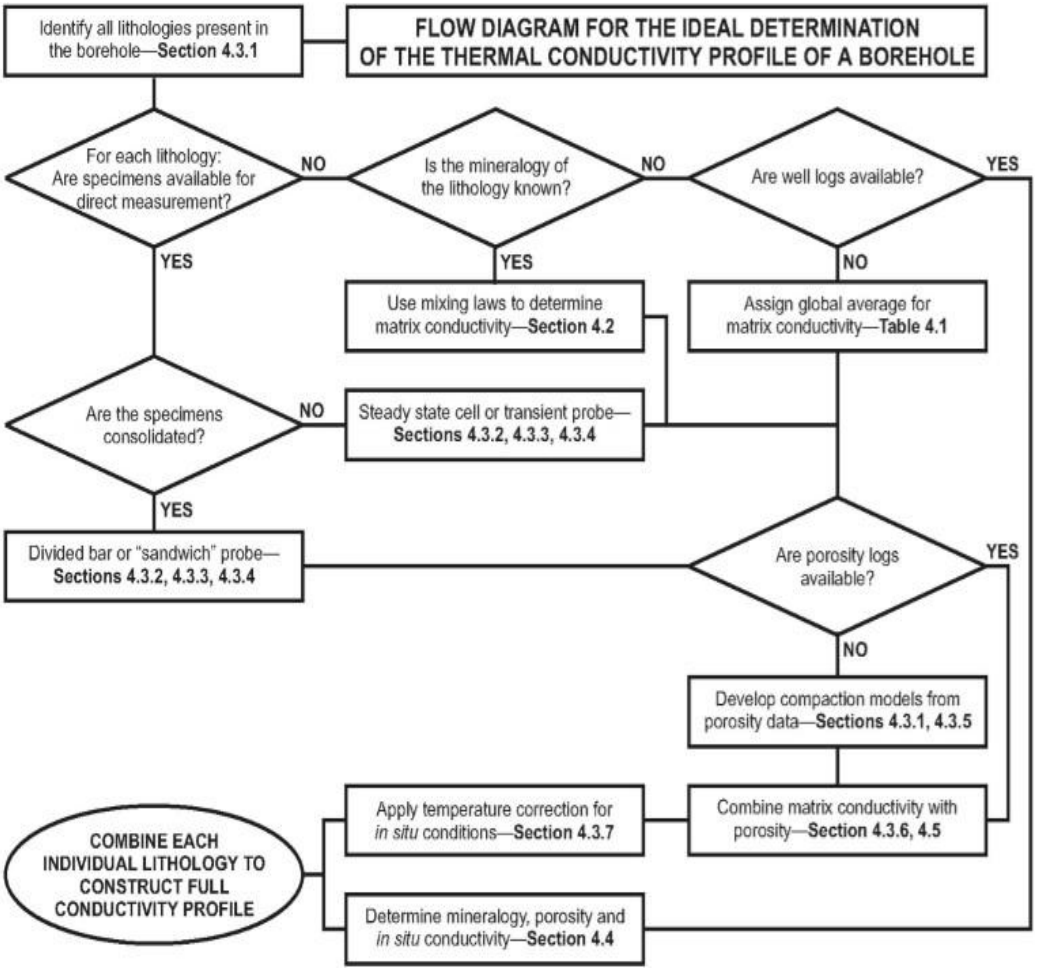

Figure 8: Flow chart for determining a vertical thermal conductivity profile (From Beardsmore & Cull, 2001).

1.6.2.2 IN SITU CONDUCTIVITY AND TEMPERATURE CORRECTION

Practically, it is almost impossible to obtain a lithology sample for thermal conductivity measurement from boreholes due to a lack of cores. This condition warrants the use of alternative techniques such as the use of nearby well logs of the same formations or a choice of matrix conductivity's value equivalent to a similar lithology in the world. Many compilations of thermal conductivity values exist but vary markedly with respect to matrix conductivity or bulk conductivity. The choice of an appropriate value for a specific location is filled with uncertainty, and the error estimates of subsequent heat flow density estimations should account for it.

With the knowledge and integration of various data of matrix conductivity of designated penetrated formations, compaction models for porosity calculation at any given depth, and lithological column, a good thermal conductivity versus depth model can be constructed. The conductivity-depth model depends on the preferred mixing law for each lithology, and the (geometric or square-root) is preferred:

$$\lambda(z) = \lambda_m^{1-\phi(z)} \lambda_f^{\phi(z)} \tag{1.16}$$

or,

$$\lambda(z) = \left[\left(1 - \phi(z)\right) \times \lambda_m^{1/2} + \phi(z) \times \lambda_f^{1/2}\right]^2 \tag{1.17}$$

where $\phi(z)$ is the compaction function, λ_m is the matrix conductivity, and λ_f is the pore fluid conductivity.

In situ temperature corrections are conducted for thermal conductivity measurement from the laboratory or obtained from global compilations as the temperature dependence of any specific formation is difficult to predict. For any arbitrary rock with a temperature range 0-300°C, Sekiguchi (1984) proposed an empirical correction at absolute temperature and is given by:

$$\lambda = \left(T_o T_m / (T_m - T_0)\right)(\lambda_0 - \lambda_m)\left((1/T) - (1/T_m)\right) + \lambda_m \tag{1.18}$$

Where λ ($Wm^{-1}K^{-1}$) is the corrected thermal conductivity, λ_0 is thermal conductivity at laboratory temperature, (T_0), T_0 is the temperature (K) at which λ_0 was taken, λm (1.05 $Wm^{-1}K^{-1}$), and Tm (1473 K) are calibration coefficients.

The temperature range for the temperature corrections for boreholes with depths down to about 6-10 km is ~300-500 K. For impenetrable crustal sections, thermal conductivity is calculated from empirical relationships that automatically integrate a temperature correction which is used to calculate thermal conductivity. For lower crustal

measurements of rocks exposed at the surface, high temperature-high pressure laboratory experiments are used to generate a temperature correction solely.

1.6.3 HEAT FLOW DENSITY

Never has heat flux been directly measured, but rather Fourier's law derives its vertical component. Heat flow density of a region is the rate at heat conveyed across Earth's surface of that region per unit area per unit time. It is known as watts per square meter (Wm-2). Heat flux estimates in an area require the vertical temperature gradient [∂T/∂z] and the rock's thermal conductivity (k) in that area to be measured. The following equation usually expresses conductive heat for steady-state:

$$Q_0 = Q_d + \int A(z)dz = \lambda_d \left[\frac{\partial T}{\partial z}\right]_d + \int A(z)dz \qquad (1.19)$$

Where Q_o is the surface heat flow, Q_d, λ_d and $[\partial T/\partial z]_d$ are the heat flow, thermal conductivity, and thermal gradient, respectively, at depth, d; and $\int A(z)dz$ is the integral of volumetric heat generation from the surface to depth.

1.6.4.1 METHODS OF CALCULATION OF HEAT FLOW DENSITY

There are two methods of combining thermal conductivity and temperature gradient information: the interval or product method and the Bullard method. Heat flux is estimated by the application of one of these methods to data derived from temperature measurements in a drill hole a few hundred meters to kilometers deep or within the upper few meters of sediments of a lake and is purely a local value characterizing a region possessing same order of dimensions as the determination depth.

(i) INTERVAL METHOD: This method involves the determination of a temperature gradient from temperature-depth data over a specific depth interval and is compounded with the representative thermal conductivity for that same interval. Depth intervals are chosen to equate to major lithologic units intersected

by the borehole. If either a single lithologic unit is intersected or the lithologic units are thin and diverse, then the entire borehole can be regarded as a single interval. The temperature gradient can be estimated from a linear least-squares regression of temperature on depth (i.e., all error is assumed to be in temperature) over a specific depth interval; alternatively, it can be calculated as the average of gradients determined between consecutive temperature-depth points throughout the interval or from a gradient logging device. A mean heat flux for the area can then be derived from the values for each lithologic section. Thermal conductivity values are measured and computed based on the chosen mixing law. The average heat flow over a section is the product of the average thermal gradient and the average thermal conductivity over the same interval. The average thermal gradient is calculated using only the top temperature and bottom temperature at that section, while the average thermal conductivity is generally the harmonic mean of the conductivities of all beds layered horizontally within the same depth section. The harmonic mean is preferred over the arithmetic mean because the change of temperature across the interval is directly proportional to thermal resistance rather than thermal conductivity (Beardsmore & Cull, 2001; Powell et. al, 1988).

(ii) BULLARD PLOTS: Based on the concept of thermal resistance. This is a more coherent method of estimation of heat flow. The thermal resistance of a material is a measure of how effectively it retards the flow of heat. Thermal resistivity (R) is the integral of the reciprocal of thermal conductivity (λ) over the depth range (z). It is expressed as

$$R = \int \left(\frac{1}{\lambda}\right) dz \tag{1.20}$$

A graphical representation of temperature against thermal resistance is known as a Bullard plot after Sir Edward Bullard (Bullard, 1939). Errors in thermal

conductivity and temperature data cause Bullard plot points to be scattered instead of lying in a straight line for constant heat flow density. Therefore, linear regression is utilized to find the best estimate of heat flow, and final estimate uncertainty is assessed statistically from the degree of scattering in the points (e.g., Kreyszig, 1983, pg. 986). It is noteworthy that it is fundamentally wrong to adopt a constant thermal gradient across a section comprising of thermal conductivity contrasts in all real situations.

The thermal resistance is best calculated with the format of the thermal conductivity data set. For individual formations conductivity data, each of thickness, Δz, and conductivity, λi, Equation (1.11) is rewritten as:

$$R = \sum_{i=1}^{n} \frac{\Delta z_i}{\lambda_i} \tag{1.21}$$

Thus, for thermal conductivity from boreholes logs is generally constant (usually 0.1524 m), and so:

$$R = \Delta z \sum_{i=1}^{n} \left(\frac{1}{\lambda_i}\right) \tag{1.22}$$

1.6.4.2 FACTORS AFFECTING HEAT FLOW METHODS

A linear Bullard plot is produced by purely conductive, steady-state vertical heat flow without heat production internally. Divergence from these conditions creates a non-linear Bullard plot.

(i) Error in thermal conditions measurements: Systematic errors in estimating thermal conductivity led to systematic error in calculated heat flow. When sediment compaction is underestimated, then porosity is modeled higher than its true value. Therefore, thermal conductivity modeled will be lower than true conductivity, and the errors will escalate with depth. The production of high heat results in a reduction in heat flow density with depth - a result, which is similar to

poor compaction modeling, especially in hard rocks. Abrupt and sustained vertical heat flow density changes at specific depths indicate heat introduction or removal from the system. Such effects in a sedimentary setting are commonly caused by fluid migration, heat refraction, or diagenetic/metamorphic processes (effect negligible).

(ii) C**limatology:** Periodic climate changes affect the Earth's surface temperature resulting in a disturbance in the thermal gradient. Long-period climatic changes usually affect the heat flow density profile to greater depths and times. Onshore heat flow data obtained closer to the surface are likely disturbed by diurnal and seasonal heating cycles.

(iii) Sedimentation: Sediments achieve water temperatures during the settling process as heat moves along their grains. The previously deposited material is buried downwards at a rate equal to the sedimentation rate irrespective of compaction effects. The magnitude and depth of the sedimentation effect depend on the rate and duration of sedimentation. Also, turbidity flows and landslides can lead to sudden thick deposits of sediment at water temperature.

(iv) Erosion: Erosion results in the movement of rocks upward in relation to a reference point on the surface. As the erosion of the ground surface occurs, surface heat flow increases. The amount of heat flow is dependent upon the elapsed time and rate of erosion. The thermal effect of erosion on the Earth's surface is opposite to that of sedimentation.

(v) Gro**undwater migration:** In the presence of hydrothermal processes, moving fluids transport heat through advection via a permeable body. This process provides a mechanism for mixing and diffusion, leading to a decrease in thermal

gradient and an increase in thermal conductivity within a rock, affecting the net vertical heat flow.

(vi) **Deep flow of hot fluids:** As hot fluids flow along an aquifer, the thermal history of the formation within a sedimentary formation change. Excess temperatures maintained within a thin aquifer for a thousand years or more can significantly raise temperatures for several hundred meters above the aquifer (Bruce et al., 1996). As heat increases, the maturity of sediments occurs for petroleum reserves.

1.6.4.3 FACTORS AFFECTING NON-VERTICAL HEAT FLOW

Heat flows are disturbed by non-horizontal surface boundaries, surface boundaries with laterally varying temperatures, non-horizontal contacts between formations and formations with laterally varying thermal conductivity. Therefore, heat flow on Earth is not always vertical. Some factors are responsible for these deviations and are:

(i) **Basement relief:** Heat flows through regions of higher thermal conductivity when escaping the interior of the Earth. Heat refraction comes from thick sediment cover regions from a blanket of low conductivity sediment and is mostly distributed through thinly covered areas in an area of undulating and high-conductivity basement rocks.

(ii) **Surface topography:** In mountainous terrain, heat flow needs to advance to reach the surface beneath a peak compared with heat flow in a valley. This implies that heat will mostly flow into the valleys in as much as it is homogeneous, resulting in variation in elevation of surface heat flow.

(iii) **Salt domes:** Diapiric salt columns are important features of sedimentary basins, with their thermal properties and geometry being differential compared to all other lithologies commonly present in a basin. They act to increase surface heat flow in three ways. Firstly, the salt comprises of higher thermal conductivity than most

other lithologies. Secondly, salt bodies resemble vertical dykes more than horizontal layers. Thirdly, salt heat transport is via advection if its ascent rate is significant due to its low density.

CHAPTER TWO: HEAT FLOW DENSITY ESTIMATION IN THE MESO CENOZOIC BASINS OF PORTUGAL

2.1 INTRODUCTION

The interpretation of the thermal history of a sedimentary basin demands the study of its tectonic evolution and the circumstances surrounding its development. Diffusion of excess heat within a basin formation and the consistent heat supply migrating from its basement is dependent on its fluid content and strata's thermal properties. The temperature history of sedimentary basins serves as a fundamental tool for assessing hydrocarbon exploration, geothermal energy potential, paleogeographic reconstruction, carbon sequestration, and hydrogeology of a region. In the best scenario, heat flow density (HFD) is determined by the evaluation of (i) borehole interval temperature gradients derived by continuous or discontinuous temperature logging under equilibrium conditions and (ii) estimations of rock thermal conductivity from the various formations through which the temperature measurement was conducted. Based on those data, steady-state conductive heat flow is usually estimated (Beck, 1965; Prensky, 1992; Jessop & Majorowicz, 1994; Förster & Merriam, 1995).

A comprehensive surface HFD estimates in the Portuguese Meso Cenozoic basins are difficult to obtain. The majority of HFD data originates from south Portugal, where explosive mining activity has favored the existence of deep mining wells. Although, in the northern areas of the Hercynian Massif, only a few HFD estimates are obtained (Correia & Ramalho, 2009**).** Two major problems limiting a significant increase in HFD estimates in the Portuguese Meso Cenozoic basin are the drilling cost for HFD work and regional regulatory requirements. These regulatory requirements require the closure of non-producing drilled holes of oil and gas and economic mineral resources and the sealing-off of abandoned sites.

Consequently, other geothermal data must be taken into contemplation. The use of the temperature data obtained from other physical parameter logs or data derived from special logging procedures is utilized as alternative sources for HFD data. The abundance and availability of bottom-hole temperature (BHT) data make it the most used but shadows a limitation on data accuracy when applied. Bottom-hole temperatures are generally recorded after drilling ceases in a well under unequilibrated conditions. There is no central database for access to BHT values, drill mud circulation, drilling regime information, or essential parameters for their various theoretical correction approaches. A similar limitation applies to their corresponding or assumed rock thermal conductivities (Beck & Ballin, 1988; Forster & Miriam, 1995).

In the present work, the major objectives are: (i) the collection of BHT values from accessible well-sites, and their corresponding rock thermal conductivities, (ii) the adoption of the best correction approaches for thermal properties (iii) estimation of HFD. A contribution to the existing geothermal database of the Portuguese Meso Cenozoic basins is the primary goal.

2.2 GEOLOGICAL SETTING OF THE PORTUGUESE MESO CENOZOIC BASINS

The Iberian or Hesperian Massif composed the most solid fragment of Hercynian base in Europe and complemented by synorogenic magmatism and regional metamorphism. The mountainous edge of the Hesperian Massif consists of sedimentary basins formed by the contrastive intensity of alpine deformations during the Meso Cenozoic era. Greater alpine deformations occurring on edges of North and South East Hesperian Massif gave rise to the Cantabrian and Iberian Cordillera, while the southern edge witnessed a deformation by flexure in the base in the Sierra Morena. Evidence of minute alpine deformation on the

West and South West edge of the Hesperian Massif created a distinction in the Southern border (Algarve) and Western or Lusiitanian border, which comprised the Portuguese Meso Cenozoic basins. (Figure 9) (Ribeiro et al., 1979; Ramos-Pereira et al., 2005).

In Portugal, the southern and western Meso Cenozoic boundaries materialized after the Palaeozoic era and are mostly consisted of limestones and sandstones, which indicates sea-level fluctuations in the course of the transgressions of the Mesozoic and Cenozoic era over the Hesperia continent (Figure 10). Salt domes existing in the Western Meso Cenozoic boundary greatly controls the existence of various hot springs, which identifies mineralization and higher water flow rates compared to Hercynian massif.

- LUSITANIAN BASIN

This sedimentary basin emerged on the Margem Ocidental Ibérica (MOI) during part of the Mesozoic, situated on both the continental shelf and the mainland of the west-central coast of Portugal. The basin is practically about 340 km long and 130 km width, and its onshore area over 23,000 km2. The basin links southward with the Alentejo and Algarve Basins and northward, via a basement ridge, to the Oporto (or Galicia) Basin. On the eastern side of the Lusitanian Basin is the Central Plateau of the Iberian Peninsula, and a marginal horst system is located to the west. It is characterized as a distensive basin, belonging to a family of periatlantic basins such as the Jeanne d'Arc Basin (Figure 10) (Enachescu, 1987; Cunha & Pena dos Reis, 1995; Ramos Pereira et al., 2005; Kullberg et al., 2006). The Jeanne d'Arc Basin is a remarkable sedimentary basin formed as a consequence of the large-scale plate tectonic forces that split the super-continent Pangea and resulting in North Atlantic Ocean sea-floor spreading (Sinclair, 2021).

The tectonic evolution of the Lusitanian Basin was constrained due to failures that developed during the episode of late-Variscan fracture around 300-280 Ma (Ribeiro et al., 1979; Ribeiro, 2002). This basin results from the opening of the North Atlantic Ocean due to Mesozoic extension. A good summary of the four phases of rifting identified in the entire formation of the basin from the Late Triassic to the Cretaceous are well detailed in Kullberg et al., (2006), and Reis et al., (2010).

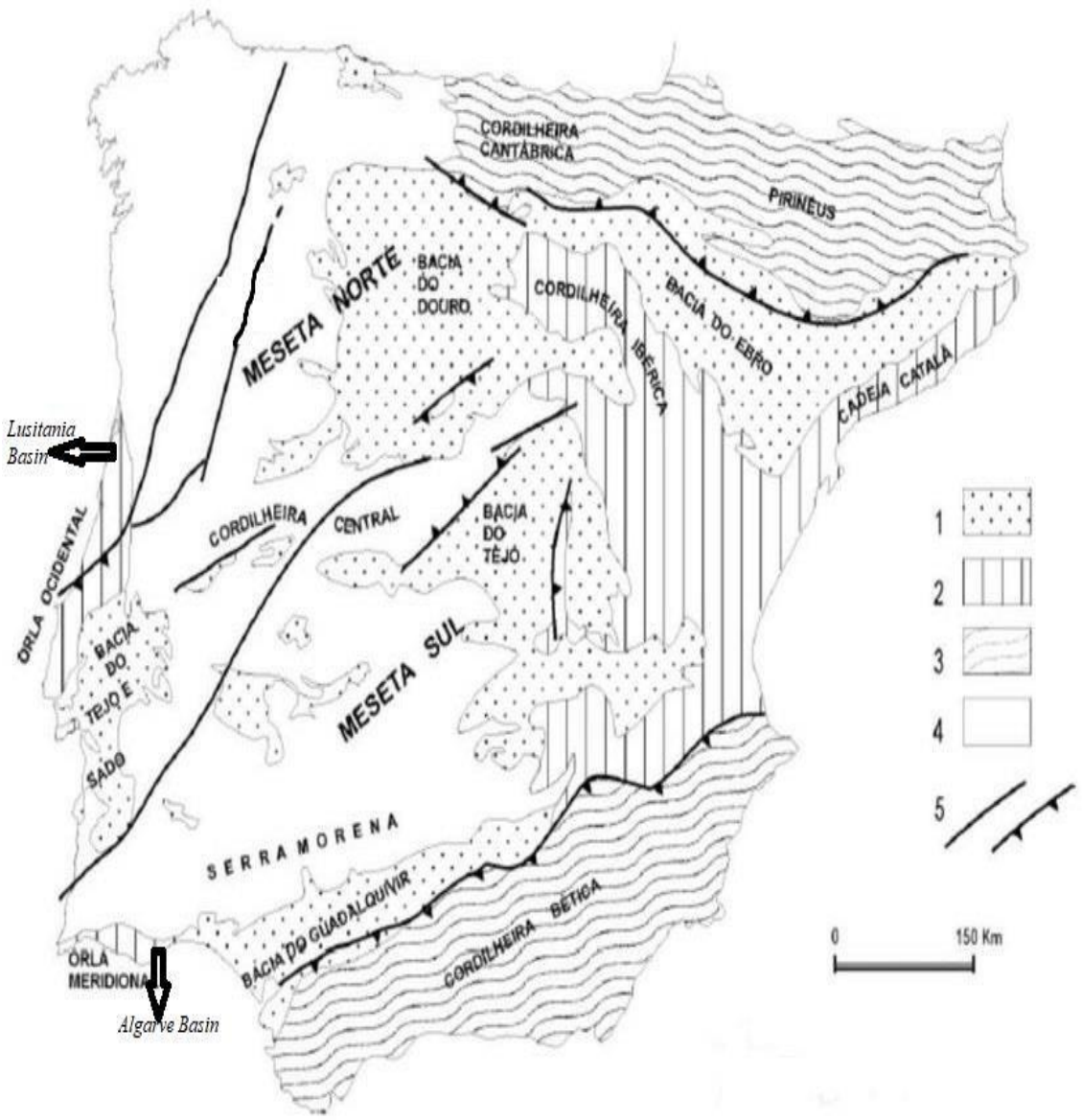

Figure 9: (a) Morpho structural units of the Iberian Peninsula, highlighting study basins 1 -Cenozoic basins, 2 -Meso Cenozoic basins, 3 -Alpine chains, 4 -Iberian massif (North and South of the central system), 5 -Main alpine faults and thrusts (Adapted from Ribeiro et al., 1979).

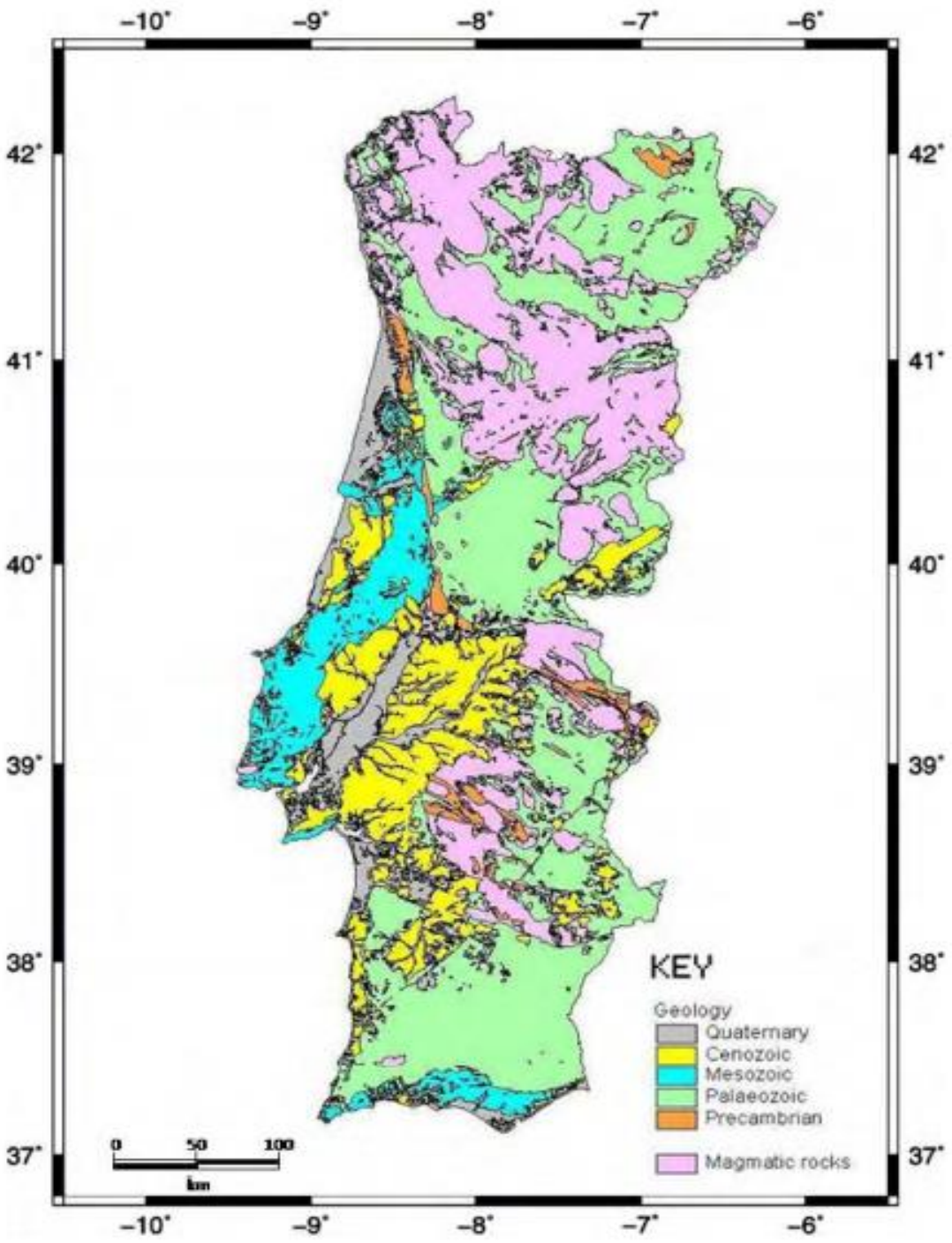

Figure 10: Geological map of Portugal showing study zone (Adapted from Correia and Ramalho, 2005).

2.3 LITERATURE REVIEW

The 2002 Edition of Atlas of Geothermal Resources stated heat flow density (HFD) values in central Portuguese Iberian Pyrite Belt province (IPB) is relatively higher than in the rest of the IPB area. This information results from an extensive study of thermal properties in the IPB using primarily mining data. Mainland Portugal has HFD values ranging from 40 to 115 mWm^{-2}, with an average value of about 75 mWm^{-2}. While in the South Portuguese Zone (SPZ), regional HFD values varying from 40 to 90 mWm^{-2} (Hurter & Haenel, 2002; Correia & Ramalho, 2005).

Correia et al. (1982) published a work presenting heat flow values for South Portugal based on the region's mining data. The heat flow density values were estimated by temperature measurement at several depths in mining wells with assumed thermal equilibrium regime and multiplying the geothermal gradients obtained by the corresponding rock thermal conductivity values generated from their core samples. A geothermal anomaly named the Alentejo Geothermal Anomaly (AGA), with HFD values as high as 160 mWm^{-2} were obtained, confirming its geological structure "zinciferous and magnetic strip of the South Alentejo." It became one of the first attempts to compile geothermal data in South Portugal, giving rise to the first heat flow density map for mainland Portugal (Figure 11).

Duque (1991) and Duque & Mendes-Victor (1993) suggested a higher value of 200 mWm^{-2} for heat flow density values for the central region of the Alentejo Geothermal Anomaly after considerable additional HFD determination and correctional measures were employed to the geothermal data. The heat flow density values were evaluated from data gathered from oil prospecting boreholes (bottom hole temperatures and lithology logs). They found and confirmed the existence of a geothermal anomaly as earlier reported.

Subsequently, new geothermal data were obtained in southern Portugal and showed lower heat flow density estimates than those previously reported, with values that range between 60 - 90 mWm^{-2} (Almeida, 1991, 1992, 1993). Geothermal anomalies are a good exploration tool for petroleum. The anticline area may correspond with positive geothermal anomalies indicated by BHTs. As petroleum is a low heat conductor compared to other formation fluids, it forms an identifiable anomaly (Ball, 1982; Meyer & McGee, 1985; McGee et al., 1989).

Nevertheless, a study revisits on the geothermal anomaly claim was conducted involving an additional new temperature dataset and revalidation of previously published data, taking into account their hydrodynamic equilibrium and thermal status. A new heat flow density value ranging from 50 – 90 mWm^{-2} was obtained against the previous estimate of >200 mWm^{-2}. It was a normal HFD estimate value for geothermal areas in other Hercynian regions in Europe. Therefore, the claim for a geothermal anomaly in southern Portugal was debunked (Correia & Ramalho, 1998).

Correia and Ramalho (1999) and Correia and Safanda (2002) attempted to construct a 1-D and 2-D geothermal models for the two main geotectonic units of Southern Portugal, i.e., the Ossa–Morena Zone (OMZ) and the South Portuguese Zone (SPZ), respectively, using heat flow density data and radiogenic heat production values generated from the region (Figure 12).

Correia and Ramalho (1999) 1-D model proposes that SPZ crustal temperatures are higher than those in OMZ, with their difference-ranging values of about 300°C at Moho depths. Contrarily, Correia and Safanda (2002) 2-D model presented calculated Moho temperatures below 700°C in the model configurations considered and are in accordance with the other geological and geophysical data and the results of a magnetotelluric survey

in specific (see Figure 12) (Correia & Jones, 1997; Jones & Correia, 1999). Ossa-Morena Zone temperatures range from 400 to 500°C, while in the South Portuguese Zone, the ranges are from 500 to 670°C. Comparing both Moho temperatures from different model configurations suggests uncertainty in the order of 50 – 100°C in the calculations. National geothermal maps were created based on this geothermal information, which is frequently updated and detailed as more geothermal data are gathered (Figure 14).

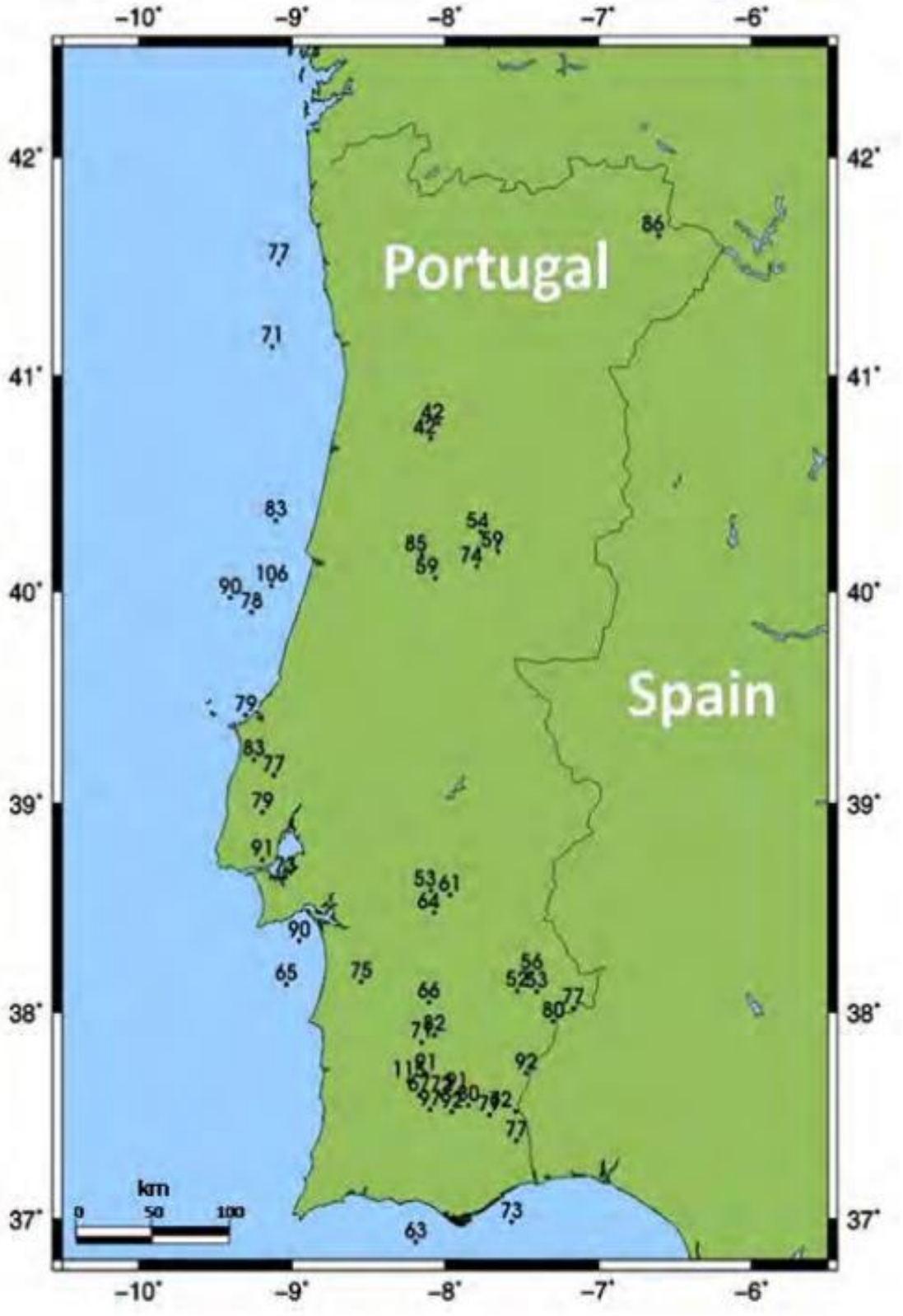

Figure 11: Heat flow density map for mainland Portugal (mWm^{-2}) (Correia & Ramalho, 2005).

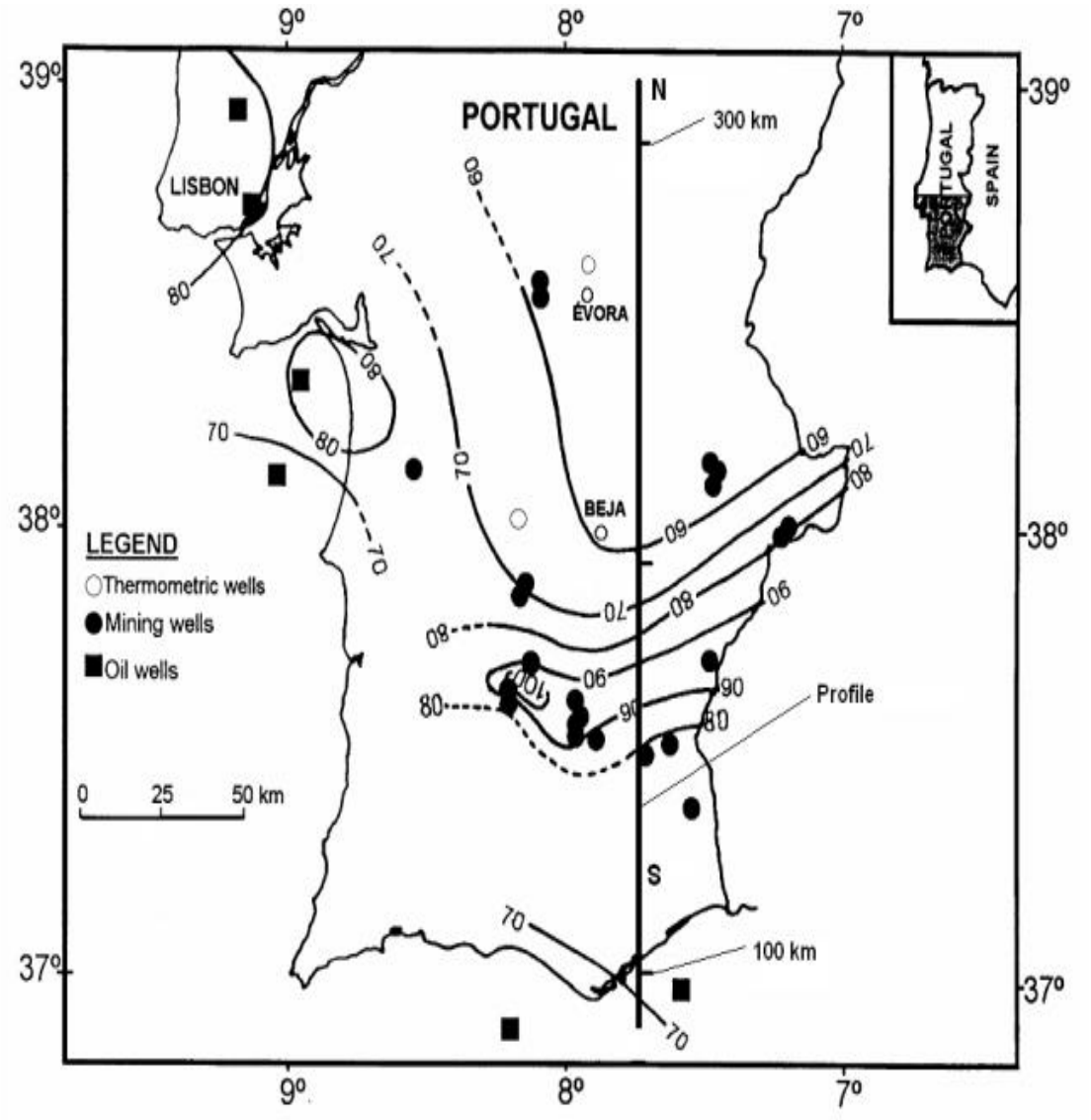

Figure 12: Profile along which the two-dimensional thermal model was constructed (Correia & Safanda, 2002).

Ramalho and Correia (2006) reprocessed and analyzed geothermal data collected by Almeida (1991) from mining prospects and water. More data was obtained from thermal parameter values based on U, Th, and K concentrations by several research institutions. They are frequently updated, stored in the National Laboratory of Energy and Geology (LNEG), making them readily available to the public utilizing interactive internet tools (http://geoportal.lneg.pt), Geothermal Atlas of Mainland Portugal.

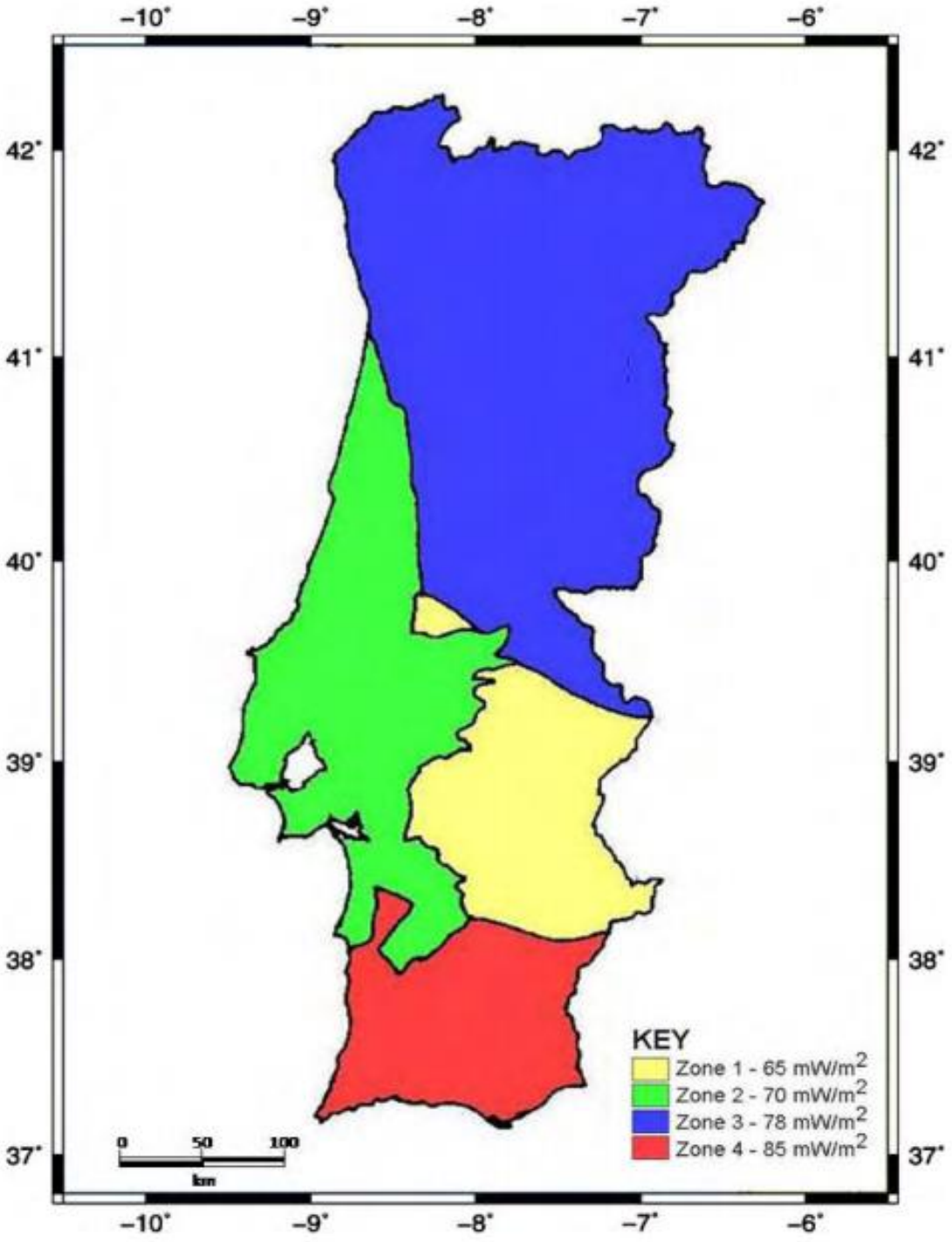

Figure 13: Heat flow density zones for mainland Portugal based on HFD values shown in Figure 11 and geological and structural features (Correia & Ramalho, 2005). Delineated four HFD zones with values having various degrees of accuracy was illustrated. The northern zone presents a less accurate value as a result of insufficient information.

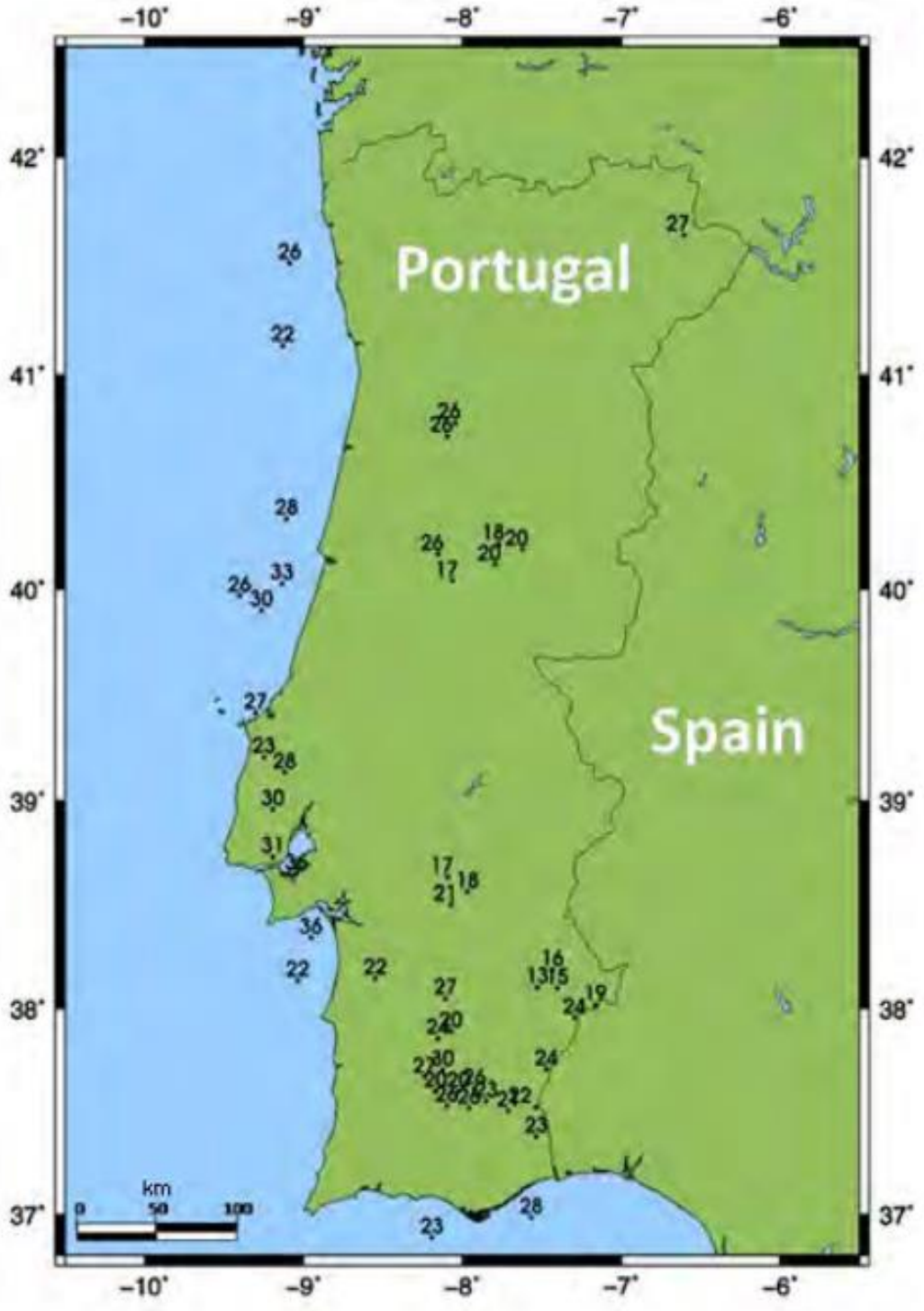

Figure 14: Geothermal gradient map for mainland Portugal (°Ckm^{-1}) (Correia & Ramalho, 2005).

2.4 CALCULATION OF THERMAL PROPERTIES

(i) **Geothermal gradient:** The most available temperature dataset is the bottom hole temperature (BHT), which is usually lower than true formation temperatures. BHT values are corrected to obtain the true formation temperature, and the simplest correction method is Horner's plot method. Also, the BHTs are accompanied by unknown certainties from well data with incomplete mud circulation times, which affects Horner's plot method. Consequently, a histogram is used to generate a mean circulation time value with the known mud circulation times. However, an assumed mean circulation time value is made for wells with unknown circulation times.

(ii) **Thermal conductivity of the rock:** The thermal conductivity of rock decreases with an increase in temperature and porosity but increases with pressure. There was no thermal conductivity information available for the wells. The well's lithology logs were used to obtain each individual well composition in terms of nine sedimentary rock types: limestone, claystone, sandstone, siltstone, sand, clay, dolomite halite, and shale. The footage not logged was provided too. The effective thermal conductivity was estimated using Eq. (1.12) and reference Tables of the compilation of thermal conductivities of various rock types.

(iii) **Heat flow density:** Heat flow is calculated by applying the interval method, which is the product of the average geothermal gradient and the effective thermal conductivity. The average geothermal gradient is estimated by computing the temperature gradient of a specific depth after correction of its bottom hole temperature. The selection of depth intervals determined each well's corresponding effective thermal conductivity, and it equates a major lithological unit throughout the whole depth of the well from the available lithological log. Their corresponding thermal conductivities of the rock types were obtained from reference Tables. The appropriate mixing law (harmonic mean) was

selected and applied based on how the strata bed were layered. Moreover, the effective thermal conductivity was computed for the well. However, a heat flow density map is obtained after calculating the overall mean heat flow density of the individual wells of the region.

CHAPTER THREE: NEW HEAT FLOW DENSITY ESTIMATION IN THE MESO CENOZOIC BASINS OF PORTUGAL

3.1 INTRODUCTION

In this chapter, new determinations of heat flow density (HFD) are generated from data (log runs, lithologic logs) obtained from the "Gabinete de Prospeção e Exploração de Petróleos (GPEP)". GPEP is responsible for promoting and regulating the activities of prospecting, research, development, and exploitation of national petroleum resources in Portugal. The bathymetric data of Portugal from the Research and Development project "Interaction between the Coastal Outcrop and the Current of Portugal – CORPAC (1986 - 1992)", and the temperature profile of the Portugal Coastline were utilized in this study.

This work consists of extraction of the drill mud circulation times and drilling regime information from temperature logs and log runs, identifying and characterizing lithology beds from lithologic logs in various well locations in the Meso Cenozoic basins of Portugal, with the sole aim of determining the temperature gradients, thermal conductivity profile and heat flow density of the region.

The study zone is located between latitudes 41°30'51.4"N and 36°13'58.0"N, and between longitudes 9°05'18.6"W and 11°05'51.0"W as shown in Figure 15. The locations of the wells, names, geographic coordinates, and depths are listed in Table 7. The results obtained from the estimation of the thermal parameters of interest are presented in this chapter, and temperature diagrams obtained in the various well boreholes are shown in Appendix.

Figure 15: Well locations.

Table 7: Well names, coordinates, and depths.

Well names	Geocoordinates	Maximum depths (m)
Pe-1	38°08'07.1"N, 9°02'08.6"W	3117
Go-1	38°30’35.2"N, 8°57’12.4"W	1790
Sm-1	38°42'45.0"N, 9°8'35.16"W	3392
Sa-1	38°55'34.0"N, 8°52'15.0"W	1811
20B-1	39°04'48.4"N, 9°36'02.4"W	2532
Alj-2	39°33'49.2"N, 8°54'42.0"W	3616
Alj-1	39°37'54.3"N, 8°58'51.4"W	2686
14C-1	39°58'07.5"N, 9°24'03.0"W	2142
13E-1	40°06'58.0"N, 9°12'20.6"W	2040
Ca-1	40°30'53.0"N, 9°02'30.0"W	2480
Lu-1	41°18'45.5"N, 8°46'4.4"W	4040
Cv-1	41°30'51.4"N, 9°05'18.6"W	2749

3.2 DETERMINATIONATION OF NEW DATA FOR HEAT FLOW DENSITY ESTIMATION

3.2.1 CALCULATION OF TEMPERATURE AND GEOTHERMAL GRADIENT

The temperature dataset presented consists of BHT values from 12 oil prospecting wells in the Meso Cenozoic basins of Portugal, which some are from abandoned or non-producing drilled holes. This is beneficial for the contribution to the study of the thermal regime of the Portuguese territory. BHTs were corrected with Zetaware software by choosing the appropriate option of the software for each specific depth BHTs. Horner-plot corrections require the temperature measurement, fluid circulation time, and time elapsed between fluid circulation times. A histogram was constructed using known fluid circulation times to determine the mean circulation time value (Figure 16). Mean circulation time was utilized for wells with incomplete circulation times for Horner-plot

correction. Table 8 identifies wells with their known fluid circulation times, and Figure 16 is the histogram chart. The expression of the geothermal gradient is given as:

$$\frac{\partial T}{\partial z} \approx \frac{T_1 - T_0}{\Delta z} \tag{2.1}$$

where T_1 (°C) = surface temperature, Δz (m) = total depth, T_0 (°C) = maximum recorded temperature.

Table 8: Wells and their known circulation times.

Well names	**Known circulation times** (hrs)
13E-1	7.0, 5.0, 6.0, 8.0, 8.5, 11.0
14C-1	13.0, 8.0, 8.0, 11.0, 6.0, 6.0
20B-1	8.0, 1.5, 9.0, 19.5, 10.0
Alj-1	
Ca-1	6.0, 5.5, 5.3, 16.5, 7.0, 7.0, 16.7
Cv-1	10.0
Go-1	6.0, 8.0
Lu-1	6.0, 7.5, 7.5
Pe-1	7.0, 10.0, 10.0, 15.0, 17.0
Sa-1	
Sm-1	
Alj-2	

3.2.1.1 HISTOGRAM

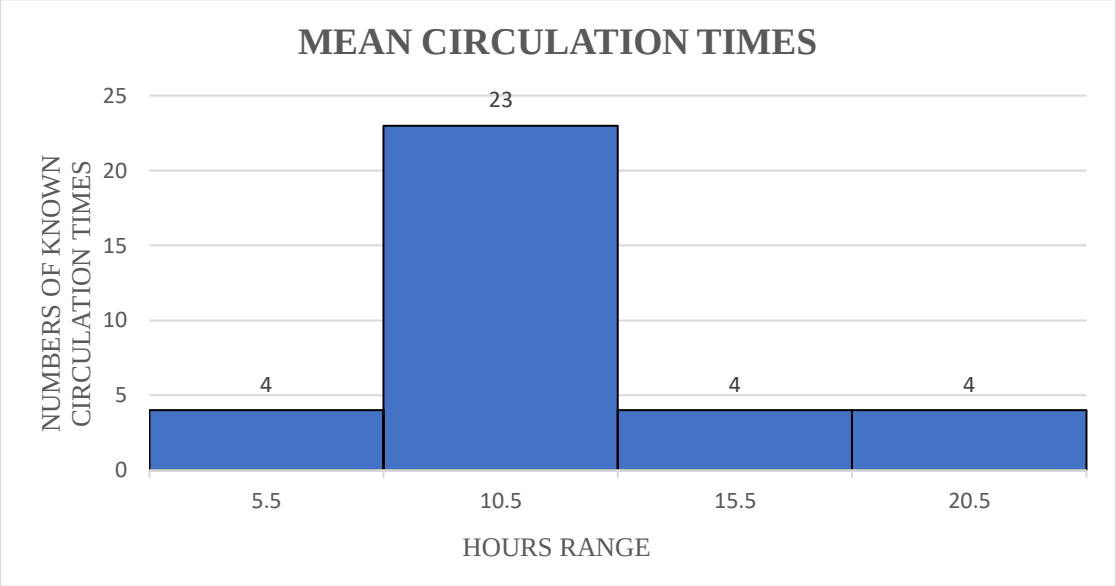

Figure 16: Histogram of known circulation times.

Circulation times = Sum of known circulation times divided by the number of circulation times

= 313.5 / 35 ≈ 9hrs

3.2.1.2 BOTTOM HOLE TEMPERATURES CORRECTION

Table 9 presents a summary of calculations for the corrected and uncorrected BHTs of the wells.

Table 9: Summary estimates of BHTs of wells.

13E-1				
Uncorrected BHT (°C)	Depths (m)	Mud circulation t_c (hrs)	Time since circulation Δt (hrs)	Corrected BHT (°C)
33.0	509	7.0	*	33.0
33.0	509	*	5.0	
42.0	1109	6.0	*	61.7
52.0	1386	*	8.0	123.5
55.0	1386	*	8.5	
64.0	2044	*	11.0	82.4

14C-1				
Uncorrected BHT (°C)	Depths (m)	Mud circulation t_c (hrs)	Time since circulation Δt (hrs)	Corrected BHT (°C)
24.0	465	13.0	8.0	44.4
34.0	908	*	8.0	38.8
35.0	908	*	11.0	
42.0	1472	*	6.0	63.8
55.0	2142	*	6.0	76.8

20B-1				
Uncorrected BHT (°C)	Depths (m)	Mud circulation t_c (hrs)	Time since circulation Δt (hrs)	Corrected BHT (°C)
29.0	418	8.0	1.5	54.4
30.0	1020	*	9.0	58.7
66.0	2532	19.5	10.0	85.0

Alj-1				
Uncorrected BHT (°C)	Depths (m)	Mud circulation t_c (hrs)	Time since circulation Δt (hrs)	Corrected BHT (°C)
80	2565	*	*	98
80	2686	*	*	98

Ca-1				
Uncorrected BHT (°C)	Depths (m)	Mud circulation t_c (hrs)	Time since circulation Δt (hrs)	Corrected BHT (°C)
37.2	927	*	6.0	18.2
38.3	927	*	5.5	
55.6	1576	*	5.3	55.6
55.6	1576	*	16.5	
66.7	2480	*	7.0	66.7
68.9	2480	*	7.0	
70.0	2480	*	16.7	

Cv-1				
Uncorrected BHT (°C)	Depths (m)	Mud circulation t_c (hrs)	Time since circulation Δt (hrs)	Corrected BHT (°C)
71.7	2749	*	10.0	89.7

Go-1				
Uncorrected BHT (°C)	Depths (m)	Mud circulation t_c (hrs)	Time since circulation Δt (hrs)	Corrected BHT (°C)
57.2	1274	*	6.0	79.0
58.9	1790	*	8.0	79.3

Lu-1				
Uncorrected BHT (°C)	Depths (m)	Mud circulation t_c (hrs)	Time since circulation Δt (hrs)	Corrected BHT (°C)
34.4	1728	6.0		
34.4	1728	7.5		
66.6	3080	7.5		84.6

Pe-1				
Uncorrected BHT (°C)	Depths (m)	Mud circulation t_c (hrs)	Time since circulation Δt (hrs)	Corrected BHT (°C)
40.0	1265	*	7.0	40.0
40.0	1265	*	10.0	
65.6	2948	*	10.0	65.6
65.6	2948	*	15.0	
72.2	3117	*	17.0	87.2

Sa-1				
Uncorrected BHT (°C)	Depths (m)	Mud circulation t_c (hrs)	Time since circulation Δt (hrs)	Corrected BHT (°C)
54.0	1007			72.0
60.0	1811			
60.0	1811			
60.0	1811			

Sm-1				
Uncorrected BHT (°C)	Depths (m)	Mud circulation t_c (hrs)	Time since circulation Δt (hrs)	Corrected BHT (°C)
88.0	3383			
88.0	3386			
88.0	3387			
88.0	3387			
88.0	3387			

Alj-2				
Uncorrected BHT (°C)	Depths (m)	Mud circulation t_c (hrs)	Time since circulation Δt (hrs)	Corrected BHT (°C)
91.0	3616	*	*	109

* = Mean circulation

3.2.1.3 ESTIMATION OF GEOTHERMAL GRADIENT

This method involves estimating the temperatures of the offshore and onshore boreholes respectively, and inputting the temperatures in the temperature plots of the corrected BHTs to generate the temperature gradient.

The temperatures of onshore boreholes are calculated by utilizing the average annual temperature of the city in which the boreholes are situated. The temperature data were obtained from the meteorological records of Instituto Português do Mar e da Atmosfera (IPMA).

The temperatures of the offshore boreholes are determined by calculating the temperatures at the borehole wellhead (which was not given) through estimation of the temperatures at the bottom of the ocean. It is assumed that the top of the wellhead is at the same level as the seabed floor. Thereby, using the depths of the seabed floor from the lithology log to

extrapolate for the temperature at the bottom of the ocean from the temperature profile of Portugal coastline (Figure 17b).

The geothermal gradient of the individual wells is computed manually from the temperature plots of the corrected BHTs of the individual wells. This is achieved by; (i) taking two temperatures at two points on the temperature axis, and with their corresponding depths points (T_1, T_0, ΔZ_1, ΔZ_0), (ii) the best fit straight line is adjusted to the points on the plots, (iii) the slope is calculated, and yields the gradient of the borehole. Table 10 illustrates the generation of the temperature of the offshore boreholes, Table 11 shows IPMA data for the temperature of the onshore borehole, and Table 12 displays the calculation of the geothermal gradient. In the appendix, the temperature plots of the corrected BHTs of the individual boreholes are included with their uncorrected BHTs temperature plots. Figure 18 is the map of geothermal gradient of the wells.

Table 10: Offshore boreholes temperature data

Well names	**Seabed floor depths**		**Wellhead temperature**
	(m)	(ft)	(°C)
13E-1	210.0		12.0
14C-1	200.0		11.9
20B-1	165.0		12.8
Ca-1	82.3	270.0	13.5
Cv-1	118.3	388.0	13.0
Go-1	134.1	440.0	12.2
Lu-1	300.0		12.0
Pe-1	183.5	602.0	12.2

Table 11: Onshore boreholes temperature data

Well names	**IPMA DATA**	
	District	Average annual temperature (°C)
Alj-1	Leiria	14.8
Alj-2	Leiria	14.8
Sa-1	Santarém	16.3

Table 12: Estimation of geothermal gradient for this study

Well names	**T_1 (°C)**	**$T_{0(approx)}$ (°C)**	**ΔT (°C)**	**ΔZ_1 (m)**	**ΔZ_0 (m)**	**ΔZ (m)**	**Grad T (°C km^{-1})**
13E-1	100	12	88	2000	0	2000	44.0
14C-1	73	12	61	2000	0	2000	30.5
20B-1	70	13	57	2000	0	2000	28.5
Alj-1	80	15	65	2000	0	2000	32.5
Ca-1	67	13	54	2500	0	2500	21.6
Cv-1	83	12	71	2500	0	2500	28.4
Go-1	50	13	37	1000	0	1000	37.0
Lu-1	83	12	71	3000	0	3000	23.7
Pe-1	83	12	71	3000	0	3000	23.7
Sa-1	61	16	45	800	0	800	56.3
Alj-2	88	15	73	3500	0	3500	20.9

T_1 = Temperature at point 1, T_0 = Temperature at point 0, ΔT = Change in temperature ($T_1 - T_0$), ΔZ_1 = Depth at T_1, ΔZ_0 = Depth at T_0, ΔZ = Change in depths ($\Delta Z_1 - \Delta Z_0$), Grad T = Gradient temperature.

3.2.1.4 ESTIMATION OF AVERAGE GEOTHERMAL GRADIENT

Using the values from Table 12, the average geothermal gradient for Portugal, Mainland Portugal and Lusitanian basin are computed. The wells in the Mainland Portugal are Alj-1, Sa-1, Alj-2, and the wells in Lusitanian basin are 13E-1, 14C-1, 20B-1, Alj-1, Ca-1, Go-1, Sa-1, and Alj-2. The wells in Porto basin are Well Cv-1 and Well Lu-1.

Average geogradient $_{(Portugal)}$ = Sum of individual well geogradient estimates divided by the number of individual wells

$$= 338.4 / 11 \approx 31 \text{ °C km}^{-1}$$

Average geogradient $_{(Mainland\ Portugal)}$ = Sum of individual well geogradient estimates divided by the number of individual wells

$$= 109.7 / 3 \approx 37 \text{ °C km}^{-1}$$

Average geogradient $_{(Lusitanian\ basin)}$ = Sum of individual well geogradient estimates divided by the number of individual wells

$$= 265.3 / 8 \approx 33 \text{ °C km}^{-1}$$

Average geogradient $_{(\text{Porto basin})}$ = Sum of individual well geogradient estimates divided by the number of individual wells

$$= 52.1 / 2 \approx 26\ ^{\circ}\text{C km}^{-1}$$

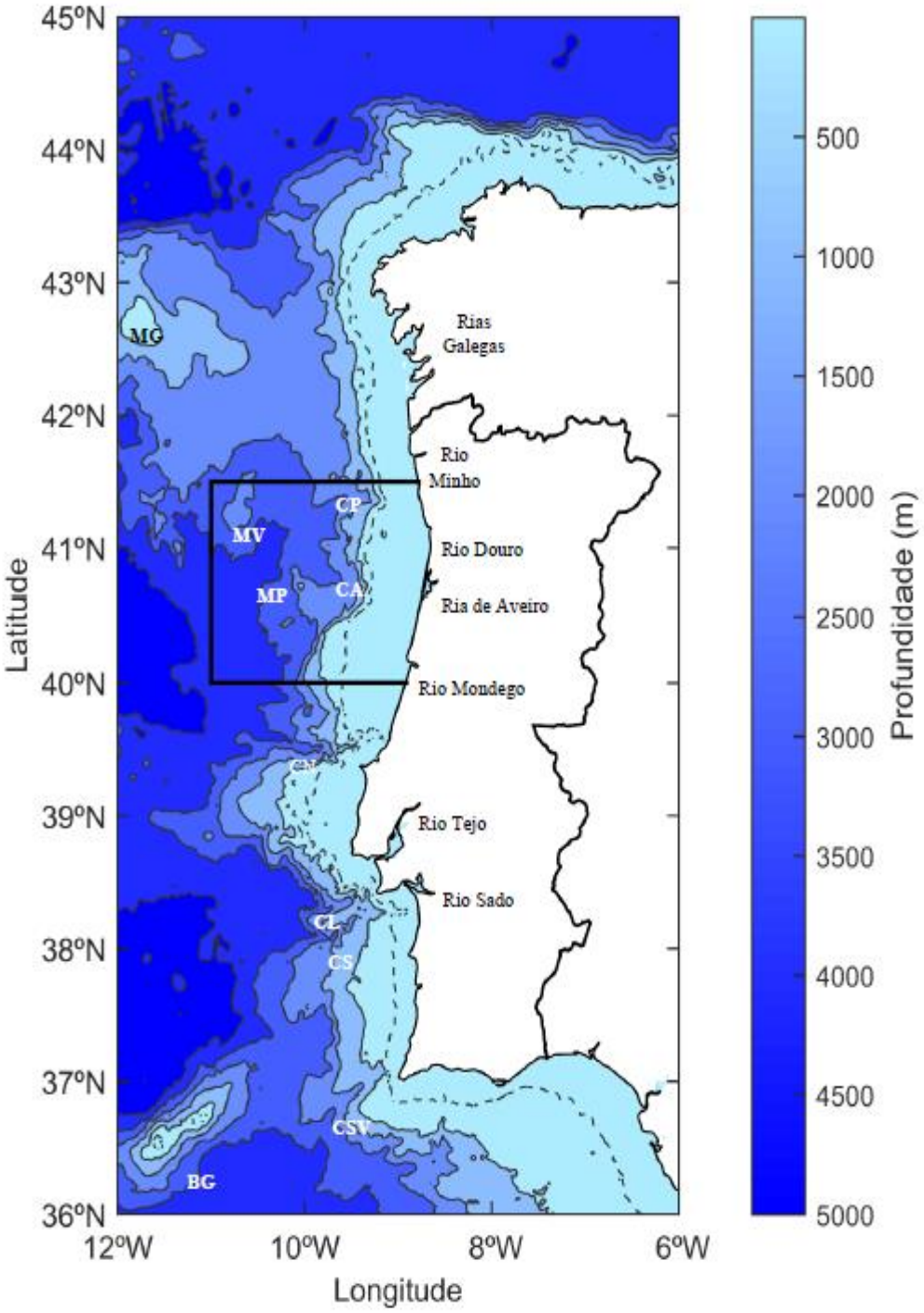

Figure 17a: Bathymetric data of Portugal during CORPAC/92 campaign (Profundidade (Portuguese) – Depth (English)) (Adapted from Hurduc, 2018).

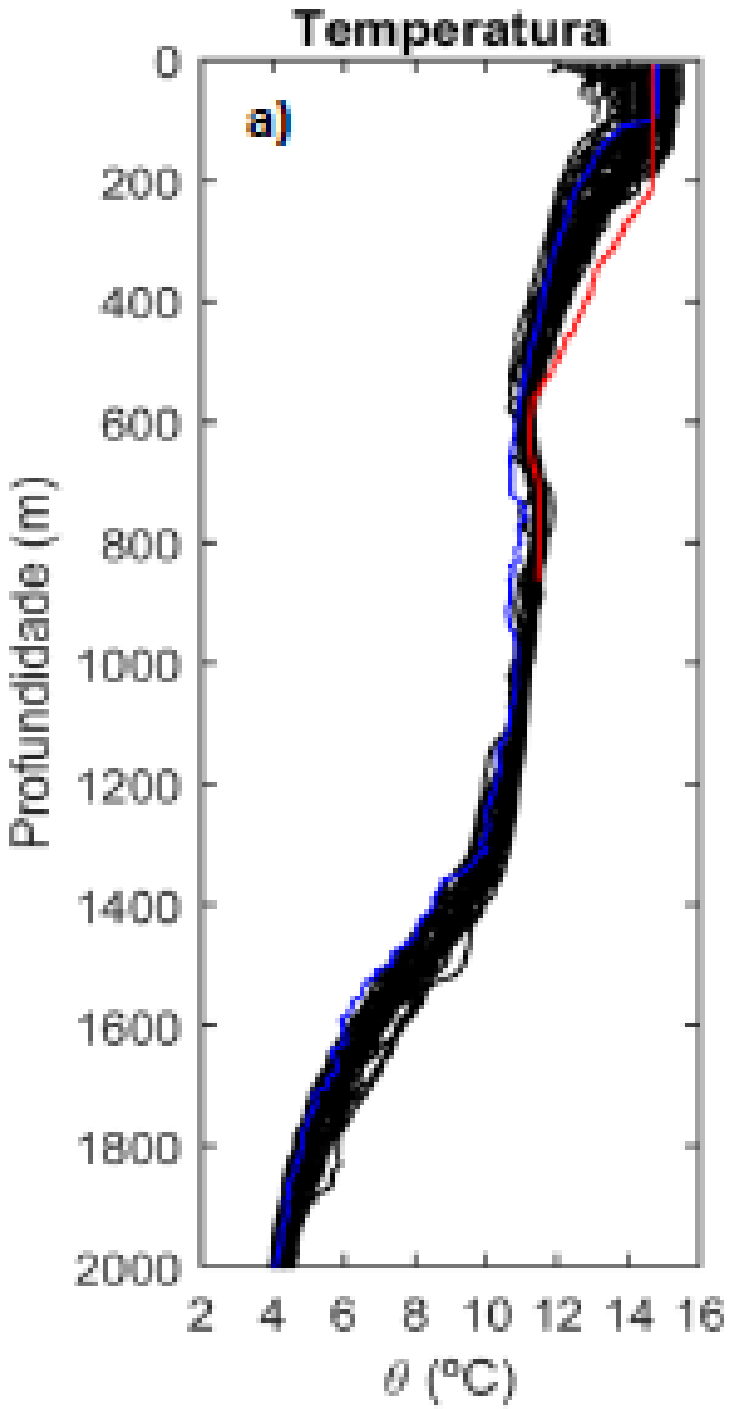

Figure 17b: Temperature profile of Portugal coastline during CORPAC/92 campaign (Temperatura, Profundidade (Portuguese) – Temperature, Depth (English)) (Adapted from Hurduc, 2018).

Figure 18: Map of geothermal gradients of wells (°C km^{-1}).

3.2.2 ESTIMATION OF THERMAL CONDUCTIVITY

To estimate the heat flow density, in addition to the calculated geothermal gradient for a given hole, it is also necessary to assume or estimate the thermal conductivity of the formations it crosses. The method of determining the effective thermal conductivity requires identifying the thickness of the formation, and the type of rock in the formation from the available lithology log of the borehole. The thickness of a formation is estimated by difference in the selected depths intervals which equates a major lithological unit. Individual lithology units of same rock type occurring throughout the whole depth of the well are computed for a particular rock. The corresponding thermal conductivities of the rock types were obtained from reference Tables as it was not available. Thereby, applying harmonic mean mixing law to calculate the effective thermal conductivity of the well which is the sum total of all the identified formation thickness divided by total of the individual rock type bed thickness over their corresponding thermal conductivities.

Table 13 displays a compilation of thermal conductivities of some rock types. Table 14 shows the calculation of lithology bed thickness, Table 15 presents the summary calculations of lithology bed thickness by thermal conductivities of each well. In Table 16, estimation of the effective thermal conductivities of the individual wells are made. The expression of the effective thermal conductivity is given below:

$$\lambda_B = \sum_{i-1}^{n} \frac{\sum_{i-1}^{n} \Delta z_i}{\sum_{i=1}^{n} \frac{\Delta z_i}{K_i}} \tag{2.2}$$

where i corresponds to the different rocky materials that the hole passes through, Δz_i (m) is the thickness of layer i, and k ($Wm^{-1}K^{-1}$) is the thermal conductivity of the material of that layer.

Table 13: Compilation of thermal conductivities of some rocks (Beardsmore, 2001).

Rock types	**Beardsmore** (1996)	**Raznjevic** (1976)	**Barker** (1996)	**Touloukian et. al.,** (1970)
Sandstone	7.1		4.7 ± 2.8	
Claystone	2.9		1.8	
Mudstone	2.9		1.9 ± 0.4	
Shale	2.9		1.8 ± 1.2	
Kaolinite				1.8 ± 0.3
Siltstone	2.9			
Limestone	3.1	2.21	2.5 ± 0.6	
Dolomite			3.7 ± 1.8	
Halite			5.9	
Loose Sand		2.44 ± 0.8		

Table 14: Summary of lithology bed thickness of the individual wells.

Wells names	**Lithology bed thickness $\sum \Delta z$ (m)**										
	Lim	Cls	Ss	Sts	Sd	Cl	Dol	Md	Hal	Sh	$\sum \Delta z$(m)
13E-1	239		672				683		168		1762
14C-1	83	371	76		213	165	429		434		1771
20B-1	2165						206				2371
Alj-1	63	689	32				254		1476		2514
Ca-1	415		195		457	219	326		250	524	2386
Cv-1	1532			290	585	208					2615
Go-1	245			180	701	428	73				1627
Lu-1	850		453	1240			385			487	3415
Pe-1	1731	328		425			227				2711
Sa-1	228				533	606	403				1770
Alj-2	2631	168	437	142			130	94			3602

Lim = Limestone, Cls = Claystone, Ss = Sandstone, Sts = Siltstone, Sd = Sand, Cl = Clay, Dol = Dolomite, Md = Mudstone, Sh = Shale, Hal = Halite.

Table 15: Summary o the lithology bed thickness divided by thermal conductivity of individual wells.

Lithology bed thickness / thermal conductivity $\sum \frac{\Delta z}{k}$ (m^2KW^{-1})												
Rock types	Thermal conductivity (K) ($Wm^{-1}K^{-1}$)	Well names										
		13E-1	14C-1	20B-1	Alj-1	Ca-1	Cv-1	Go-1	Lu-1	Pe-1	Sa-1	Alj-2
Limestone	3.1	77.097	26.774	698.387	20.323	133.871	494.194	79.032	274.194	558.387	73.548	848.710
Claystone	2.9		127.931		237.586					113.103		57.931
Sandstone	7.1	94.648	10.704		4.507	27.465			63.803			61.550
Siltstone	2.9						100.000	62.069	427.586	146.552		48.966
Sand	2.44		87.295			187.295	239.754	287.295			218.442	
Clay	1.8		91.667			121.667	115.556	23.778			336.667	
Dolomite	3.7	184.594	115.946	55.676	68.649	88.108		19.730	104.054	108.919	108.919	35.135
Mudstone	2.9											32.414
Halite	5.9	28.475	73.559		250.169	42.373						
Shale	2.9					180.690			167.931			
TOTAL		384.814	533.876	754.063	581.113	781.469	946.504	471.904	1037.568	926.961	737.576	1084.706

Table 16: Determination of the effective thermal conductivities of the wells.

Well Names	Lithology thickness $\sum \Delta z$ (m)	Lithology bed thickness / thermal conductivity $\frac{\sum \Delta z}{k}$ (m^2KW^{-1})	Effective thermal conductivity $\frac{\sum \Delta z}{\sum \frac{\Delta z}{k}}$ ($W\ m^{-1}K^{-1}$)
13E-1	1762	384.814	4.579
14C-1	1771	533.876	3.317
20B-1	2371	754.063	3.144
Alj-1	2514	581.113	4.326
Ca-1	2386	781.469	3.053
Cv-1	2615	946.504	2.763
Go-1	1627	471.904	3.448
Lu-1	3415	1037.568	3.291
Pe-1	2711	926.961	2.925
Sa-1	1770	737.576	2.400
Alj-2	3602	1084.706	3.321

3.2.3 ESTIMATION OF HEAT FLOW DENSITY

Well formations are assumed to be laterally homogeneous, isotropic, and with thermal conductivity independent of temperature, which implies that heat transfer movement is stationary. Heat flow density is determined as the product of the average geothermal gradient and their corresponding effective thermal conductivity in each well. Table 17 presents a summary of the estimate of the heat flow density of the wells. Figure 19 shows a map of the heat flow values of wells.

Table 17: Estimation of heat flow density of the boreholes.

Well names	Geothermal gradient (°C km^{-1})	Effective thermal conductivity (W $m^{-1}K^{-1}$)	Heat flow density (mWm^{-2})
13E-1	38.0	4.579	174.0
14C-1	30.5	3.317	101.2
20B-1	28.5	3.144	89.6
Alj-1	32.5	4.326	140.6
Ca-1	21.6	3.053	65.9
Cv-1	28.4	2.763	78.5
Go-1	37.0	3.448	127.6
Lu-1	23.7	3.291	78.0
Pe-1	21.0	2.925	61.4
Sa-1	56.3	2.400	135.1
Alj-2	20.9	3.321	69.4

Values of the effective thermal conductivity obtained from reference table, and the values of HFD and geothermal gradient are from this study.

3.2.3.1 ESTIMATION OF AVERAGE HEAT FLOW DENSITY

Using the values from Table 17, the average heat flow density for Portugal, Mainland Portugal and Lusitanian basin are computed.

Average HFD $_{(Portugal)}$ = Sum of individual well HFD estimates in Portugal divided by the number of individual wells

$$= 1121.3 / 11 \approx 80 \text{ mWm-}^{2}$$

Average HFD $_{(Mainland\ Portugal)}$ = Sum of individual well HFD estimates divided by the number of individual wells

$$= 345.1 / 3 \approx 115 \text{ mWm-}^{2}$$

Average HFD $_{(Lusitanian\ basin)}$ = Sum of individual well HFD estimates divided by the number of individual wells

$$= 903.4 / 8 \approx 113 \text{ mWm-}^{2}$$

Average HFD $_{(\text{Porto basin})}$ = Sum of individual well HFD estimates divided by the number of individual wells

$$= 156.5 / 2 \approx 78 \text{ mWm-}^{2}$$

Figure 19: New heat flow density values (mWm^{-2}).

CHAPTER FOUR: RESULT DISCUSSION AND INTERPRETATION OF NEW DATA

4.1 DATA COMPILATION

Twelve well log data from oil prospecting locations in the Portuguese Meso Cenozoic basins are considered in this study (Figure 15). Eight of the boreholes were situated offshore, and the remaining boreholes (Sa-1, Sm-1, Alj-1 & Alj-2) onshore. All the boreholes were found to be in the Lusitanian basins with two exceptions; Well Pe-1 is in the Alentejo basin (Pimental & Reis, 2012), and Well Cv-1, Well Lu-1 are considered to be in the Porto basin (Alves et al., 2006, 2009, Casacão et al., 2015). The geocoordinates of some of the boreholes were wrongly stated, but the geocoordinates of nearest cities to the boreholes were used. They are as follows:

Well Sa-1 (Samora Correia, Portugal): 38°55'34.0"N, 8°52'15.0"W,

Well Sm-1 (São Mamede, Portugal): 38°42'45.0"N, 9°8'35.16"W

Well Lu-1 (Porto basin): 41°18'45.5"N, 8°46'4.4"W.

The criteria for thermal properties for estimating the heat flow density indicates that for

(i) Geothermal gradient: BHTs to be considered are to be corrected, and individual well temperature datasets must have both their time elapsed between the end of mud circulation and the temperature measurement and mud circulation times.

(ii) Thermal conductivity: Thermal conductivity of rock formations and lithological information must be known or derived from tables of thermal conductivity of similar rock types.

Well log suites were available and comprised of temperature logs, lithology logs, sonic logs, neutron logs, gamma-ray logs, micro log, and computer-processed logs**.** All the boreholes had lithology logs, but most of the borehole's well log data contain incomplete

or null details for the fluid circulation times. Well Alj-1, Sa-1, Sm-1, and Alj-2 had no mud circulation times and time since circulations, and Well Cv-1 had only one circulation time. Well Lu-1 had circulation times given in a 24-hour time format with some of the depths indicating unreliable BHTs in the log's remarks. In boreholes with no circulation times, a mean circulation time of 9hrs generated from the histogram was used (Figure 16). Most of the depth measurements of the boreholes were in feet and temperature readings in Fahrenheit (Well Ca-1, Cv-1, Go-1, and Pe-1) but were converted to meters and degrees Celsius, respectively. Only Well Sm-1 was rejected for not meeting the criteria for HFD estimates. Temperature diagrams obtained in the various well boreholes are shown in Appendix 1-11. The wells have different depths, and they are fair of profound depth more than 500m.

Furthermore, for the purpose of this study, they are all considered to be deep enough to be in thermal equilibrium. Some rock types from lithology logs were categorized according to classification based on sedimentary rocks (Rock salt, Anhydrite, Gypsum - Halite, Clay - Kaolinite), which were beneficial in determination for effective thermal conductivity of the wells. The thermal conductivities of the rock types were not provided, so they were obtained from reference tables.

4.2 RESULT DISCUSSION AND DATA INTERPRETATION

The HFD estimates obtained appear to be high when compared with previous estimates of various authors. According to Correia et al. (2010), an HFD estimate in Mainland Portugal was observed to be in the range of 40 – 115 mWm^{-2}. The average geothermal gradient and average HFD estimate were 33 °C km^{-1} and 75 mWm^{-2}, respectively. Although, an average geothermal gradient of 21°C km^{-1} was suggested by Carvalho et al., (1990) and a higher HFD value of 200 mWm^{-2} for the central region by Duque and Mendes-Victor (1993). In Mainland Portugal, the HFD estimate was found to be within

the range of 69 – 141 mWm^{-2}, with an average HFD estimate of 115 $mWm^{-2}$and an average geothermal gradient of 37 ℃ km^{-1} which can be considered normal for the region. The Portuguese average HFD estimate for this study is 32 ℃ km^{-1}, and their average HFD estimate is 80 mWm^{-2}. Well Alj – 2, Ca – 1, Pe-1 and Lu-1 had the lowest geothermal gradients in the range of 21 -24 ℃ km^{-1}, while well 13E – 1 had the highest HFD estimate of 174 mWm^{-2}.

The Porto basin is analogized to a region with high heat flow density estimates. The northern region of the Hesperia Massif has an HFD estimate value of 65 mWm^{-2} as heat flow density increases (Fernandèz et al., 1998). Wells situated in this region had an averge HFD estimate value of 78 mWm^{-2}.

In Portugal, the Sedimentary basins were noted to have a regional heat flow density estimate ranging from 40 – 90 mWm^{-2} (Correria et. al., 2010). The Porto basin, Alentejo basin, and Lusitania basins were encountered in this study, having a very high regional HFD estimate varying from 61 – 174 mWm^{-2} against the stipulated similar region estimate.

Trend variation in temperature diagrams (Appendix 1 - 11) is a consequence of attempts on plotting over different segments within a particular borehole. The different segments stem from inconsistent depth intervals at which BHT was recorded. The ocean's surface, leading to a relatively uniform temperature of the ocean as heat is distributed to deeper water.

In all the boreholes, no thermal conductivity measurements were made available; so, for those boreholes where no thermal conductivity values are available, thermal conductivity values from tables from Beardsmore (1996), Raznjevic (1976), Barker (1996), and Touloukian et al. (1970) were used. However, a geothermal gradient map and heat flow density map were generated from the estimates of this study.

4.3 CONCLUSION

The average geothermal gradient in the Lusitanian basins of the Portuguese Meso Cenozoic basin was found to be 33 ℃ km^{-1}, and the average heat flow density estimate 113 mWm^{-2}, Porto (24 ℃ km^{-1}, 78 mWm^{-2}) and Alentejo (21 ℃ km^{-1}, 61 mWm^{-2}) respectively. In comparison with previous HFD estimates, the new HFD estimates obtained can be considered to be having a fair correspondence. The high HFD estimates of the Porto basin were considered normal as it is situated in the northern part of the Massif, which is associated with a region for increasing heat flow (Fernandèz et al., 1998). Nevertheless, a geothermal gradient map and a heat flow density map of the region were generated, and an attempt to a geothermal characterization of the Portuguese Meso Cenozoic basins is made.

The influence of climatic changes on surface temperatures and groundwater migration cannot be excluded for poor geothermal gradient estimates generated as most well log data utilized in this work were obtained from offshore locations. No error analysis for the wells was undertaken as it is performed only on data with actual measurements of thermal properties, which was not the case in this study. Irregularities on estimates obtained could be attributed to insufficient well-log information available, wrong boreholes geocoordinates and analogue well log data.

The use of Zetaware software for the correction of bottom-hole temperatures (BHTs) was efficient and yielded results with the least uncertainties. Only in one of the depths of Well Lu-1 was correction not affected as it did not conform to criteria of correction of the software. Only the best well log suites were considered for data compilation for each well. The use of analogized well log data proved time-consuming and cumbersome in deciphering driller's log information and in language translation as some well log information was in Spanish. The geocoordinates of nearest city to well sites were assumed

in situations where erroneous geo coordinates from the driller's log or lithology log were observed. More HFD researches are recommended.

REFERENCES

Almeida, L.C. (1991). Geothermal prospecting - Determination of geothermal gradients in drill holes. Boletim Informativo do INMG (in portuguese), pg. 149.

Almeida, L. C. (1992). Geothermal prospecting - Determination of geothermal gradients in boreholes. Boletim Informativo do INMG (in Portuguese).

Almeida, L. C. (1993). Geothermal prospecting - Calculation of thermal condutividades in rocky samples. Boletim Informativo do INMG, Lisboa, pg.7.

Alves, T., Moita, C., Sandnes, F., Cunha, T., Monteiro, J., & Pinheiro, L. (2006). Mesozoic-Cenozoic evolution of North Atlantic continental slope basins: The Peniche Basin, western Iberian margin. AAPG Bulletin. 90. 10.1306/08110504138.

Alves, T., Moita, C., Cunha, T., Ullnaess, M., Myklebust, R., Monteiro, J., & Manuppella, G. (2009). Diachronous evolution of Late Jurassic–Cretaceous continental rifting in the northeast Atlantic (west Iberian margin). Tectonics. 28. 10.1029/2008TC002337.

Anderson, D. L (1989). Theory of Earth. Blackwell Scientific Publications. ISBN: 0865423350.

Arevalo Jr, R., McDonough, W. F., & Luong, M. (2009). The K/U ratio of the silicate Earth: Insights into mantle composition, structure, and thermal evolution. Earth and Planetary Science Letters, 278(3), pg. 361–369.

Ball, S. M. (1 982). Exploration application of temperatures recorded on log heading and up-the-odds method of hydrocarbon-charged porosity prediction. Am. Assoc. Petroleum Geologists Bull., v.66(8), pg.1108-1123.

Barker, C. (1996). Thermal Modeling of Petroleum Generation: Theory and Applications. Amsterdam: Elsevier.

Beardsmore, G. R. (1996). The Thermal History of the Browse Basin and its Implications for Petroleum Exploration. Ph.D. dissertation, Monash University, Victoria, Australia.

Beardsmore, G. R., & Cull, J.P. (2001). Crustal Heat Flow: A Guide to Measurement and Modelling. Cambridge University Press, New York. Pg.47-87. ISBN 0-521- 79289-4.

Beck, A. E. (1965). Techniques of Measuring Heat Flow on Land. Amer. Geophys. Union, Natl. Acad. Sci., Natl. Res. Council, Geophys. Monograph Ser.; (United States). 8. DOI:10.1029/GM008p0024.

Beck, A. E. (1988). Methods for determining thermal conductivity and thermal diffusivity. In Handbook of terrestrial heat-flow density determination. Pg. 87 -124.

Beck, A. E., & Balling, N. (1988). Determination of virgin rock temperatures. In Handbook of terrestrial heat-flow density determination. Pg. 59-83.

Benfield, A. E. (1939). Terrestrial heat flow in Great Britain, Proc. Roy. Soc. London, A, 173, pg. 428- 450.

Bucker, C., & Rybach, L. (1996). A simple method to determine heat production from gamma logs. Marine and Petroleum Geology, 13(4), pg. 373-375.

Blackwell, D., & Richards, M. (2004). Geothermal Map of North America, Am. Assoc. of Pet. Geol., Tulsa, Okla.

Blackwell, D. D., & Steele, J.L. (1989). Thermal conductivity of sedimentary rocks: Measurement and significance. In Thermal History of Sedimentary Basins, eds. N.D. Naeser and T.H. McCulloch, pg. 45-96. New York: Springer-Verlag.

Blackwell, D. D., Wisian, K.W., & Beardsmore, G.R. (1997). Application of temperature logging technology to increasing the accuracy of basin thermal models. In Applications of

Emerging Technologies: Unconventional Methods in Exploration for Petroleum and Natural Gas, vol. 5, eds. R.J. Kruizenga et al., pp. 41-65. Dallas, Texas: Institute for the Study of Earth and Man, Southern Methodist University.

Bullard, E .C. (1939). Heat flow in South Africa, Proceedings of the Royal Society of Cambridge. Cambridge University Press.

Bruce, R.H., Middleton, M. F., Holyland, P., Loewenthal, D., & Bruner, I. (1996). Modelling of petroleum formation associated with heat transfer due to hydrodynamic processes. Petroleum Exploration Society of Australia Journal, 24, 6-12.

Casacão, J., Pimentel, N., Silva, C., & Reis, R. (2015). Port basin. Casacao_et.al_2015.

Cathles, L. M., & Smith, A. T. (1983). Thermal constraints on the formation of Mississippi Valley-type lead-zinc deposits and their implications for episodic basin dewatering and deposit genesis, Econ. Geol., 78, pg. 983–1002.

Carvalho, J. M., Berthou, P.Y., & Silva, L.F. (1990). Introduction to the Geothermal Resources of the Lisbon Region, Book tribute to Carlos Romariz - Applied and Economical Geology Section, Lisbon, 332-356.

Cermak, V., & Rybach, L. (1982). Thermal Conductivity and Specific Heat of Minerals and Rocks. Subvolume A of Volume 1 'Physical Properties of Rocks' of Landolt-Börnstein - Group V Geophysics, doi: 10.1007/10201894_62.

Cermak, V. (1979). Heat flow map of Europe. In: V. Cermak and L. Rybach (Edit.), Springer-Verlag, Berlin (1979), pg. 261-266.

Clauser, C., & Huenges, E. (1995). Thermal Conductivity of Rocks and Minerals. Rock Physics and Phase Relations: A Handbook of Physical Constants, AGU Reference Shelf 3, pg 105-126. https://www.researchgate.net/publication/256372062.

Condie, K. C. (1997). Plate Tectonics and Crustal Evolution (Fourth edition). Butterworth Heinemann, An imprint of Elsevier Science.

Correia, A., Duque, R., Maciel, C., Camelo, S., Almeida, L.C., & Mendes Victor, L. A. (1982). First determinations of heat flux in Portugal. INMG, Boletim Informativo nº56, pp.3-13 (in Portuguese).

Correia, A, & Jones, F.W. (1997). On the existence of a geothermal anomaly in southern Portugal, Tectonophysics, 271, pg. 123-134.

Correia, A., & Ramalho, E. (1998). New heat flow density data from southern Portugal: a geothermal anomaly revisited, Tectonophysics, 291, pg. 55-62.

Correia, A., & Ramalho, E. (1999). One-dimensional thermal models constrained by seismic velocities and surface radiogenic heat production for two main geotectonic units in southern Portugal. Tectonophysics. 306, pg. 261-268. DOI:10.1016/S0040-1951(99)00059-1.

Correia, A., & Safanda, J. (1999). Preliminary ground surface temperature history in mainland Portugal reconstructed from borehole temperature logs. Tectonophysics, 306, pg. 269-275.

Correia, A., & Safanda, J. (2001). Ground surface temperature history at a single site in southern PoÍugal reconstructed from borehole temperatures. Global and Planetary Change, 29, pg. 155-165.

Correia, A., & Safanda, J. (2002). Geothermal modeling along a two-dimensional crustal profile in Southern Portugal, Journal of Geodynamics, 34,47-61.

Correia, A., & Ramalho, E.C. (2005). Updated Surface Heat Flow Density Map in Mainland Portugal. Proceedings World Geothermal Congress 2005, paper 2641. Correia, A., & Ramalho, E. (2009). Heat flow density estimations in the

Portuguese northern Hercynian Massif using silica geothermometry. Transactions - Geothermal Resources Council. 33. 813-816.

Correia, A., & Ramalho, E.C. (2010). Update Heat Flow Density Map for. Proceedings of the World Geothermal Congress 2010.

Cunha, P., & Reis, R. (1995). Cretaceous sedimentary and tectonic evolution of the northern sector of the Lusitanian Basin (Portugal). Cretaceous Research - CRETACEOUS RES. 16. 155-170. 10.1006/cres.1995.1013.

Davies, G. (1980). Review of oceanic and global heat flow estimates, Rev. Geophys., 18, pg. 718-722.

Davis, E. E. (1988). Oceanic heat flow density. In Handbook of Terrestrial Heat-Flow Density Determination, eds. R. Haenel, L. Rybach and L. Stegena, pp. 223-60. Dordrecht: Kluwer Academic Publishers.DOI:10.1007/978-94-009-2847-3_6.

Davies, J. H., & Davies, D. R. (2010). Earth's surface heat flux, Solid Earth, l,5-24.

Demongodin, L., Pinoteau, B., Vasseur, G., & Gable, R. (1991). Thermal conductivity and well logs: A case study in the Paris Basin. Geophysics Journal International, 105, 675-91Davies, J. H., and D. R. Davies (2010), Earth’s surface heat flux, Solid Earth, 1, pg. 5–24.

Diment, W. H., & Pratt, H.R. (1988). Thermal Conductivity of Some Rock-Forming Minerals: A Tabulation. USGS open file report no. 88-690. Reston, Virginia: United States Geological Survey.

Duque, M. R., & Mendes-Victor, L. (1988). Heat Flow and Thermal Gradients in Portugal.

Duque, R. (1991). Contribution of heat flux for the characterization of the lithosphere in Alentenjo, Unpublished thesis, Ph.d, University of Evora (in Portuguese).

Duque, R., & Mendes-Victor, L. (1993). Heat flow and deep temperature in South Portugal. Studia Geophysica et Geodaetica, Vol.37, pg. 279-292.

Dye, S. T. (2012). Geoneutrinos and the radioactive power of the Earth, Rev. Geophys., 50, RG3007, doi:10.1029/ 2012RG000400.

Enachescu, M. E. (1987). "The tectonic and structural framework of the northeast Newfoundland margin". In Beaumont, C. and Tankard, A.J. (eds.). Sedimentary Basins and Basin-forming Mechanisms. Memoir 12. Can. Soc. Petrol. Geol. pp. 117–146. ISBN 978-0-920230-43-5.

Etiope, G., & R. W. Klusman (2002), Geologic emissions of methane to the atmosphere, Chemosphere, 49, pg. 777–789.

Fahnestock, H., Abdalati. W., Joughin. I., Brozena. J., & Gogineni, P. (2001). High geothermal heat flow, basal melt, and the origin of rapid ice flow in central Greenland, Science, 294, pg. 2338–2342.

Fernandez, M., Marzan, I., Ramalho, E., & Correia, A. (1998). Heat flow and lithospheric thermal regime in the Iberian Peninsula, Tectonophysics, 291, 29-53.

Fiorentini, G., Lissia, M., & Mantovani, F. (2007), Geo-neutrinos and earth's interior, Physics Reports, 453(5-6), pg. 117-172, doi: 10.1016/j.physrep.2007.09.001.

Förster, A., & Merriam, D.F. (1995). A bottom-hole temperature analysis in the American Midcontinent (Kansas): Implications to the applicability of BHTs in geothermal studies. World Geothermal Congress (Florence, Italy) Proceedings. 2, pg. 777-782.

Gasparini, P., Mantovani, M. S. M., Corrado, G., & Rapolla, A. (1979). Depth of Curie Temperature in Continental Shields: A Compositional Boundary? Nature, 278, 845- 6. Horner, D.R.

(1951). Pressure Build-up in Wells. Proceedings of the Third World Petroleum Congress, The Hague, 2, pg. 924-31.

Gasparini, P., Mantovani, M.S.M., Corrado, G., & Rapolla, A. (1979). Depth of Curie temperature in continental shields: A compositional boundary? Nature, 278, 845-6.

Glover, P. W. J. (2014). Petrophysics and Geological analysis of logs. Copyright for Petrophysics MSc Course notes. Department of Geology and Geological Engineering, Laval University, Canada.

Hamza, V., & Beck, A. (1972). Terrestrial Heat Flow, the Neutrino Problem, and a Possible Energy Source in the Core. Nature. 240. 343-344. 10.1038/240343a0.

Horai, K., & Simmons, G. (1969). Thermal conductivity of rock-forming minerals. Earth and Planetary Science Letters, 6, pg. 359-68.

Hurduc, A. (2018). Hidrologia e Dinâmica do Oceano Costeiro de Portugal na Região do Cabo Mondego. Published MSc thesis. http://hdl.handle.net/10451/35534

Hurter, S., & Haenel, R. (2002). Atlas of Geothermal Resources in Europe. Directorate-General for Research and Innovation, European Commission. GGA, Hannover, Germany. 92p., 89 plates. pg. 47-49. ISBN92-828-0999-4.

Instituto Português do Mar e da Atmosfera (IPMA) (2020). Sea surface temperatures. In IPMA. Retrieved from https://www.ipma.pt/en/maritima/sst/

Issler, D. R., & Beaumont, C. (1989). A finite element model of the subsidence and thermal evolution of extensional basins: Application to the Labrador continental margin. In Thermal History of Sedimentary Basins: Methods and Case Histories, eds. N.D. Naeser and T.H. McCulloh, pg. 239-67. New York: Springer-Verlag.

Jaupart, C., & Mareschal, J. C. (2007). Heat flow and thermal structure of the lithosphere, in: Treatise on Geophysics, Vol. 6, edited by: Schubert, G., 217–252, Oxford, Elsevier Ltd.

Jessop, A. M., Hobart, M. A., & Sclater, V. (1976). The World Heat Flow Data Collection, 1975, 125 pp., Earth Phys. Branch; Energ. Mines and Resour. Canada, Ottawa, Ont.

Jessop, M. A., & Majorowicz, A. J. (1994). Fluid flow and heat transfer in sedimentary basins. Geological Society, London, Special Publications, Volume 78, pg. 43-54. DOI: 10.1144/GSL.SP.1994.078.01.05.

Jones, F. W., & Correia, A. (1999). Comparison of 2-D and 3-D models of a magnetotelluric survey in southern Portugal. In: Three-Dimensional Electromagnetics, Michael Oristaglio and Brian Spies (eds.), Geophysical Developments nº 7, Society of Exploration Geophysicists, pg. 375-386.

Kreyszig, E. (1983). Advanced Engineering Mathematics. Wiley, Fifth Edition. ISBN 10: 0471862517 / ISBN 13: 9780471862512.

Kullberg, J.C., Rocha, R. B., Soares, A.F., Rey, J., Terrinha, P., Callapez, P., & Martins, L. (2006). A Bacia Lusitaniana: Estratigrafia, Paleogeografia e Tectónica. Geologia de Portugal No Contexto da Ibéria. pg.317-368.

Lee, W. H. K., & MacDonald, G. J. F. (1963). The global variation of terrestrial heat flow: Jour. Geophys. Res., v. 68, pg. 6481-6492.

Lee, W. H. K., & Uyeda, S. (1965). Review of heat flow data, in Terrestrial Heat Flow, edited by W. H. K. Lee, pg. 87– 190, A. G. U., Washington, D. C.

Lowrie, W. (2007). Fundamentals of Geophysics. Cambridge University Press. ISBN 0521 46164 2.

Majorowicz, J. A., Gough, D. I., & Lewis, T. J. (1993). Electrical conductivity and temperature in the Canadian Cordilleran crust. Earth and Planetary Science Letters, 115, pg. 57-64.

Mashayek, A., Ferrari. R., & W. R. Peltier (2013). Geothermal heat flux and enhanced abyssal mixing: Implications for the Antarctic bottom water circulation, Geophys. Res. Abstr., 15, EGU2013–6310.

McDonough, W. F., & Sun, S. S. (1995). The composition of the Earth, Chemical Geology, 120, 223-253, doi: 10.1016/0009-2541(94)00140-4.

McGee, H.W., Meyer, H.J., & Pringle, T.R. (1989). Shallow geothermal anomalies overlying deeper oil and gas deposits in Rocky Mountain region. Am. Assoc. Petroleum Geologists Bull., v.73(5), pg.576-597.

Meyer, H. J., & McGee, H.W. (1985). Oil and gas fields accompanied by geothermal anomalies in Rocky Mountain region. Am. Assoc. Petroleum Geologists Bull, v.69(6) pg. 933-945.

Mojiri, A. (2013). "Spectral beam splitting for efficient conversion of solar energy- A review". Renewable and Sustainable Energy Reviews. 28: pg. 654–663.

Morgan, P. (2000). Heat flow. Publication no. 243 of the ARC National Key Centre for Geochemical Evolution and Metallogeny of Continents.

Morgan, P. (2014). Continental Heat Flow. In: Reference Module in Earth Systems and Environmental Sciences, Elsevier. DOI: 10.1016/B978-0-12-409548-9.09439-2.

Mörner, N. A., & Etiope, G. (2002). Carbon degassing from the lithosphere, Global Planet. Change, 33, pg. 185–203.

Muffler, P., & Cataldi, R. (1978). Methods for regional assessment of geothermal resources, Geothermics, 7, pg. 53–89.

Nielsen, S. B. (1986). The continuous temperature log: method and application. Ph.D. thesis. University of West Ontario, London, Canada.

O'Reilly, S.Y., & Griffin, W.L. (1985). A xenolith-derived geotherm for southeastern Australia and its geophysical implications. Tectonophysics, Volume 111, pg. 41-63.

Pollack, H. N., Hurter, S. J., & Johnson, J. R. (1993). Heatflow from the Earth's Interior-Analysis of the global data set, Rev. Geophys., 31, pg. 267–280.

Ramos, P., Trindade, J., & Neves, M. (2005). Portugal: Coastal dynamics, A field trip guide-A1. Sixth international conference on geomorphology, Zaragoza.

Ramalho, E. C., & Correia, A. (2006). Contribution for the thermal characterization of the crust in mainland Portugal. INETI Report, 32 pp. (in Portuguese).

Pimentel, N., & Reis, R. (2012). The Mesozoic Evolution of South-Western Portugal – Algarve and Alentejo Basins, Portugal. Field-trip Guide, III Conjugate Margins Conference, 48 pp. PIPCo RSG Ltd, Dublin.

Prensky, S. (1992). Temperature measurements in boreholes: An overview of engineering and scientific applications. The Log Analyst. 33, pg.313-333.

Pribnow, D., Williams, C. F., & Burkhardt, H. (1993). Well log-derived estimates of thermal conductivity in crystalline rocks penetrated by the 4-km deep KTB Vorbohrung, Geophys. Res. Lett., 20(12), pg.1155-I 158.

Prol-Ledesma, R. M., & Juarez, G. (1986). Geothermal Map of Mexico. Journal of Volcanology and Geothermal Research. 28, 351-362.

Raznjevic, K. (1976). Handbook of Thermodynamic Tables and Charts. Washington DC: Hemisphere Publishing Corp.

Reis, R., & Pimentel, N., & Garcia, A. (2010). The Lusitanian Basin (Portugal): Stratigraphic analysis and geodynamic evolution. Boletim de Geociencias da Petrobras. 19, pg. 23-52.

Ribeiro, A., Antunes, M. T., Ferreira, M. P., Rocha, R. B., Soares, A. F., Zbyszewski, G., Aleida, F. M., Carvalho, D., & Monteiro, J. H. (1979). Introduction à la Géologie Génerale du Portugal. Serv. Geol. Portugal, pg. 114, Lisbon.

Ribeiro, A. (2002). Soft Plate and Impact Tectonics. Springer, Berlin, ISBN 3-540- 67963-4. DOI:10.1007/978-3-642-56396-6.

Rybach, L. (1976). Radioactive heat production in rocks and its relation to other petrophysical parameters. Pure Appl. Geophys.,114, pg. 309–318.

Rybach, L. (1988). Determination of heat production rate. In Handbook of Terrestrial Heat Flow Density Determination, ed. R. Haenel, L. Rybach and L. Stegena, Dordrecht: Kluwer Academic Publishers, pg. 48.

Safanda, J., Rajver, D., Correia, A., & Dedecek, P. (2007). Repeated temperature logs from the sites of the Czech, Slovenian and Portuguese borehole climate observatories. Climate of the Past, 3, 453-462.Safronov, V. S. (1972), 'Evolution of the protoplanetary cloud and formation of the Earth and Planets', NASA TT F-677 (Originally published in Russian in 1969).

Sclater, J. G., & Christie, P. A. F. (1980a). Continental stretching: An explanation of the post Mid-Cretaceous subsidence of Central North Sea Basin. Journal of Geophysical Research, 85(B7), 3711-39.

Sclater, J. G., Jaupart, C., & Galson, D. (1980b). The heat flow through oceanic and continental crust and the heat loss of the Earth, Rev. Geophys. Space Phys., 18, pg. 269-311.

Scott, J. R., Marotzke, J., & Adcroft, A. (2001). Geothermal heating and its influence on the meridional overturning circulation, J. Geophys. Res., 106, 31,141–31,154.

Sekiguchi, K. (1984). A method for determining terrestrial heat flow in oil basinal areas. Tectonophysics, 103, pg. 67-79.

Simmons, G., & Horai, K. (1968). Heat flow data 2, J. Geophys. Res, 73, pg. 6608–6609.

Sinclair, I. (2021). Tectonism and sedimentation in the Jeanne d'Arc Basin, Grand Banks of Newfoundland.

Stein, C. (1995). Heat Flow of the Earth. Doi: 10.1029/RF001p0144. https://www.researchgate.net/publication/255653835.

Tissot, B. P., Pelet, R., & Ungerer, P. (1987), Thermal history of sedimentary basins, maturation indices, and kinetics of oil and gas generation, AAPG Bull., 71, pg. 1445–1466.

Touloukian, Y.S., Powell, R. W., Ho, C.Y., & Klemens, P.G. (1970b). Thermal Properties of Matter, vol. 2, Thermal Conductivity, Non-Metallic Solids. New York and Washington: IFI/Plenum.

Turcotte, D. L., & Oxburgh, E. R. (2014). Mantle convection and the new global tectonics, Ann. Rev. Fluid Mech., 4, pg. 33-68.

Weiss, 0. (1938). Temperature measurements with an electrical resistance thermometer in a deep borehole on the East Rand, J.Chem. Met. Min. Soc. South Africa, 89, pg. 149-166.

Williams, C. F., & Anderson, R.N. (1990). Thermophysical properties of the Earth's crust: In situ measurements from continental and ocean drilling. Journal of Geophysical Research, 95(B6), pg.9209-36.

Williams, D. L., & Von Herzen, R. P. (1974). Heat loss from the Earth: new estimate, Geology, 2, pg. 327–328. www.ihfc-iugg.org.

ZetaWare, Utilities (2003). Bottom Hole Temperature Horner Correction. In Zetaware Inc, retrieved from https://www.zetaware.com/utilities/bht/horner.html.

APPENDIX 1

UNCORRECTED BHT VS DEPTH

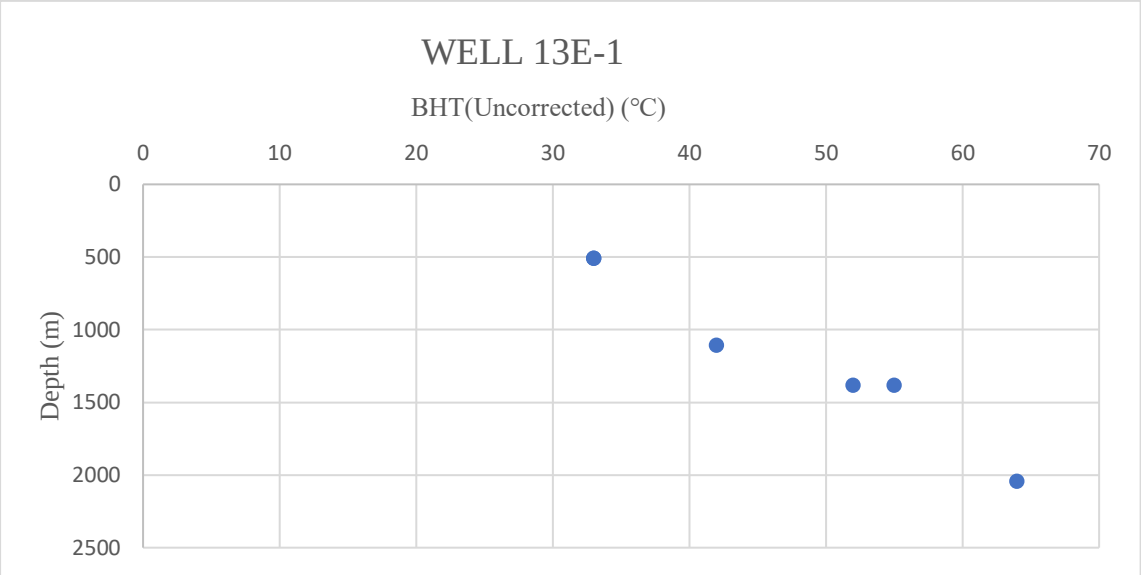

CORRECTED BHT VS DEPTH

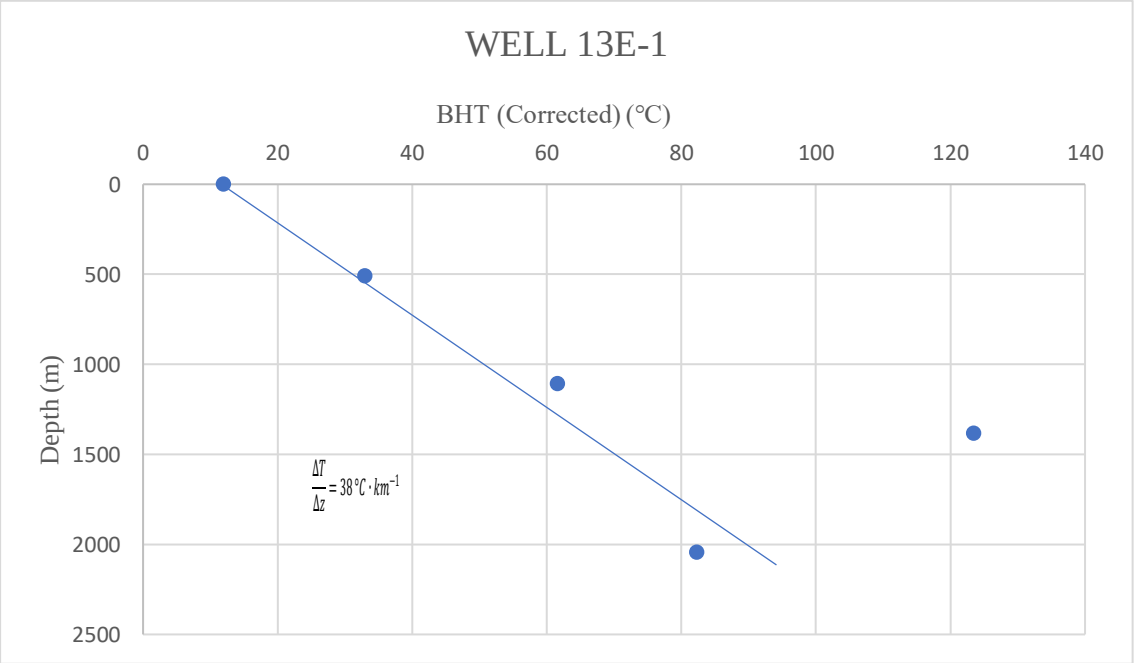

APPENDIX 2

UNCORRECTED BHT VS DEPTH

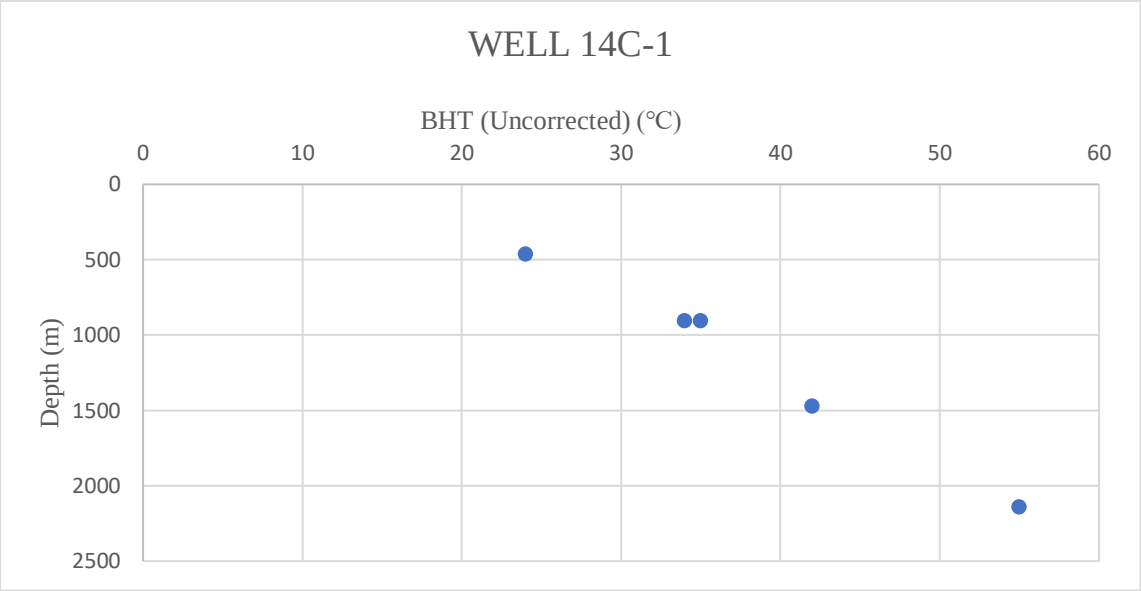

CORRECTED BHT VS DEPTH

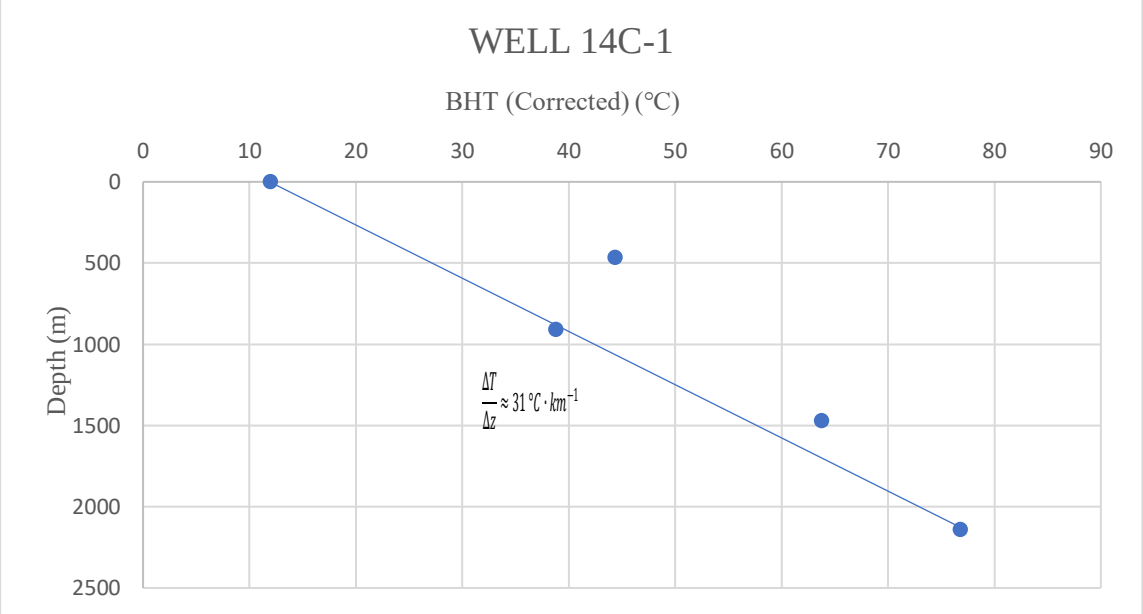

APPENDIX 3

UNCORRECTED BHT VS DEPTH

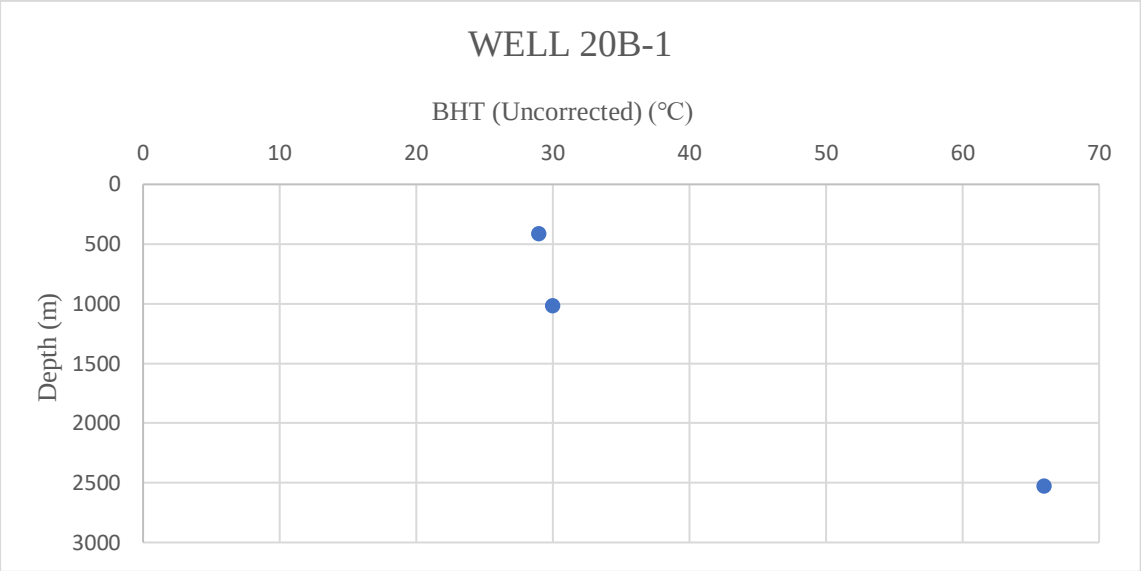

CORRECTED BHT VS DEPTH

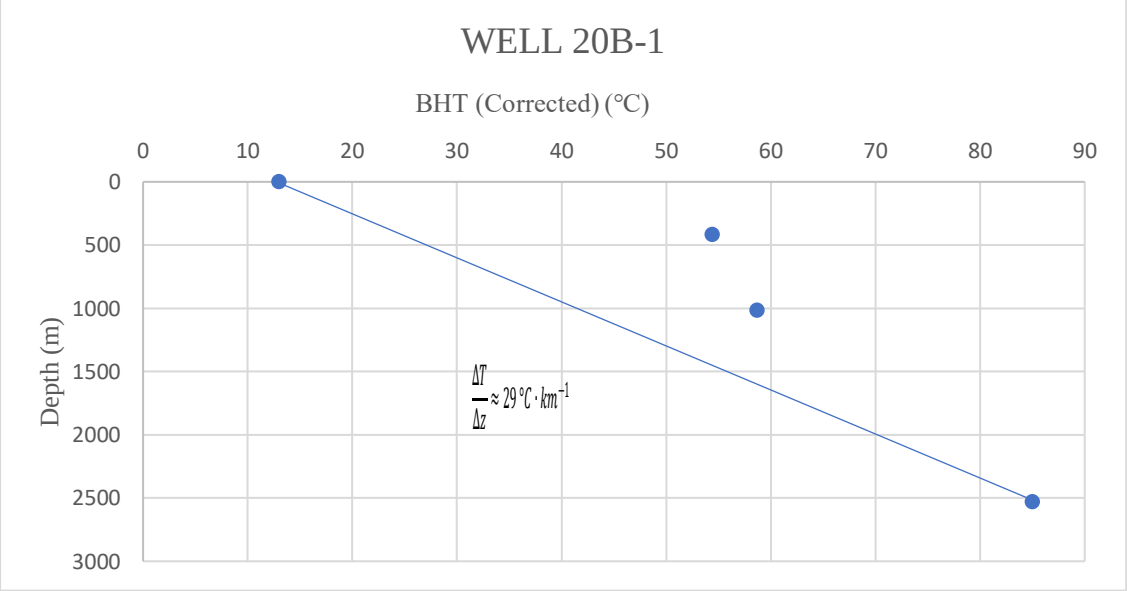

APPENDIX 4

UNCORRECTED BHT VS DEPTH

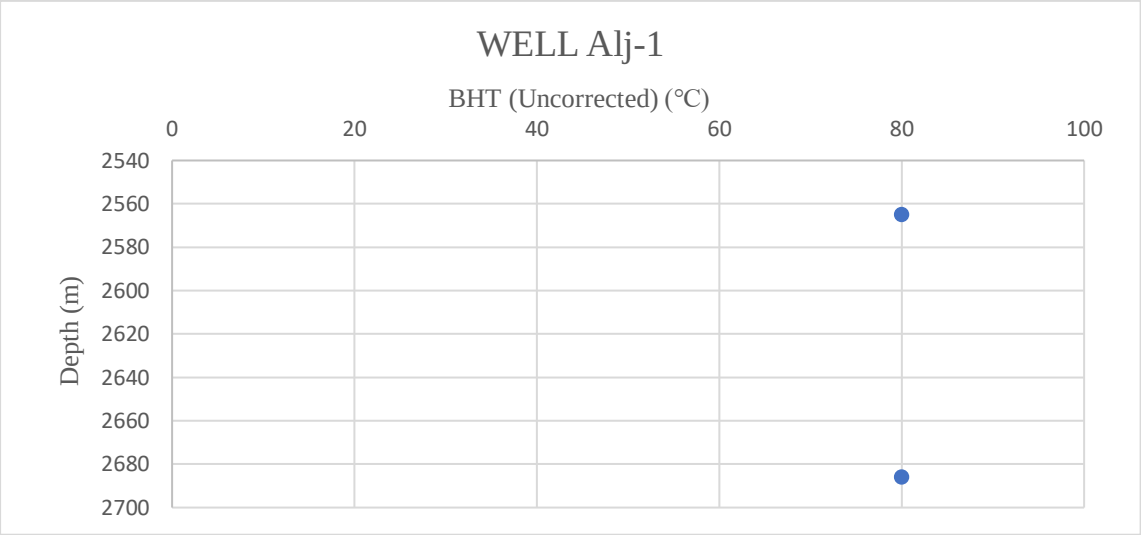

CORRECTED BHT VS DEPTH

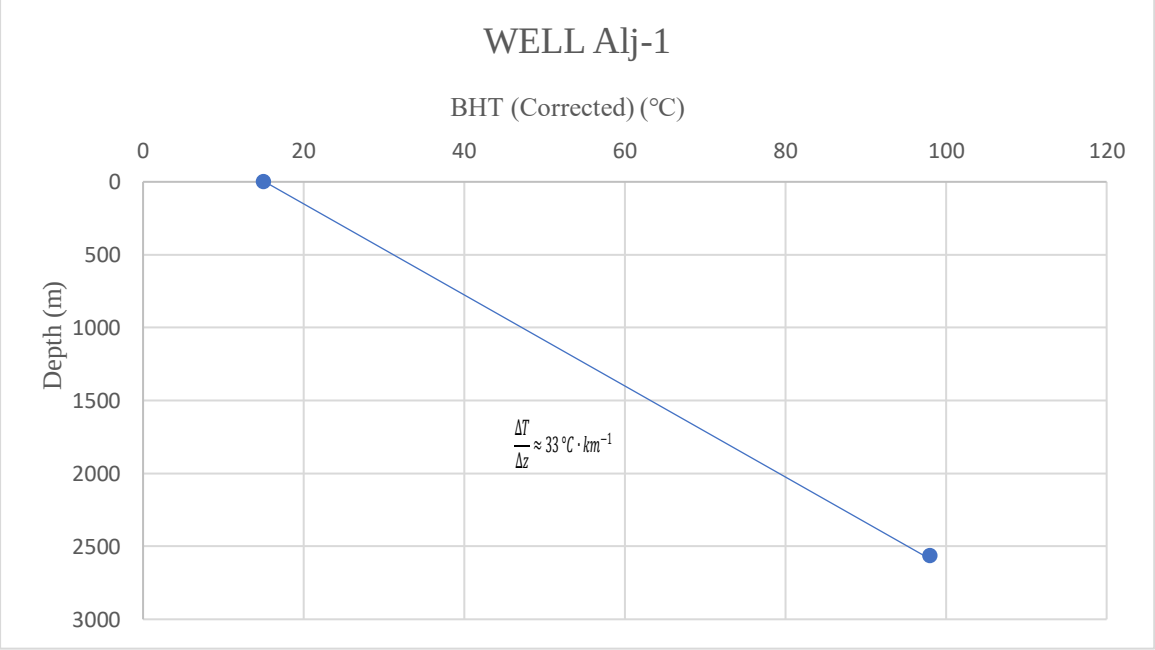

APPENDIX 5

UNCORRECTED BHT VS DEPTH

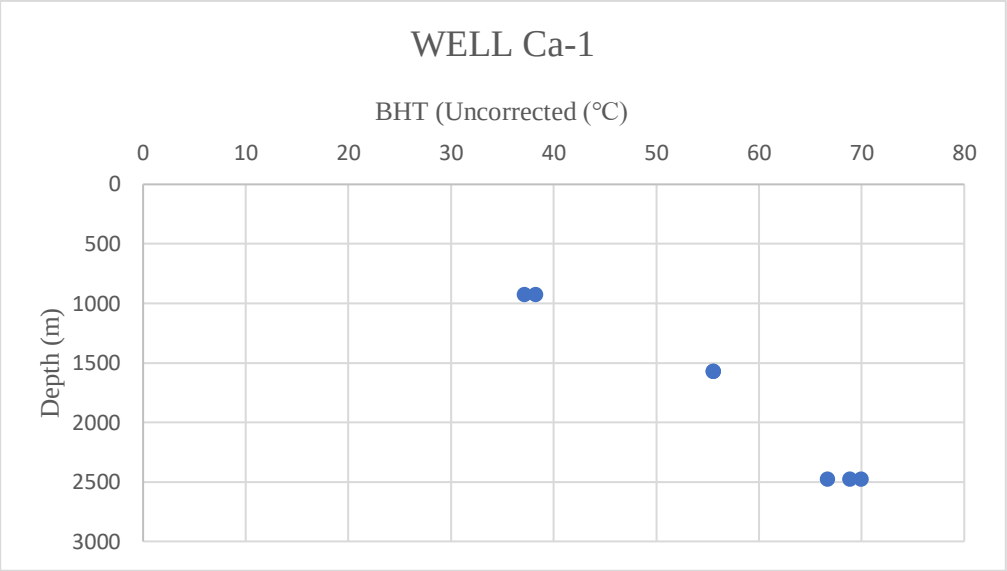

CORRECTED BHT VS DEPTH

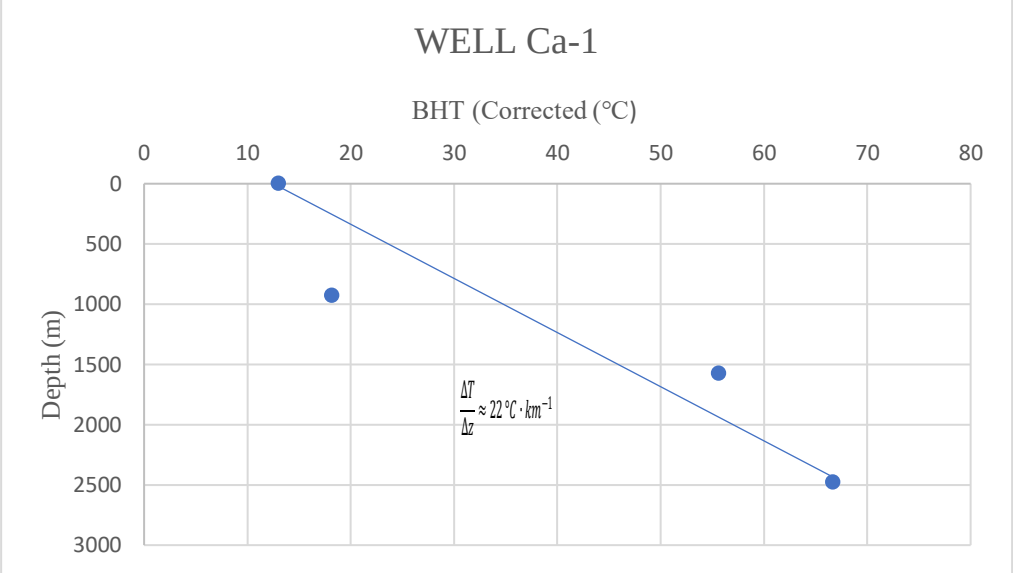

APPENDIX 6

UNCORRECTED BHT VS DEPTH

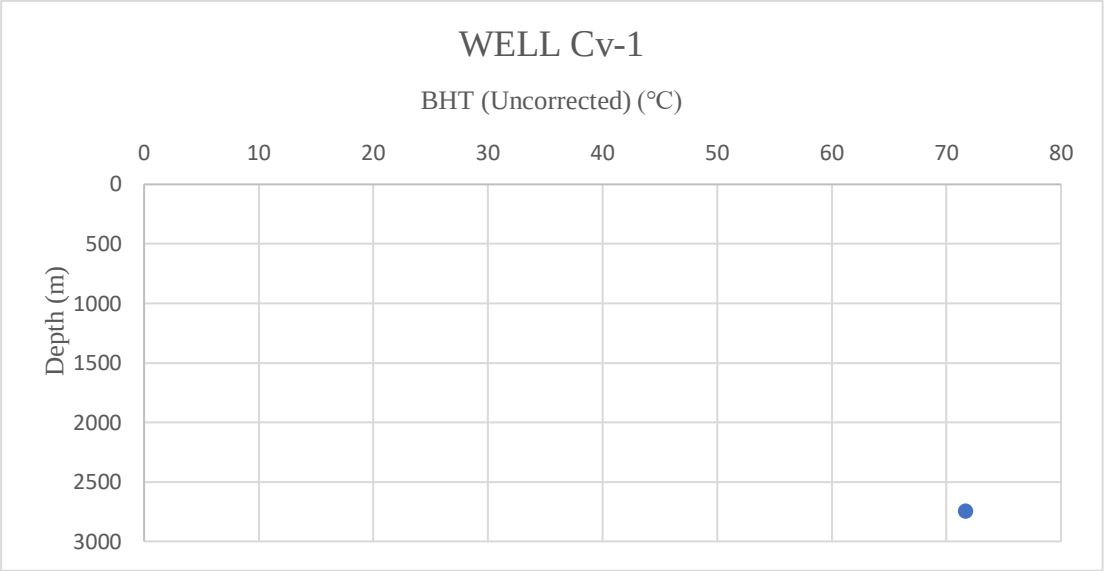

CORRECTED BHT VS DEPTH

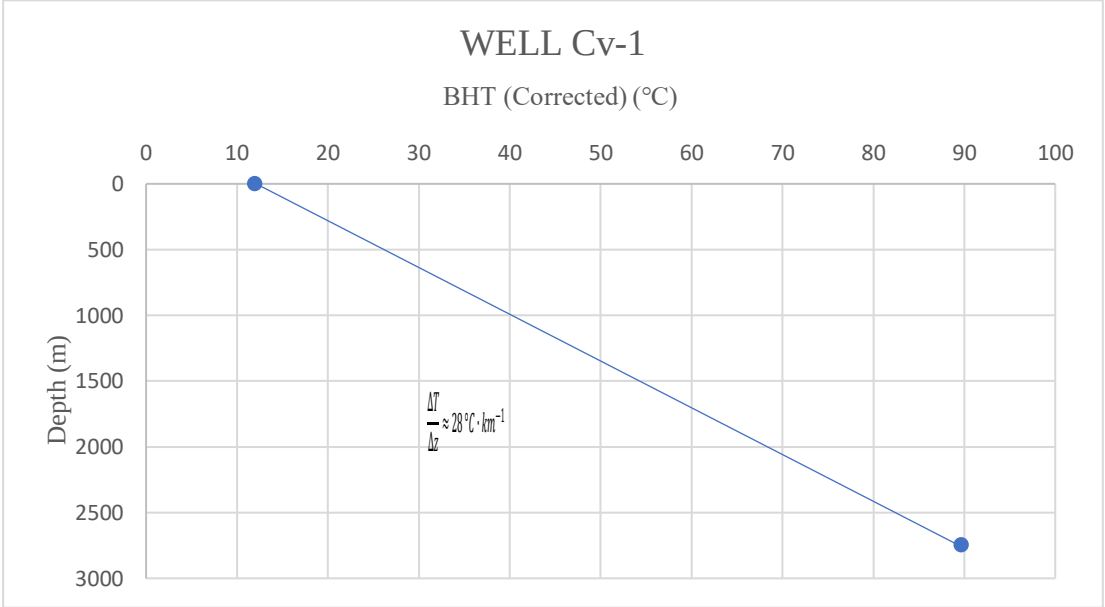

APPENDIX 7

UNCORRECTED BHT VS DEPTH

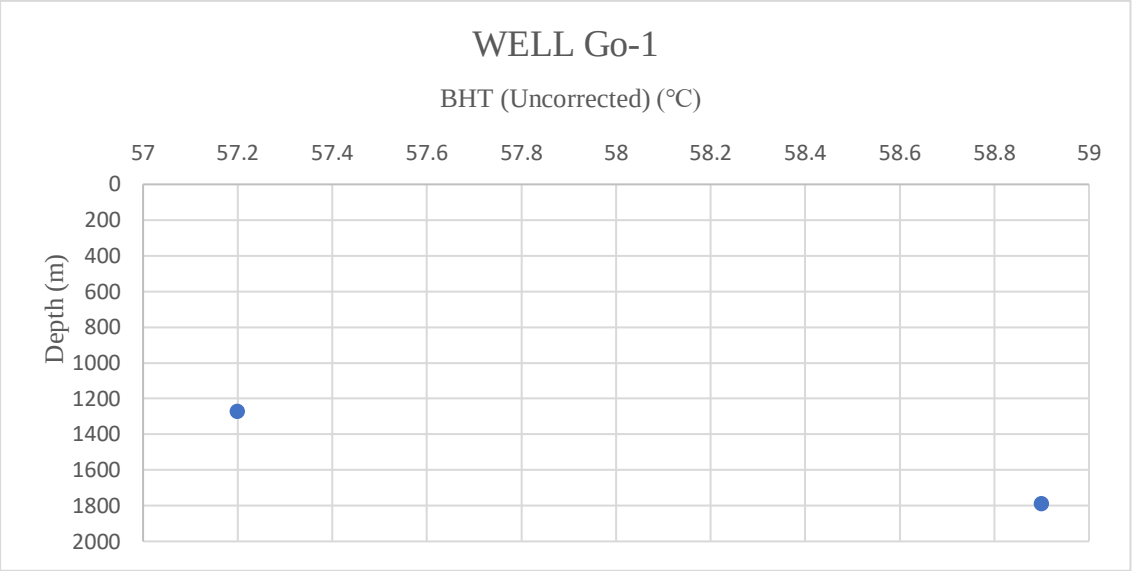

CORRECTED BHT VS DEPTH

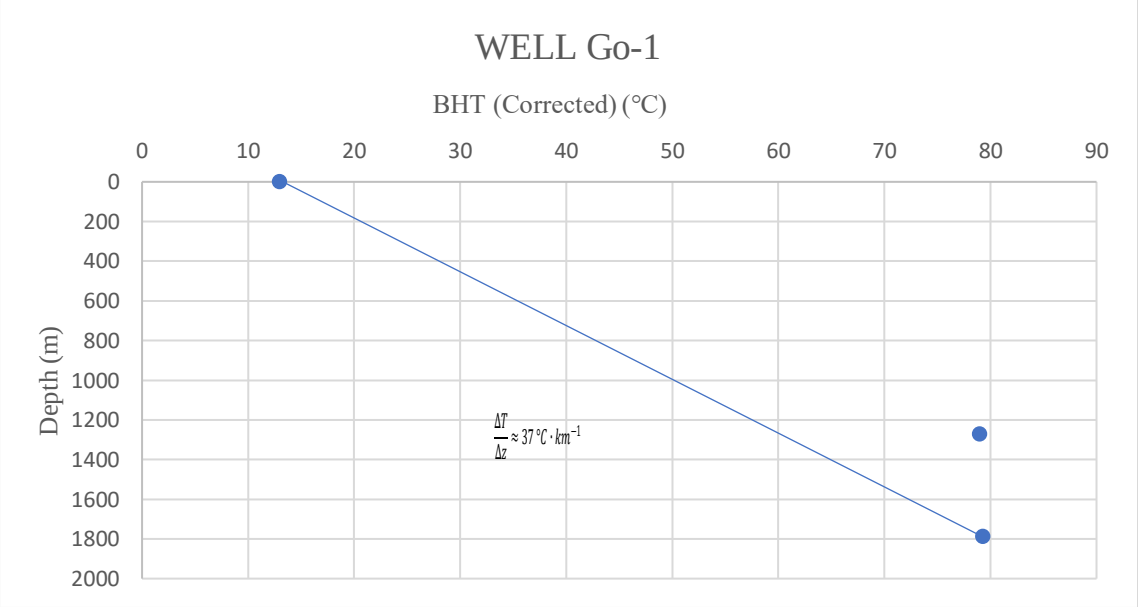

APPENDIX 8

UNCORRECTED BHT VS DEPTH

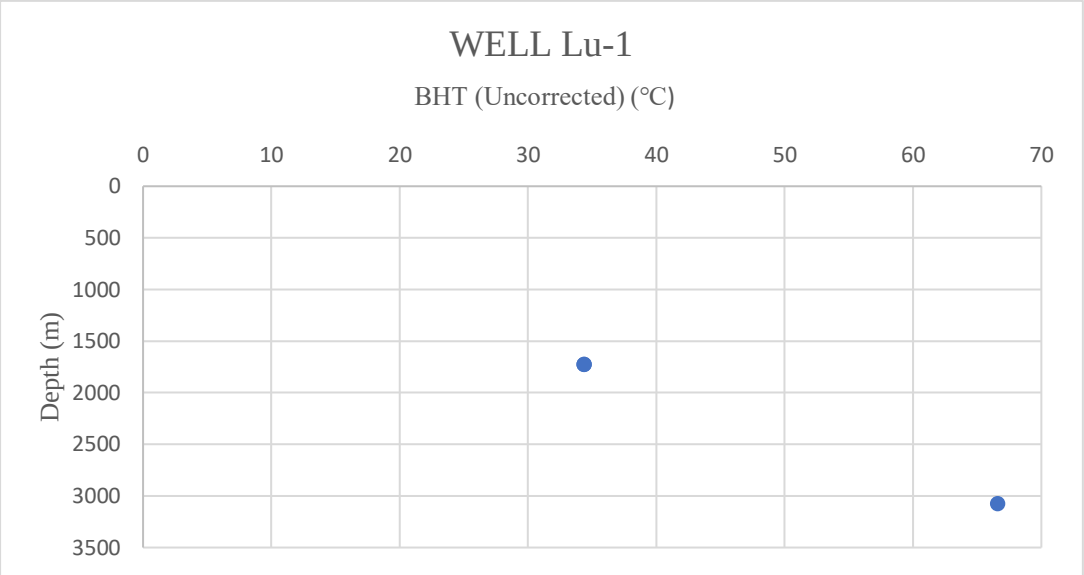

CORRECTED BHT VS DEPTH

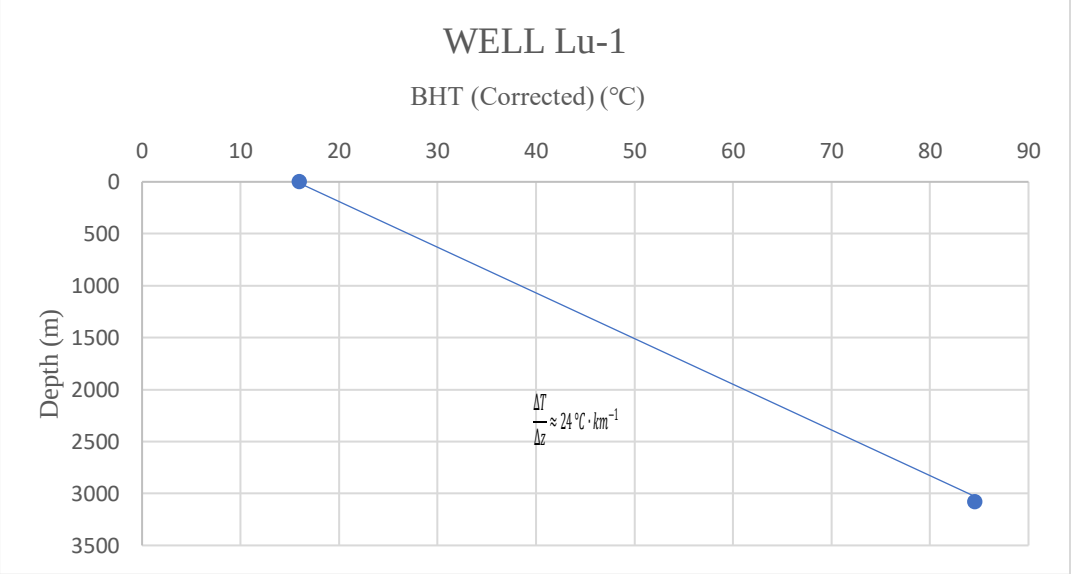

APPENDIX 9

UNCORRECTED BHT VS DEPTH

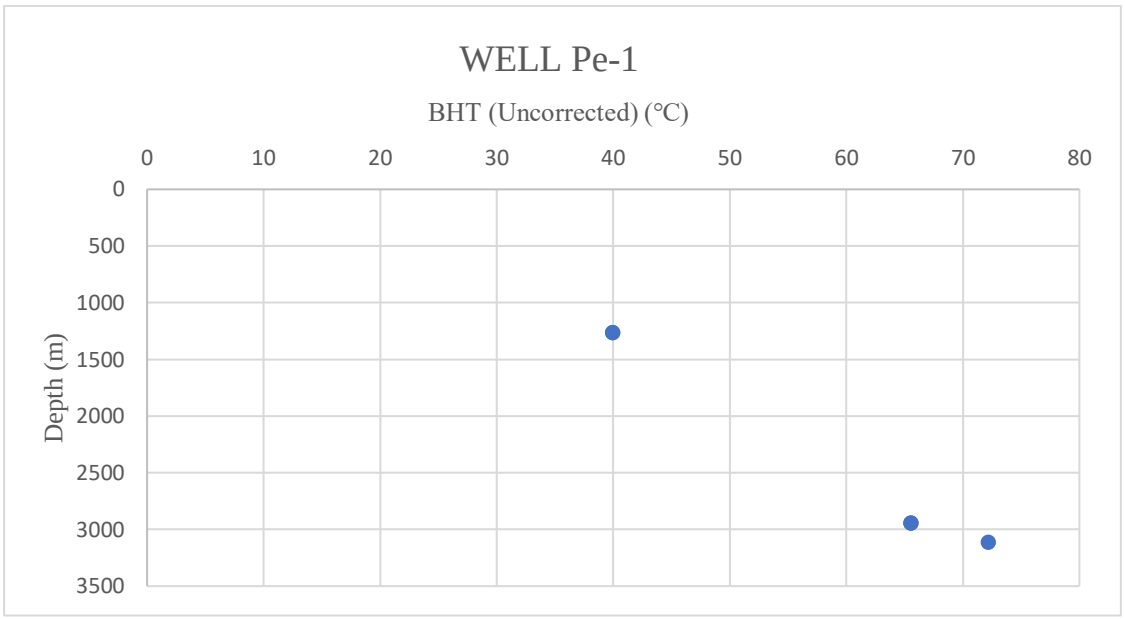

CORRECTED BHT VS DEPTH

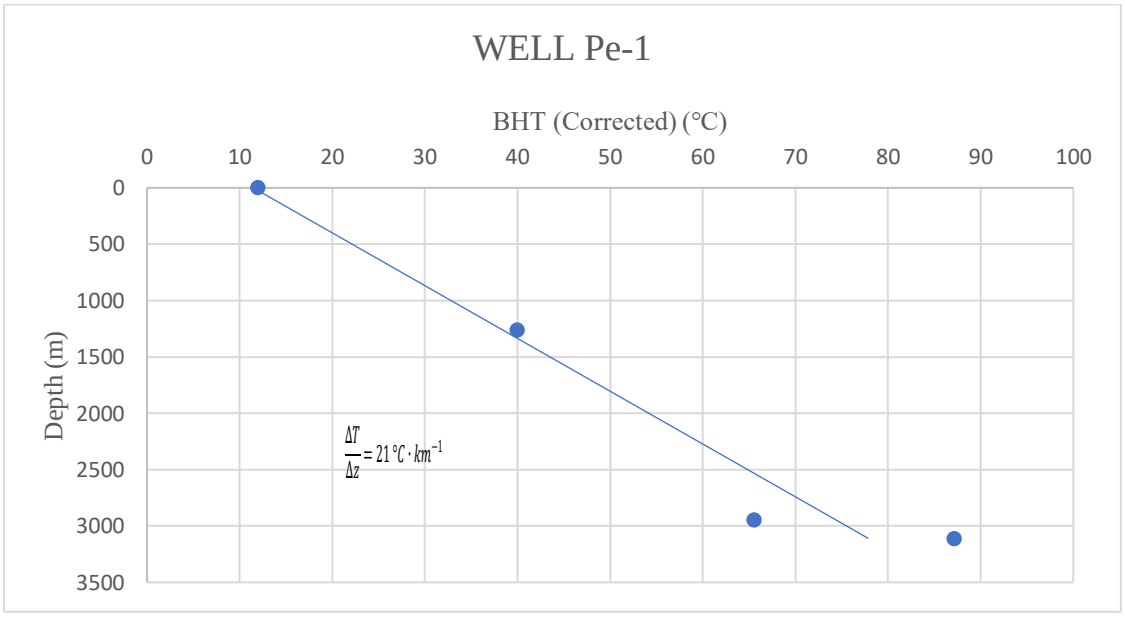

APPENDIX 10

UNCORRECTED BHT VS DEPTH

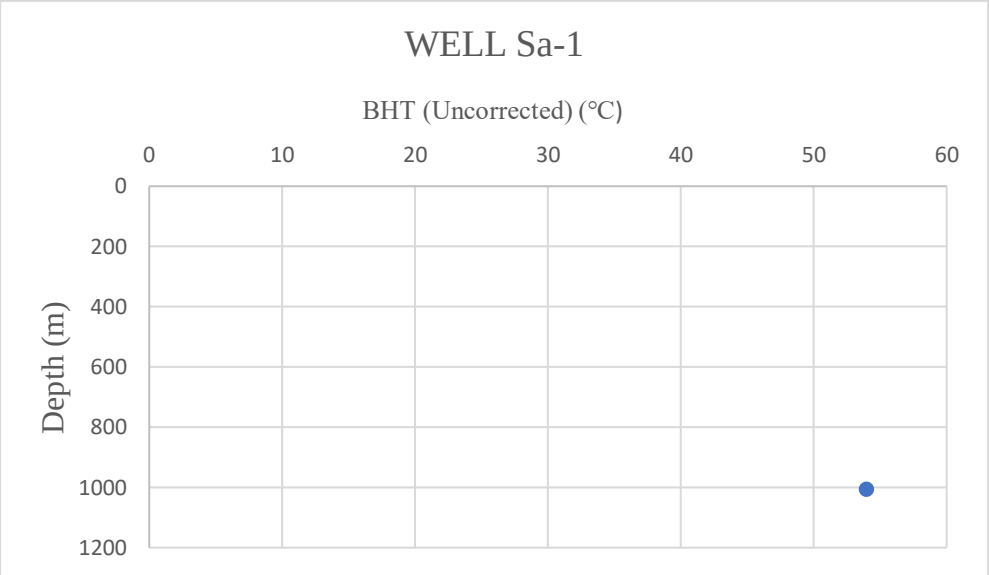

CORRECTED BHT VS DEPTH

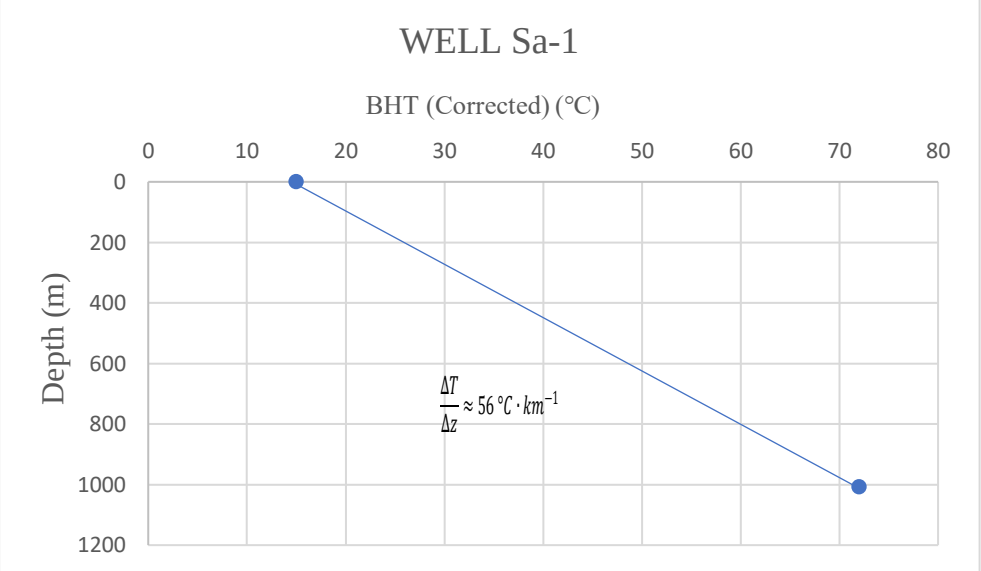

APPENDIX 11

UNCORRECTED BHT VS DEPTH

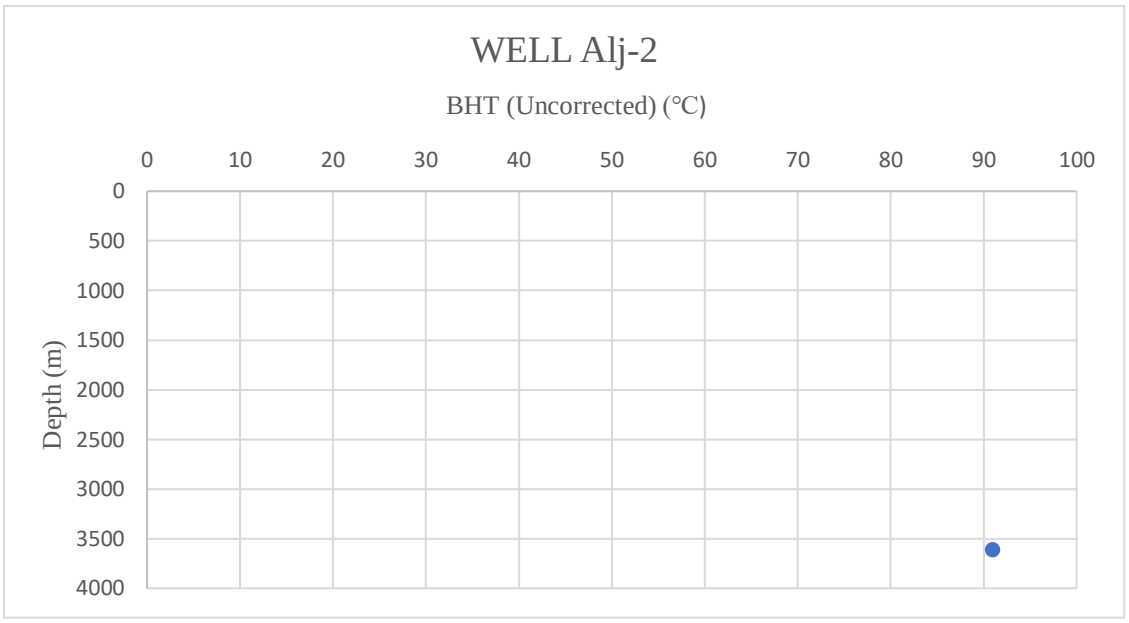

CORRECTED BHT VS DEPTH